NASA Contractor Report 165700

MLS–Airplane System Modeling

A. D. Thompson, B. P. Stapleton, D. B. Walen, P. F. Rieder, and D. G. Moss

Boeing Commercial Airplane Company
P.O. Box 3707
Seattle, Washington 98124

CONTRACT NAS1-14880
APRIL 1981

National Aeronautics and
Space Administration

Langley Research Center
Hampton, Virginia 23665

CONTENTS

TABLES

FIGURES

FIGURES (Continued)

FIGURES (Continued)

1.0 SUMMARY

Procedures and results associated with a variety of analyses and simulations conducted as part of a multiyear microwave landing system (MLS) study are reported in this document. Emphasis of the overall contract is directed toward the more important airplane-related items associated with MLS. This report details the following areas addressed in FY 80:

a. Airplane MLS antenna modeling
b. Airplane antenna-to-receiver RF system configurations
c. Direct path signal strength performance
d. MLS impact upon the airplane's autoflight system
e. Development of the initial stages of a fast-time MLS/flight control simulation model

Through use of a geometrical theory of diffraction (GTD) computer code, representative top-forward and bottom-rear antenna configurations have been developed and characterized for each member of the Boeing family of commercial airplanes. The top antennas give adequate coverage for the front sector, and the bottom antennas provide good coverage in the rear sector. Combining the two antennas into a single system by use of a switching element produces a unit with the potential for near-omnidirectional azimuth coverage.

RF system configurations for the MLS installation on Boeing jet transports were analyzed for several available options. These included trade studies relating to variation in coaxial cable type to minimize attenuation at the expense of weight, use of remote preamplifiers to improve system sensitivity, and employment of power dividers to provide triple redundancy. To meet the 5-dB cable attenuation specification requires the use of either waveguide, a 2.2-cm (0.875-in) diameter pressurized coaxial cable, or a remote preamplifier for all the rear antenna locations and for all the front antennas with the exception of the 707, 727, and 737 airplanes. Both the waveguide and 2.2-cm (0.875-in) coaxial cable are judged to be undesirable options for the airlines. The preamplifier does offer a potential solution for the aft antenna and for triple redundant applications where the requisite three-way power divider adds another 5- to 6-dB attenuation.

Antenna and RF system performance attributes were derived as a function of the airplane body angle relationships encountered on a representative flight track employing complex approach maneuvers and conventional finals. System performance was measured in terms of the signal power delivered to the receiver from the ground station elevation guidance element. These results were generated for candidate single and dual antenna systems for each Boeing jet model. For the single, forward antenna solution, only the 737 meets the required signal level for the entire approach because of the lower cable loss (i.e., 4 dB compared to 7.4 dB for the 757) and because the 737 antenna gain rolls off slower in the aft direction than most of the other airplanes. For the dual antenna system, all airplanes exceed the specification value by at least 2.5 dB. Again the 737 has superior performance and the 747 has the most marginal performance as a result of the difference in cable length runs associated with the rear antenna installation.

Three increasingly complex roles of MLS usage were examined to qualitatively assess their effects on current and next-generation aircraft autoflight systems, including flight management computer system (FMCS), flight control computer system, and thrust control computer system. The first role, that of MLS in direct substitutional use for instrument landing system (ILS), involved zero to very slight effect on software of the autoflight system (AFS), and no evident effect on the hardware capacity. The second role, wherein

the final leg of approach (course and glidepath) again remained nonselectable in azimuth and elevation but the interception point on this leg was defined by precision distance measuring equipment (PDME) gate, involved an intercept leg of autoguidance requiring new control logic for computations and commands by the FMCS. The third role, that of MLS (with associated PDME) serving as the principal guidance sensor for complex curved approaches, allowed the selection or assignment of azimuth and elevation angles different from the nominal course and glidepath. Additionally, it provided for initial approach guidance in which arcs and straight line segments were defined in terms of the three-dimensional geometrical data available from the ground facility.

Evaluation of automatic flight control algorithms in the MLS environment requires that realistic direct and multipath channel models and representative receiver models be incorporated into a high-fidelity AFCS simulator. Toward this overall procedure, development effort this year was centered primarily around the integration of a phenomenological MLS channel model with a lateral model of a 747-type widebody airplane. Existing ILS AFCS algorithms were employed and the ILS-derived information as supplied from the MLS receiver was used to drive the simulation. Both the low-frequency path-following errors and high-frequency control motion noise were included, and a mean touchdown lateral dispersion of approximately 1.5m (5 ft) was observed.

2.0 INTRODUCTION

NASA-Langley Task Requirement A-108 was designed to address several important airplane-related aspects of the microwave landing system (MLS). This effort represents the second phase of a multiyear program, which has as its objectives—

a. Provision of airplane MLS design options at various levels of sophistication to accommodate situations where airplane operators desire differing system capabilities; e.g., a single-antenna solution with no position biasing compensation as compared to a multiple-antenna configuration with autopilot biasing to dynamically account for the difference in antenna location and wheel position
b. Development of a procedure whereby the salient effects of the direct and multipath channels, coupled with flight dynamics, can be accounted for in the airborne guidance and flight management computer (FMC) algorithms

Toward these goals, the following studies and program developments were conducted during FY 80:

a. Airplane antenna pattern generation
b. Airborne RF system configuration
c. Airplane antenna coverage performance
d. MLS/FMC functional description
e. MLS/AFCS simulator development

These items are documented in sections 4.0 through 8.0, respectively. A description of the direct path channel model, developed in FY 79 and 80 and used to generate the results of the antenna coverage performance study, is given in appendix A.

3.0 SYMBOLS AND ABBREVIATIONS

AFCS	automatic flight control system
AFS	autoflight system
ATC	air traffic control
AWOP	All-Weather Operations Panel
AZ	azimuth
AZR	azimuth antenna look-angles at airplane receiver
AZT	azimuth antenna look-angles at transmitter
B	one-half wing span
C_e	total aerodynamic rolling moment
cg	center of gravity
C_L	coefficient of lift
CMN	control motion noise
C_n	total aerodynamic yawing force
C_{xb}	stability derivatives
C_y	total aerodynamic side force
DME	distance measuring equipment
DPSK	differential phase shift keying
EE	electronic equipment
EL	elevation
ELR	elevation antenna look-angles at airplane receiver
ELT	elevation antenna look-angles at transmitter
FCCS	flight control computer system
FFT	fast Fourier transform
FMCS	flight management computer system
FMS	flight management system
g	acceleration due to gravity
G_o	antenna peak gain, dB
GRP	ground reference point
GTD	geometrical theory of diffraction
h_{cg}	height of aircraft cg above touchdown elevation, m (ft)
h'_{cg}	height of aircraft cg above ground reference line, m (ft)
ICAO	International Civil Aviation Organization
IFR	instrument flight rules
ILS	instrument landing system
IRS	inertial reference system
I_{xx}	moment of inertia about x axis
I_{xz}	product of inertia in x-z system
I_{zz}	moment of inertia about z axis
LNAV	lateral navigation
LRC	Langley Research Center

m	mass
MLS	microwave landing system
n	load factor, nondimensional
P_B	body roll rate
PDME	precision distance measuring equipment
PFE	path-following error
P_s	body roll rate-stability axes
Q	aerodynamic pressure
R	radius of curvature in the x-y plane, m (ft)
R_B	body yaw rate
RF	radio frequency
R_f	flare radius of curvature in the x-z plane, m (ft)
R_s	yaw rate-stability axes
S	wing surface area, m^2 (ft^2)
SARP	standard and recommended practice
SID	standard instrument departure
S/N	signal to noise
STAR	standard terminal arrival
TCCS	thrust control computer system
TERP	terminal instrumentation procedure
U_{Bo}	forward velocity perturbation
V_B	side velocity perturbation
V_g	groundspeed, m/s (kn)
VNAV	vertical navigation
V_P	total velocity
V_t	true airspeed, m/s (kn)
W	aircraft weight, kg (lb)
W_{Bo}	vertical velocity perturbation
X_{cg}	x coordinate of cg location, m (ft)
Z_{cg}	z coordinate of cg location, m (ft)
α_{FP}	flightpath angle, rad
α_i	wing angle of incidence, rad
α_o	flare flightpath angle, rad
α_w	wing angle of attack, rad
β	bank angle, rad
δ A	aileron deflection
δ R	rudder deflection
θ	body angle, rad
ϕ	roll
ψ	heading

4.0 AIRBORNE MLS ANTENNAS

The airborne antenna pattern coverage is an important factor affecting the performance of the microwave landing system (MLS). The airborne MLS antennas must provide adequate coverage to ensure reliable MLS operation for all airplane orientations during approach. Therefore, this portion of the MLS study focused on measuring and calculating radiation pattern coverage for prospective antenna installations on Boeing airplanes. Results of the measurements and calculations were then used in section 6.0, Airplane Antenna Coverage Performance.

To take full advantage of the MLS guidance capabilities, omnidirectional azimuth pattern coverage is required. The elevation angle limits for the omnidirectional coverage are determined by the approach maneuvers of the airplane. Based on analyses of the airborne antenna look-angles for possible commercial transport airplane approaches, coverage is required at elevation angles from 25° above the horizon to 40° below the horizon. There must be sufficient antenna gain in this sector to produce a reliable link between the airplane and ground station.

On the Boeing commercial transport airplanes, a single antenna will not satisfy the requirement for omnidirectional azimuth coverage. A vertical monopole antenna above the cockpit was selected to provide the primary coverage in the front sector. By locating this antenna where the fuselage starts curving down to the windshield, the maximum forward gain is near the horizon. Few reflecting objects, such as other antennas or lights, would produce pattern variation. However, the gain aft is low because of the fuselage curvature and vertical fin shadowing. An antenna on the bottom centerline under the nose could produce forward coverage, but landing gear and doors would cause pattern variation during the approach maneuvers.

An aft antenna is used to fill the coverage nulls of the front antenna to supply coverage required for some MLS approaches and missed approaches. The aft antenna is located on the bottom of the fuselage where the fuselage begins to curve up to the tail. Therefore, the gain aft peaks near the horizon, but the forward coverage is minimal at the horizon.

4.1 ANTENNA MODELING

Antenna radiation patterns were determined using scale model measurements and computer calculations. The computer program, developed at Ohio State University, uses the geometrical theory of diffraction (GTD) to calculate the radiation patterns. NASA and Boeing measured radiation patterns using scale model airplanes. All patterns were recorded using the coordinate system of figure 1 with the elevation angles represented by theta and the azimuth angles by phi.

The GTD computer program developed at Ohio State University uses elliptical cylinders and flat plates to model the airplane (ref. 1). Using two models for each antenna allows the radiation patterns to be calculated for the entire antenna radiation sphere. GTD models were set up for top fuselage and bottom fuselage antennas on Boeing commercial transport airplanes. Then the models were input to the computer program to calculate radiation pattern amplitude over the antenna's radiation sphere. Similar models have been developed for some Boeing airplanes by Old Dominion University (ref. 2), and these were used as guides to develop our models.

NASA measured radiation patterns for several MLS antennas on an 1/11-scale Boeing 737 model (ref. 3). These measured data have been used to verify the model procedure used for the GTD computer calculations. Boeing obtained the NASA-measured data for a vertical monopole antenna above the cockpit and monopole on the bottom of the fuselage. The measured radiation pattern coverage data were used directly in the performance simulation of section 6.0.

Boeing measured radiation patterns for a vertical monopole antenna above the cockpit on the 767 airplane, using a 1/4-scale 767 forward fuselage section. The measured patterns were compared to data calculated using a GTD model. The scale model and elevation plane GTD model are compared in figure 2. The ellipses model the fuselage and a flat plate represents the edge of the front bulkhead. Similarily the roll plane model uses ellipses for the fuselage and flat plates for the wings and stabilizers. Comparisons of the measured and calculated pitch, roll, and 90° conic patterns are shown in figures 3, 4, and 5. Numerically comparing the measured and calculated data shows a mean difference of 1.3 dB in the forward coverage sector $\pm 30^{\circ}$ from the horizon and $\pm 60^{\circ}$ from the nose. Aft of the airplane, the difference increases because of the difference between the scale model and GTD model.

4.2 ANTENNA PATTERN RESULTS

Scale model measurements and GTD calculations were performed at 5.0 GHz for the Boeing commercial transport airplanes. Results of the measurements and calculations were stored on computer files, with each file containing the amplitude of the MLS antenna radiation, recorded every 2° in azimuth and elevation. Antenna radiation amplitude was used to calculate the antenna peak directivity by integrating over the radiation sphere. Then the data files were used in the MLS direct path characterization program.

In addition to using the radiation pattern coverage data in the system simulation, the data were presented in polar analog radiation patterns and in percentage coverage plots. The percentage coverage plots show the percentage of area over a particular angular sector of the radiation sphere where the directivity exceeds a specified level. For the top antennas, the percentage coverage was calculated for the sector with elevation angles of 65° to 130° and with azimuth angles from 270° to 90° ($\pm 90^{\circ}$ from the nose).

The bottom antenna percentage coverage was calculated over the sector with elevation angles from 65° to 130° and azimuth angles from 90° to 270° ($\pm 90^{\circ}$ from the tail). Finally, the top and bottom antenna radiation pattern data files were combined to make a file with the highest antenna directivity for each look-angle. The MLS receiver can select the antenna receiving the highest signal level. Therefore, this combined coverage file approximates the peak power available to the MLS receiver at each look-angle. This file was used to calculate the combined percentage coverage for the sector, including all azimuth angles between 65° and 130° elevation.

Table 1 lists the percentage coverage of 0 dBi for the top and bottom antennas and for the combined pattern coverage files. The 0-dBi level is significant because it has been used to develop the received signal level at the receiver (ref. 4). This table points out the coverage improvement when the top and bottom antenna coverage files are combined. For example, the top 737 antenna exceeds 0 dBi over 66% of the front sector, while the bottom 737 antenna exceeds that level over 68% of the rear sector. However with the combined pattern coverage over the two sectors, the percentage coverage increases to

87% of the area. The percentage coverage plots for the top and bottom antennas and the combined coverage are shown in figures 6 through 23.

The calculated percentage coverage uses only the directivity of the antennas and does not account for the cable loss to the receiver. The cable losses to the top and bottom antennas will not be the same. Therefore, the combined antenna pattern coverage at the receiver will have a different distribution than indicated by the combined coverage of table 1. Effects of the cable losses are described in section 5.0 and accounted for in the system coverage analysis of section 6.0.

4.3 CONCLUSIONS

The antenna pattern coverage measurements and calculations show that at least two MLS antennas are required for omnidirectional azimuth coverage. The top antennas give adequate gain for the front sector, and the bottom antennas give good coverage in the rear sector. Combining the coverage of the two antennas improves the pattern coverage over all azimuth angles.

Only vertical monopole antennas were used for the radiation pattern analysis, and the only locations investigated were above the cockpit and on the bottom of the rear fuselage. On final approach, an antenna nearer the main landing gear may be preferred to decrease the height of the antenna above the landing gear, although autopilot processing could be used for height correction. Forward pattern coverage could be produced by an antenna mounted on the airplane bottom centerline near the nose. However, available scale models and GTD models could not accurately model the landing gear, doors, and other hardware that would affect the radiation pattern coverage. A directional antenna may be required to produce uniform forward coverage in the presence of landing gear, gear doors, other antennas, etc. Further work is required to identify the location and the type of antenna required for this coverage.

5.0 RF SYSTEM CONFIGURATION

5.1 GENERAL

The basic MLS system configuration on a transport aircraft was studied for various installations. Trade studies included variations in coaxial cable type to minimize attenuation at the expense of weight, use of remote preamplifiers to improve system sensitivity, and use of power dividers to provide triple redundancy. The basic antenna system consists of a vertical monopole on fuselage top centerline above the crew cab, supplemented by a second antenna located far aft on the fuselage underside for approach and missed approach aft-azimuth* guidance. The MLS receiver is assumed to be located in the main electronic equipment (EE) rack. Figure 24 shows the basic system with parameter definitions. Data included give the length, attenuation, and weight of MLS cable runs on Boeing commercial transport aircraft.

The prime choice for location of a single MLS antenna is above the crew cab using the forward-sloping ground plane to produce a peak in the antenna pattern a few degrees below the horizon. This location is considered to be the best candidate location for a single antenna solution and will provide a gain of isotropic (0 dBi) or better over a high percentage for the forward sector, as shown in section 4.0.

The link budgets shown in the FAA MLS signal format and system-level functional requirements (ref. 4) assume an airborne antenna gain of 0 dBi. The statistical data presented in section 4.0 support the choice of this value of gain.

Table 2 gives a link budget for the differential phase shift keying (DPSK) data signal, using parameters given in reference 4.

Miscellaneous losses account for rainfall, multipath, atmospheric absorption, polarization loss, and transmitter power degradation, all of which are assumed to be statistically independent. A signal-to-noise (S/N) ratio of 5 dB is required for a 72% probability of successful decoding; thus, there is a 6.24-dB margin in the system. The minimum power density guaranteed over the specified coverage zone is -89.5 dBW/m^2. At 5 GHz this results in a received signal of -95 dBm at the output port of a 0-dBi airborne antenna.

5.2 CANDIDATE COAXIAL CABLES

The basic airborne system configuration consists of at least one antenna on fuselage top centerline with the MLS receiver located in the main EE rack. The choice of the coaxial cable configuration determines the sensitivity of the airborne receiver.

Because of the MLS frequency, cable attenuation is a serious consideration. Existing ILS systems use RG 214 type coaxial lines or smaller. This study considered three different candidate cables ranging from RG 214 to a 1.27-cm (0.5-in) diameter semirigid foam dielectric cable (Andrew Heliax FHJ4-50B). Table 3 gives the attenuation and weight per 100m for the three candidate cables at 5 GHz.

* Aft-azimuth is used to designate signal reception from the rearward direction of the airplane; i.e., local airplane azimuthal look-angles between 90° and 270°.

RG 393 is similar in construction to RG 214 with a larger diameter and can be installed in the same manner as RG 214. Andrew FHJ4-50B has a corrugated outer conductor and foam dielectric with a minimum bend radius of 12.7 cm (5 in). Connectors are nonstandard. Both airlines and airframe manufacturers would be reluctant to install the FHJ4-50B cable.

Comparison of the data in table 3 indicates a small weight differential between RG 393 and FHJ4-50B but significantly lower attenuation for FHJ4-50B cable. RG 393 offers better attenuation than RG 214 at the expense of a weight penalty and offers no significant increase in installation complexity compared with RG 214.

5.3 BOEING TRANSPORT AIRCRAFT CABLE RUNS

Table 4 gives the cable length, attenuation, and weight for a fuselage top centerline MLS antenna installation on Boeing aircraft with the MLS receiver in the radio rack. The antenna location chosen on each aircraft is intended to provide the same type of radiation pattern coverage as shown in figures 3, 4, and 5.

The 747 has the greatest cable length and therefore requires the most sensitive receiver. FAA MLS functional requirements in reference 4 indicate an aircraft cable loss limit for the full capability system of 5 dB, which corresponds to a receiver sensitivity of -100 dBm. Based on the data from table 4, none of the Boeing aircraft can use RG 214 for the MLS system and only three can use RG 393. The remaining aircraft will be required to use the FHJ4-50B type cable, which will impose both an installation and weight penalty on the aircraft.

The situation is even worse for the aft antenna because cable lengths are considerably longer. Table 5 gives the cable length, weight, and attenuation for a candidate antenna location far aft on fuselage bottom centerline for Boeing aircraft. For aft-azimuth coverage, the bottom centerline antenna must be located far aft to benefit from the upward slope of the fuselage and give coverage above the horizon. This is required for the missed approach maneuver where the aircraft will be climbing at a modest pitchup angle. A fuselage top centerline antenna location would not provide satisfactory aft coverage because of the null directly aft caused by the vertical fin.

Again the 747 has the greatest cable length; however, all aircraft exceed the 5-dB attenuation value given in reference 4, even with the largest diameter cable. Reference 4 requires aft-azimuth coverage to 13.9 km (7.5 nmi), which corresponds to a free space path loss decrease of 8.5 dB. One interpretation of this requirement is that the cable attenuation for the aft antenna could be 8.5 dB higher than the top centerline antenna or a total of 13.5 dB. The minimum power density from the aft-azimuth transmitter over the required coverage zone is -81 dBW/m^2 (ref. 4), which is consistent with the shorter range requirement. In spite of this increase in permitted cable loss, table 5 indicates that the FHJ4-50B still will be required on all aircraft. However, as will be shown in section 6.0, the aft antenna is required for certain approaches where the aircraft is required to fly away from the front azimuth transmitter because the top centerline antenna has poor aft coverage. Thus, for a full capability installation, the cable loss from the aft antenna would still be limited to 5 dB.

To achieve full 20-nmi range aft would require either the use of waveguide, a 2.2-cm (0.875-in) diameter pressurized coaxial cable, or a remote preamplifier located near the antenna. Both the waveguide and 2.2-cm (0.875-in) coax are judged to be unsatisfactory

solutions to airlines. The preamplifier does offer a potential solution both for the aft antenna and redundancy.

5.4 MLS CONFIGURATIONS WITH PREAMPLIFIER

Figure 25 shows a system block diagram for an MLS receiver in the main electronic equipment (EE) rack with a preamplifier located near the aft antenna on a 767 aircraft. This installation permits use of the lighter RG 214 coaxial cable throughout. The 11-dB noise figure of the receiver is currently specified in reference 4 and is representative of a receiver with no RF amplifier. The signal goes directly into a mixer after some filtering. The MLS receiver sensitivity certainly could be improved by use of an RF amplifier before the first mixer, but avionics manufacturers seem reluctant to add the complexity and cost of an RF amplifier. The preamplifier selected in figure 25 is based on a first-stage transistor noise figure of 4 dB preceded by a narrowband filter with a 1-dB insertion loss to eliminate undesired signals from sources such as C-band weather radar, which is used on some aircraft. To achieve a 30-dB gain will require the use of several transistors at 5 GHz; this gain is considered a realistic value without stability problems at this frequency. Recognizing that the overall system noise figure permitted in reference 4 is 16 dB (11-dB receiver noise figure plus 5-dB cable loss), the system configuration shown in figure 25 will result in a system noise figure of 15.2 dB yielding coverage in excess of 37 040m (20 nmi).

In general, use of a preamplifier will result in decreased dynamic range because a preamplifier will be more susceptible to overload than a mixer. The preamplifier may also be required in the top centerline antenna system because aircraft will undoubtedly require a dual or triple MLS receiver installation. Figure 26 is a system block diagram for a 767 triple-redundant installation using one MLS antenna on fuselage top centerline with an integral three-way power divider. The power divider induces an additional 5- to 6-dB attenuation before the preamplifier to raise its noise figure to 11 dB. Reexamination of table 4 indicates that even with the FHJ4-50B coaxial cable the system without preamplification cannot accept an additional 5- to 6-dB loss. Thus, from figure 26, the addition of a modest gain preamplifier (15 dB) achieves an overall system noise figure of less than 12 dB and provides greater than 37 km (20 nmi) coverage for three receivers using one antenna.

If an airline were reluctant to accept the remote preamplifier configuration and chose to locate it at the main electronic equipment rack on the same shelf in front of the MLS receiver, the system noise figure would be 18.4 dB, assuming the same preamplifier characteristics as in figure 26. This is only 2.4 dB in excess of the specified system noise figure and does permit a single antenna to be used for a triple receiver installation. A dual receiver installation with only a 3.5-dB loss for power division and a slightly lower noise figure in the preamplifier would yield a system noise figure less than the specified 16 dB.

5.5 FUTURE MLS/AIRPLANE STUDY AREAS

Future efforts will examine the preamplifier in greater detail and perhaps will also consider remote mixers that would permit even lighter weight cables.

The use of a single antenna structure with an integral two- or three-way power divider is considered to be a sufficiently reliable component for an airborne MLS installation, but

FAA approval is still an open question. The development of an MLS antenna with an integral power divider is another item for future work.

Use of the top centerline antenna is proposed for final approach, recognizing that this location places the antenna in excess of the ICAO 5.8m (19-ft) glidepath to landing gear path reference. Clearly the aft bottom centerline location is unacceptable for final approach. The only remaining alternative is a third antenna located forward of the nose gear on fuselage bottom centerline or on the lower portion of the nose bulkhead behind the radome. Reference 5 treats the nose bulkhead antenna location in greater detail. The top centerline antenna location provides superior coverage over a bottom centerline antenna because the aircraft will normally bank toward the MLS facility during approach maneuvers. Because of the superiority of the fuselage top centerline location as discussed in section 4.0, further work is recommended to investigate schemes to bias the autopilot using the advanced capabilities of MLS.

The data presented indicate that the fuselage top centerline antenna will require the FHJ4-50B coaxial cable to maintain cable losses less than 5 dB on the 747, 757, and 767 aircraft. Using this same cable for the bottom centerline antenna produces cable attenuation greater than 5 dB on all Boeing aircraft.

The examples using the preamplifiers indicate the advantages achieved because system noise figure is preserved while using RG 214 type coaxial cable. Certainly, improving the sensitivity of the airborne receiver can be recommended because the addition of an RF amplifier ahead of the first mixer should lower the noise figure to 5 dB.

6.0 AIRPLANE ANTENNA COVERAGE PERFORMANCE

Proper exploitation of the MLS guidance landing capabilities requires that within the MLS coverage zone signal levels greater than or equal to specified minima be obtained at the airplane receiver. These levels are a function of several parameters, including the effective radiated power of the ground transmitter, gain characteristics of the ground antenna system, distance from the transmitter-to-receiver elements, airborne antenna gain, and line losses between the airborne antenna and the MLS receiver. In this section, we pay particular attention to airborne antenna system performance properties as a function of airplane body angle relationships encountered on a representative flight track employing aft-azimuth intercepts, curved approaches, and conventional finals.

6.1 ANALYSIS METHOD AND PARAMETERS

The antenna performance evaluation procedure consists of using the direct path channel model developed in FY 79 and FY 80 (see app. A) coupled with selected aircraft radiation distribution plots to arrive at received power as a function of time for a specified flight track. Analyses were conducted using the candidate single and dual antenna systems as described in section 4.0 for each of the following Boeing airplanes: 707, 727, 737, 747, 757, and 767. These 12 antenna-airplane configurations were exercised over a flight track that closely resembles the STAR DORA5 profile flown in the 1978 ICAO Montreal MLS demonstration.

A three-dimensional representation of the STAR DORA5 profile is given in figure 27 and a plan view is shown in figure 28. A 3^{o} descent angle was invoked and the runway threshold is located at (x=0, y=0). The flight begins at a distance of approximately 13 km (7 nmi) from the airport and consists of an initial aft-azimuth approach followed by a fairly broad curved segment that takes the airplane out to a distance of roughly 18.5 km (10 nmi). Following this, the airplane meanders 3.7 km (2 nmi) off the runway centerline extension to effect a noise abatement procedure. Figure 28 also shows that the time has been indicated on the flight track for correlation with the output data of this analysis.

For all flight simulations, the link budget analysis was conducted for the 2^{o} beamwidth elevation element of the MLS guidance complement, which was modeled at a location of x = -243.8m (-800 ft), y = 76.2m (250 ft), z = 2.4m (8 ft).

The ground station antenna radiation distribution in the horizontal plane is illustrated in appendix A, figure A-9, and a total effective radiated power at beam peak gain was taken to be 54.5 dBm. This value is in accord with the latest FAA system-level functional requirements as reported in reference 4. Also according to this report, for the purpose of airborne power budget calculations, a miscellaneous loss of 3.9 dB was employed in the computer program; this quantity represents a root-sum-square protection factor to account for polarization loss, rain attenuation, atmospheric absorption, multipath induced direct signal cancellation, and monitor loss.

Coaxial cable type RG 393 (see sec. 5.0) was selected for the transmission line between the front airplane antenna and the receiver, whereas a lower loss cable type FHJ4-50B was assumed for the rear antenna-to-receiver cable run. RG 393 has an attenuation on the order of 68.9 dB/100m (21 dB/100 ft) and is considered to be a good compromise between installation complexity and RF power loss. On the other hand FHJ4-50B poses an installation penalty but has a loss of roughly 29.5 dB/100m (9 dB/100 ft) and thus

outperforms RG 393 by 10 to 15 dB on the rear cable runs, which may exceed 42.7m (140 ft) (e.g., 747).

In the FAA requirements document, the required direct path signal level at the receiver to meet the 0.2° control motion noise limit is -98.5 dBm, which corresponds to an 11-dB receiver noise figure, a 150-kHz noise power bandwidth, and a 6-dB design margin. In the ensuing analysis it is this value of -98.5 dBm to which the model-predicted signal strengths should be compared when ascertaining the performance of the links direct path.

6.2 RESULTS

Results of this analysis are given in figures 29 through 40 where the nominal received power is plotted against time along the STAR DORA5 flight track. Table 6 is given as an aid in correlating figure number with airplane type and antenna system configuration. Table 6 also shows the number of seconds of flight time by which the received signal strength does not meet the -98.5-dBm specification level. The following conclusions can be noted from these figures and tables:

a. For the single forward antenna solution, only the 737 airplane meets the -98.5-dBm level for the entire approach. This is partly because of the lower cable loss (i.e., 4 dB as compared to 7.4 dB for the 757) and partly because the 737 antenna gain rolls off more slowly in the aft-azimuth direction than most of the other airplanes. The aft-azimuth portion of the approach flight track (i.e., t = 0 to 50 sec) is where the other single antenna systems produce received signal levels under the -98.5-dBm value.
b. For the dual antenna system, all airplanes exceed the specification value by at least 2.5 dB. The 737 has the superior performance and the 747 has the most marginal performance as a result of the difference in cable length runs associated with the rear antenna installation.
c. On an individual airplane basis, the rear antenna system is employed only on approximately the first 40 sec of the flight track, which corresponds to the aft-azimuth portion of the landing approach.
d. For the larger airplanes, particularly the 747, there are distinct signal level drops at t = 145 sec and t = 218 sec. These drops are caused entirely by the airplane's antenna radiation pattern and are associated with those regions of the curved path portion where the airplane is banked away from the ground transmitter and thus produces fairly large negative elevation airplane look-angles with respect to the airplane's coordinate system. Because of the top-centerline location, the airplane's antenna gain falls off fairly rapidly in this region, and the larger the airplane the more rapid the rolloff (see app. B).

Finally, we also note that the first half of this flight scenario takes place at a range of roughly 11.1 km to 16.7 km (6 to 9 nmi) from the runway threshold, whereas the MLS overall specifications call for performance out to a maximum range of 37 km (20 nmi). Thus one cannot directly use the results of this section to evaluate system performance at the extremes of the defined operational limits. However, an estimate of the 37-km (20-nmi) performance may be obtained by subtracting 7 to 9 dB from the results for the first 150 sec of the flight track.

7.0 EFFECTS OF MLS IMPLEMENTATION ON AUTOFLIGHT SYSTEM MODES OF OPERATION

7.1 PURPOSE

The purpose of the investigation reported here was to delineate the major effects of incorporation of the microwave landing system into the family of avionic devices used for automatic flight control and terminal area navigation in current and future-generation large transport aircraft. Specifically addressed are the effects of MLS operation on the functions and operational modes of the flight management computer system (FMCS), the flight control computer system (FCCS), and the thrust control computer system (TCCS), all of which are subsystems of the autoflight system (AFS) as defined by ARINC (ref. 6).

7.2 METHOD

To evaluate the MLS effects on the various modes of automated flight, the role of the MLS and the options of AFS operational complexity were grouped so that ascending degrees of overall complexity could be compared. Some assumptions were required about as yet undecided operational features of the involved systems; these assumptions are flagged in the appropriate context. The groupings made are shown in table 7. Note that the "MLS/ILS Capture," "MLS/DME Gate," and "MLS-AZ/EL Select" mode titles are contrived for use in this report. The "Autoland (Modified)" mode title is explained in section 7.6.

7.3 GENERAL DISCUSSION

With reference to ARINC Characteristics 701, 702, and 703, the general partitioning of automated flight functions between the three subsystems (FMCS, FCCS, and TCCS) is illustrated in figure 41. Those functions that are shown included within the boundaries of more than one subsystem will not be duplicated within the architecture chosen for a particular aircraft type; they will be performed by one subsystem or the other, depending on the chosen system architecture. For purposes of this discussion, the decision was made to assign these "dual-set" functions as discussed in this section, which will represent the function partitioning assumed throughout the remainder of this report section.

Consideration of MLS impact and effects on the autoflight system, at this date, also requires some assumptions about MLS avionic characteristics because not all details have as yet been agreed on. The ground rules for these assumptions are the following:

a. There will be no consideration of required redundancy to achieve the required reliability.
b. Effects of MLS upon control and display devices will not be discussed here.
c. ARINC Characteristics 701 (Flight Control Computer System, published March 1, 1979), 702-1 (Flight Management Computer System, published January 29, 1980), and 703 (Thrust Control Computer System, published March 1, 1979) are principal references for function definitions of the autoflight system.
d. The DOT/FAA Engineering Requirement "MLS Signal Format and System Level Functional Requirements," FAA-ER-700-08C, May 10, 1979 (including change 1, May 16, 1980) is the principal reference for topics within its title.

The assumptions, themselves, are as follows:

a. All redundancy is adequate to the conditions of flight guidance to be examined.
b. Airborne MLS antenna coverage is adequate for reception of signals involved in all described roles of MLS usage.
c. Except for conversion of azimuth and elevation angles into course deviation measurements within the proportional guidance sector, the MLS receiver does not perform any navigation computation but serves only as the data decoding interface between the MLS ground subsystem and the aircraft AFS.
d. Air traffic control (ATC) procedures for sequencing IFR arrivals into approach positions will not be significantly modified by implementation of MLS, based as they are on certain separation criteria that evolve from physical limitations that MLS cannot alter (e.g., numbers and geometry of runways, usable volume of terminal area airspace, overlapping of airport terminal areas, numbers and geometry of airways converging on a terminal area.

The following are short descriptions of the FMCS, FCCS, and TCCS functions (as used in this report) involved in the modes of flight affected by MLS in its different roles of use.

7.3.1 FMCS Functions

The FMCS integrates information from the air data, inertial reference, radio navigation, and engine and fuel sensors; its own internal data base; and crew-entered data to perform the following functions:

a. Lateral navigation (LNAV) and vertical navigation (VNAV)
b. Guidance
c. Performance management
d. Data display (not discussed)
e. Maintenance-related fault data storage (not discussed)

Internal data base might be divided into the following two levels:

a. Basic, including navaids, selected airports, selected runways, and performance, airframe, and engine data
b. Expanded, including all the basic, plus waypoints, ground reference points (GRP), standard instrument departures (SID), standard terminal arrivals (STAR), and possibly company routes

Command data for performance management and autoflight guidance are supplied to the FCCS and TCCS for the selected modes of flight.

7.3.2 FCCS Functions

The FCCS integrates commands and parameter (or flight submode) selections from the FMCS and crew, together with air data, inertial reference, radio navigation, and control surface position sensor information, to perform the following functions:

a. Autoflight tasks of –
    1. Coupled approach
    2. Autoland
    3. Rollout
    4. Go-around

b. Autoflight functions of –
   1. Vertical speed select
   2. Airspeed select and hold
   3. Mach select and hold
   4. Altitude select and hold
   5. Heading select and hold
c. Pilot assist functions of –
   1. Control wheel steering (not discussed)
   2. Flight director commands (not discussed)

The FCCS tasks and functions use generic control laws, singly or in combination, as illustrated by the following possibilities:

a. Vertical position control law—used for altitude select, altitude hold, glidepath track, and flare on landing.
b. Localizer control law—used for localizer course track (both front and back course)
c. Vertical position control law—combined with localizer control law and autothrottle control law (in the TCCS) to provide coupled approach and autoland

7.3.3 TCCS Functions

The TCCS integrates commands and parameter (or flight submode) selections from the FMCS, the FCCS, and crew with air data, inertial reference, radio navigation, and engine, throttle, and configuration sensor information to perform the following functions:

a. Thrust rating computation and display (not discussed)
b. Autothrottle
c. Flight envelope protection
d. Thrust control during nonstabilized flight phases
e. Engine trimming (not discussed)
f. Maintenance testing (not discussed)

This functional listing for the TCCS conforms to the expanded, optional listing of ARINC 703. It was chosen for use in this report because it allows simpler diagramming of AFS functions than when all the major autopilot functions are lumped into the FCCS.

7.4 EFFECTS ON THE AFS OF THE MLS DIRECTLY SUBSTITUTING FOR ILS

It is evident that the least impact of MLS on an aircraft's autoflight system operation should occur in the case of the MLS receiver outputs being used in direct functional substitution for ILS receiver outputs. It also appears evident that this employment of MLS would have the least overall impact on air traffic operations in terminal areas and for that reason will probably be the major mode of use of MLS for many years after start of implementation.

The MLS functions required to provide ILS substitutional outputs for use by the AFS are front-course azimuth and elevation acquisition, validation, and track; back-course azimuth acquisition, validation, and track; and PDME acquisition and validation. The front- and back-course azimuths will be on extended runway centerline, and the front-course glidepath will be (by chosen convention) either the minimum selectable glidepath or some constant value like 3°; in either case it will be a value determined by the ground subsystem as is the case with ILS.

ARINC Characteristic 701 for the flight control computer system (published March 1, 1979) does not as yet list specific input signals from the MLS (see Attachment 7); however, the required signals for this operational role of the MLS are inferred from the ILS inputs to the FCCS, which are simply localizer deviation and glide slope deviation.

Employing ILS, the autoland functional inputs required by FCCS are ILS guidance, radio altimeter data, and airspeed data.

With MLS guidance directly substituting for ILS, operation of the AFS would be as follows. After the aircraft has been maneuvered to a selected start-of-approach waypoint (within MLS lateral proportional coverage) by use of heading/altitude select modes, the MLS/ILS capture mode is engaged, with runway heading, MLS tuning, and PDME tuning commands having been previously entered into the AFS. Lateral approach guidance is provided by FCCS-generated aileron commands, first aligning the aircraft with MLS center azimuth, then tracking that azimuth. Vertical guidance is provided by FCCS-generated altitude hold elevator commands that cause the aircraft to acquire the nominal glidepath, at which point altitude hold disengages and autoland mode becomes operative with vertical guidance on the tracked nominal glidepath. A selected approach speed can be effected in the TCCS operation for autoland by use of an autothrottle speed mode. At approximately 15.2m (50 ft) above the runway, measured by the radio altimeter, the FCCS outputs commands for automatic flare of the aircraft. At approximately 9.1m (30 ft) above the runway, the TCCS will commence retarding throttles. Rollout guidance along the runway is provided by FCCS steering commands to the rudder and nose wheel. A functional diagram of the preceding operational description is given in figure 42.

The preceding description applies to an approach and landing at a Category III ground facility for which the PDME input to the FCCS is required. For autoland at Category I and II facilities, the PDME input would not be essential (except that in absence of marker beacons DME information would be required for pilot monitor of the autopilot-coupled approach to decision height.)

With reference to the MLS ground-subsystem-transmitted facility and guidance information (ref. 4), contained in basic data and auxiliary data, only two portions of the basic data words need to be identified and decoded for the MLS to provide an output directly substituting for an ILS receiver output. The two basic data portions are (1) the distance from azimuth antenna to threshold and (2) the minimum selectable glidepath (used as the nominal glidepath in this role of operation). Optionally, a third piece of data, the approach azimuth proportional coverage sector, may also be used by the receiver to resolve possible ambiguity in the output to displays and autopilot, which could occur during transition through clearance coverage into the proportional guidance sector. None of these data are essential to functions performed outside the MLS receiver itself. Consequently, for MLS operating as a minimum capability receiver directly substituting for ILS, the AFS control logic would be unaffected.

Using the full range of up-linked data available in the basic data and auxiliary data words, if the MLS is still operating in an ILS substitution role, some modifications will be required in the FMCS control logic to accommodate potential changes in ground facility status during approach (e.g., possible downgrading of facility category from Category III to Category II or I. The changes are not evident to the receiver in the quality of received signal but would require flags and decoupling from autoland at different points in the approach.

7.5 EFFECTS ON THE AFS WHEN MLS PERMITS LIMITED SELECTION OF INTERCEPTION ANGLE WITH FINAL APPROACH COURSE

"Limited selection of intercept" is defined here to mean that the azimuth intercept angle is within 90° either side of extended runway centerline and the elevation intercept angle is approximately -3° to $+17^{\circ}$ with respect to the minimum selectable glidepath angle. Reasons for selecting these ranges are (1) consideration of airborne antenna coverage in the forward direction and (2) preservation of a scale of increasing complexity (i.e., this role of MLS usage is considered to be in the nature of an operationally more elastic ILS).

The MLS, in this role, would provide capability for a two-segment approach (initial and final approach segments) in both heading and glidepath, and thus allow much closer in captures of final approach than are currently operationally possible with ILS.

PDME is essential in conjunction with MLS for operation in this mode because the selected intercept distance from threshold governs the functioning of the AFS in maneuvering the aircraft from its initial heading and altitude to the heading, altitude, and descent angle required at the intercept point. As it is for an ILS approach, the MLS final approach segment azimuth (extended runway centerline) and elevation angles (minimum selectable) are fixed, not selectable by the pilot.

The MLS receiver output to the AFS will include the detected azimuth and elevation angles rather than course deviation signals only (as would be output from an ILS receiver). Additionally, the following basic and auxiliary data information will be used by the AFS for maneuver to the chosen on-course distance out from threshold (at which point the AFS would presumably operate as described for the autoland mode in section 7.4.

a. Basic
    1. Approach azimuth to threshold distance
    2. Minimum glidepath
    3. DME distance (from DME to MLS datum point)
b. Auxiliary
    1. Azimuth offset angle
    2. DME antenna offset
    3. Approach azimuth coordinate (system)
    4. Approach elevation coordinate (system)
    5. DME range offset
    6. Runway heading/runway direction

Operation of MLS and AFS in this operational role is as follows.

After the aircraft has been maneuvered to an ATC-selected waypoint within MLS front course coverage by LNAV/VNAV guidance, the pilot selects the appropriate navigation mode (MLS/DME gate) and enters the DME gate intercept point data (chosen by approach control), MLS tuning, and DME tuning commands.

Lateral and vertical path navigation computations are performed by the FMCS for a path between current position and heading (as sensed by inertial reference system (IRS), MLS, and PDME) and front course position and heading at intercept, including the initial and final transition turns and descent angle changes. Lateral guidance commands to the ailerons and rudder for alignment with and maintenance of the path are generated by the FCCS. Vertical guidance commands to the elevators, also generated by the FCCS, are

based on vertical speed required for the change in altitude over the path segment. FCCS also generates airspeed required (unless this has been pilot selected), and the TCCS performs autothrottle functions based on this command.

Once the aircraft is in reception of both lateral and vertical proportional guidance signals (equivalent to both ILS localizer and glide slope course coverage), the navigation function of the FMCS is terminated and autoland guidance is taken over entirely by the FCCS (in the autoland mode), generating lateral and vertical motion commands to control surfaces based on MLS receiver course deviation outputs.

A functional diagram of this operational description is shown in figure 43.

Definition of the first path segment described above would involve development of a new autoguidance control law for the FMCS and would employ initial position, heading, and speed relative to selected (final) position, heading, and speed, with both initial and final position and heading data being sensed by IRS and MLS and DME receivers; bank angle limit and airspeed would be either pilot selected or flight envelope constrained. This path segment corresponds to a vector by ATC but has potential for much greater accuracy of the target reached by the vector.

There would have to be logic considerations of changes in flight mode required by change in category status of the ground facility during the first path segment. Depending, as it would, on the chosen DME gate intercept and the distance to intercept still remaining when a category downgrade flag is received, this algorithm could become quite complex. Its development would necessitate an extensive analysis of ATC procedural effects. The effects on the AFS of using the MLS in this role are almost entirely a result of the MLS/DME gate path segment and of the accommodation by the FMCS guidance logic of the required basic and auxiliary data from the MLS. Some further effects can be expected from the possible necessity for the AFS to confirm that the ATC-chosen DME gate intercept is usable in terms of the following constraints: flight envelope, antenna coverage, and MLS clearance guidance sector restrictions.

The possibility of this last constraint occurring is remote because approach control would be using a method defined by a terminal instrumentation procedure (TERP) that would be based on avoidance of guidance through sectors of unreliable signals.

In addition, if the selected DME gate is rejected because of either or both of the first two restrictions, the AFS should determine and display to the pilot the next closest DME gate intercept achievable.

Alternatively, the AFS could display to the pilot the acceptable range of choice for DME gate upon selection of this autoguidance mode. This would demand some look-ahead in the logic to allow for delay in pilot response.

Instead of on-course DME gate and airspeed selection as fixed parameters for this autoguidance mode, with time to DME gate and to touchdown calculable therefrom, the same two-segment path could be defined by pilot selection of airspeed and time to either DME gate or to touchdown. The DME gate point would then be the solved variable. However, it appears essential that the pilot be informed by AFS of the allowable time-to window within which selection is allowable—after he has selected airspeed—in order to avoid AFS rejection of the pilot's choice of time. In addition, the pilot would need to be

informed by the AFS of the resultant on-course DME gate, and then inform ATC. This is reversed from normal procedures for sequencing and spacing.

7.6 EFFECTS ON THE AFS WITH MLS AS A PRINCIPAL GUIDANCE SENSOR FOR COMPLEX CURVED APPROACHES

A complex curved or multisegment approach using MLS and PDME will require all-round reception capability from the airborne MLS antenna, together with antenna and signal selection logic (not required of the MLS receiver equipment implied in the previous two MLS roles).

Definition of the path geometry would normally be by one of two methods:

a. Pilot entry into the FMCS-stored flight plan of the bottom-of-descent waypoint (from en route), and the selected STAR to be used commencing at that waypoint
b. Pilot entry of the bottom-of-descent waypoint into the flight plan, followed by path segment headings (or arcs referenced to PDME), and subsequent waypoint coordinates and altitudes leading to intercept of the chosen azimuth and elevation angles of the MLS at a chosen altitude or PDME gate

The first method would require that a selection of STAR's be available in the FMCS data base for each terminal area with MLS ground facilities. It would significantly reduce pilot workload from that involved in the second method by necessitating less keyboard entry to the FMCS and less coordinative communications between aircraft and approach control.

Again, as in the previously described role (sec. 7.5) for the MLS, MLS receiver output to the AFS will include the detected azimuth and elevation angles rather than simply course deviation signals. Nearly the full range of available basic and auxiliary data information will be used by the MLS and AFS for maneuver to the last waypoint for final approach.

Operation of MLS and AFS in this role is as follows.

Prior to arrival at an ATC-selected waypoint within MLS/PDME front course coverage, at which the complex curved approach commences, these things have occurred:

a. An ATC-approved STAR has been selected for use in autoguidance from the initial waypoint to a PDME gate point on final leg.
b. MLS and PDME tuning commands have been selected.
c. The MLS-AZ/EL select mode has been selected to be armed at the waypoint.
d. The ATC-approved MLS azimuth and elevation angles for final leg of approach have been entered into the FMCS and MLS.

At the starting waypoint for the approach, LNAV and VNAV guidance computations are performed by the FMCS, based on position, heading, and speed data (sensed by MLS/PDME, inertial reference, and path data). The FMCS issues autoguidance commands to the FCCS, which in turn generates lateral guidance commands to ailerons and rudder and vertical guidance commands to the elevators for alignment with and maintenance of the path. The TCCS performs autothrottle functions based on pilot-selected (or STAR-associated) airspeed. Once the aircraft has received both lateral and vertical proportional guidance signals about the selected azimuth and elevation angles (at the PDME gate that defines the start of "final approach"), a modified autoland mode guidance is engaged. In this mode the FMCS determines from approach and ground facility geometry data whether

FCCS will couple to the MLS receiver course and glidepath deviation outputs or whether the FMCS needs to stay in the guidance loop, issuing MLS-like correction signals to the FCCS. The FCCS generates lateral and vertical motion commands to control surfaces to track the final-approach path. Selected approach speed (within flight envelope constraints) is effected by autothrottle speed mode of TCCS operation. Flare and rollout operation are accomplished as previously described in sections 7.4 and 7.5.

A functional diagram of this operational description is shown in figure 44.

Sections 7.4 and 7.5 describe how guidance for the final leg of approach is accomplished by the autoland mode of AFS operation, and table 7 shows this same mode used for the final approach segment for complex curved approaches. In fact, this last role of MLS use will require changes in control logic for this mode because the selected course azimuth must at some point transition to 0° for path alignment with runway.

For selected MLS azimuth angles increasingly different from 0°, the PDME gate for transition to 0° azimuth would be farther and farther downwind from threshold. Computation of this gate point would be affected not only by flight envelope (and passenger comfort) constraints but also by ground facility geometry factors (i.e., single site or split site, azimuth antenna offset from runway centerline, azimuth 0° offset from runway centerline, etc.). It is evident that the FMCS algorithm for only this transition phase of flight prior to flare touchdown would be quite complex and that certification of the autoflight system and its software for this type of operation would entail extensive testing at selected MLS sites with differing geometries.

(Note: The scope of this report does not involve discussion of effects of MLS operation on displays associated with autoflight systems. However, it should be noted that the role of MLS usage described in this section—and possibly that of the previous section—may introduce aspects of crew autoflight path monitoring that require unique attention in display design features.)

7.7 SUMMARY

Three increasingly complex roles of MLS usage were examined to qualitatively assess their varying effects on the autoflight systems (including flight management computer system, flight control computer system, and thrust control computer system) of current and next-generation transport aircraft.

The first role, that of MLS in direct substitutional use for ILS, involved zero to very slight effect on the software of the AFS and no evident effect on the hardware capacity. Attendant with this minimal effect would be the direct usability of current published procedures (or new procedures, based upon standard ILS criteria) and little or no increased difficulty of certification of the autoflight system.

The second role, wherein the final leg of approach (course and glidepath) again remained nonselectable in azimuth and elevation but the interception point on this final leg was defined by PDME gate, involved an intercept leg of autoguidance requiring new control logic for computations and commands by the FMCS. In effect, this new logic would compute and command transition turns into and out of a descending intercept leg whose target is a PDME gate on the MLS nominal course and glidepath. This function would replace vector instructions by approach control such as "change heading to __ and descend to intercept localizer for runway __," and other instructions for correction of

heading. Besides this, it would provide quite precise on-course intercept points, much closer to threshold than ILS allows. The new control logic would probably be of moderate complexity and might involve an increase in FMCS processor capacity.

The third role, that of the MLS (with associated PDME) serving as the principal guidance sensor for complex curved approaches, allowed the selection (or assignment) of azimuth and elevation angles different from the nominal course and glidepath. Additionally, it provided for initial approach path guidance (within MLS/PDME coverage) in which arcs and straight line segments were defined in terms of the three-dimensional geometrical data available from the ground facility. (It was assumed that complex curved approach path-defining data would normally be available within the AFS data base as a STAR). Start of the final approach leg was defined as a "target" PDME gate within the proportional coverage sector of both the selected azimuth and selected elevation. Transition from selected azimuth to runway centerline alignment prior to flare would require development of complex control logic, which would probably eventuate in extensive certification testing at MLS ground facilities with varied geometries.

Table 8 is a summary chart of MLS-associated mode effects on the autoflight system.

8.0 MLS/AFCS SIMULATOR DEVELOPMENT

Efficient evaluation of automatic flight control algorithms in the MLS environment requires that realistic direct and multipath channel models and representative receiver models be incorporated into a high-fidelity AFCS simulator. Such a simulation facility is available at Boeing (Renton) and is presently being put into a configuration that can be employed to include MLS system and channel properties. Ultimately the MLS propagation channel model will include (1) effects of both the path-following error (PFE) and control motion noise (CMN) components of the total direct and multipath channels; (2) the signal coverage attributes of the complete system, including the airplane's antenna radiation distribution as modeled from the signal acquisition standpoint; and (3) aspects relating to the aircraft antenna switching instabilities (i.e., the receiver smoothing filters do not compensate for antenna location in the airplane) and landing bias compensations. The overall integration of the MLS and AFCS models will be completed next fiscal year and will be used to (1) establish baseline path tracking performance for existing autoland systems using raw MLS receiver signals, (2) determine levels of control surface and column or wheel activity to be expected for existing autoland control laws, (3) derive MLS signal filtering requirements to achieve acceptable control activity and satisfactory path tracking, and (4) determine MLS airplane system redundancy to provide full fail-operational capability.

Toward this overall procedure, development effort this year was centered primarily around the integration of a phenomenological MLS channel model with lateral and vertical models of a 747-type widebody airplane. Existing ILS AFCS algorithms were employed and the ILS-derived information as supplied from the MLS receiver was used to drive the simulation. Basic features of this simulation are illustrated in figure 45.

8.1 MLS CHANNEL MODEL

The FY 80 MLS total channel model was configured to emulate the permissible levels and time variations of PFE and CMN contaminations as dictated by the system-level requirements delineated in reference 4. In this regard, the total channel properties represent a pseudo-phenomenological process that is useful for determining the impact of these specifications upon the airplane guidance and control surface activity performances. The basic procedure consists of defining the PFE and CMN complex spectra in the frequency domain and then applying an inverse fast Fourier transform (FFT) operation to generate the requisite time domain sequences. This sequence is then added to the contamination-free azimuth and elevation angle coordinates of airplane position. For the ensuing analysis, it was assumed that the real and imaginary components were drawn from a random gaussian process with zero mean and variance proportional to the specified PFE or CMN tolerance specification. The real and imaginary components are assumed to be statistically independent as are all samples in the positive realm of the periodogram (the discrete spectral components). To produce a real-time output, the negative elements of the periodogram are set equal to the complex conjugate of their positive frequency counterparts. Also, to ensure that the guidance signals do not possess a constant bias the dc term of the spectrum was set equal to zero.

The frequency realms over which the PFE and CMN contamination are defined are illustrated in figure 46. It is also noted that—

$F_p = 0.5/2\pi$ Hz

$F_c = 10.0/2\pi$ Hz

$$2\int_{o}^{F_p} A(f)A^*(f)df = \sigma_p^2 = (0.032)^2$$

$$2\int_{F_p}^{F_c} A(f)A^*(f)df = \sigma_c^2 = (0.025)^2$$

$$N(t) = F^{-1}\ A(f)$$

$$\frac{\int_{o}^{T} N(t)^2\, dt}{T} = \sigma_T^2 = \sigma_p^2 + \sigma_c^2$$

σ_p^2 = PFE variance

σ_c^2 = CMN variance

Also $\sigma_{sp} = \sigma_p/\sqrt{N_p}$

$\sigma_{sc} = \sigma_c/\sqrt{N_c}$

where N_p and N_c are the number of points in the periodogram over which the PFE and CMN errors are modeled and N(t) is the noise contamination added to the airplane's actual position.

In accord with the system-level requirements as spelled out in reference 4, the standard deviation values for the PFE and CMN signals were set equal to 0.032^o and 0.025^o respectively. These values pertain to the recommended accuracy for a 1^o azimuth element beam width as spelled out in the ICAO standard and recommended practices (SARP).

Again we emphasize that this particular error spectral distribution (i.e., white) and level were selected to provide a first-order evaluation of the effects of the specification upon airplane guidance properties and control surface activity.

8.2 AFCS/AIRPLANE MODEL

During this phase of the study (1) the Boeing 747 was selected for the airplane model as operating with its fail-operational ILS control system, (2) MLS receiver ILS equivalent outputs were used to drive the guidance system control laws, and (3) analysis was restricted to the lateral (i.e., localizer) portion of the guidance system.

Equations describing the lateral motion of the aircraft are given in figure 47. These relationships are based upon the small perturbation assumption and contain terms for airplane body roll rate (P_B), body yaw rate (R_B), side velocity perturbation (V_B), total aerodynamic rolling moment (C_e), total aerodynamic yawing force (C_n), total aerodynamic side force (C_y), roll (ϕ), heading (ψ), body roll rate-stability axes (P_s), yaw rate-stability axes (R_s), rudder deflection (δ_R), and aileron deflection (δ_A). Definitions of additional parameters used in this figure follow:

S	wing surface area
I_{xz}	product of inertia in x-z system
I_{xx}	moment of inertia about x axis
I_{zz}	moment of inertia about z axis
B	one-half wing span
g	acceleration due to gravity
m	mass
W_{Bo}	vertical velocity perturbation
U_{Bo}	forward velocity perturbation
Q	aerodynamic pressure
V_P	total velocity
C_{xb}	stability derivatives

Figures 48 and 49 show, in block diagram form, the mathematics involved in the lateral control law and the yaw damper/turn coordinator models, respectively. The lateral control law drives the aileron surfaces whereas the yaw damper/turn coordinator feeds the airplane rudder. For the results presented in the following section, these algorithms were implemented without gain schedules, rate limits, and amplitude limits; future applications will include these factors.

8.3 RESULTS

It has been previously stated that the bulk of the MLS/AFCS simulation work will be conducted during the next phase of this study. During the present reporting period, initial stages of the overall model were developed and will be used in the next few months to ascertain the effects of the specified MLS channel PFE and CMN derogations on airplane control surface activity and tracking performance. Preliminary results from this application are given in this section for the 747 lateral dynamics as coupled with its fail-operational ILS autopilot control law. The ILS signals are derived from the MLS receiver ILS equivalent output data.

For this study the airplane was assumed to be on an initial track 10 972.8m (36 000 ft) (t = 0 sec) from the runway threshold along the runway centerline extension. The MLS

guidance signal as described in section 8.1 was then applied to the autopilot control laws with the resultant performance until touchdown (t = 150 sec), which is recorded in figures 50 through 53. These figures contain the following data plotted in strip-chart form with time as the horizontal coordinate.

a. Figure 50, MLS channel noise
b. Figure 51, exact azimuth angle
c. Figure 52, airplane side velocity
d. Figure 53, airplane lateral displacement from centerline extension
e. Figure 54, roll angle
f. Figure 55, yaw angle
g. Figure 56, rudder angle
h. Figure 57, aileron angle

From these data traces, the following observations are noted:

a. The MLS channel noise has maximum deviations on the order of +0.12° to -0.16° and exhibits distinct low-frequency (PFE) and high-frequency components (CMN). For this sample run, the error was determined to be 0.045° in accord with the model statistic generation described in section 8.1. The airplane's actual azimuth angle represents a filtered version of the total noise perturbation.
b. As expected, the off-course lateral deviation, y, tends to decrease as the plane approaches touchdown. At touchdown an error on the order of 3m (10 ft) is recorded. Ten runs similar to this were also conducted using different random number seeds for the spectrum generation; these produced an RMS touchdown lateral dispersion on the order of 1.49m (4.9 ft), a value in accord with the reference 4 specification.
c. Airplane noise-induced roll and yaw perturbations are typically less than 1.4° and 0.8°, respectively.
d. Rudder and aileron fluctuation exhibit a substantial amount of high-frequency motion and are deflected up to 1.2° and 2.5°, respectively.

These data are intended to represent a sample application of the MLS/AFCS preliminary simulation model. Future work conducted early in the next contract phase will refine the AFCS model (i.e., gain schedules, rate limits, etc.), include an MLS guidance algorithm, and examine a range of possible PFE and CMN spectra distributions. The resulting outputs will then be used to evaluate the effectiveness of the MLS control system algorithms and determine the effect of the high-frequency CMN fluctuation upon control surfaces.

APPENDIX A

DIRECT PATH CHANNEL MODEL

The direct path channel model has been configured to include the basic microwave landing system (MLS) guidance system components (i.e., azimuth, elevation, sector coverage). Presently the attributes of all the Boeing jet commercial models are embedded in the program; this includes the aircraft's flight dynamic properties. Provisions are made for single or multiple airplane antenna systems, and both conventional and curved flight tracks may be analyzed.

This appendix describes the basic components of the channel model. The description begins with an overview of the computer facility on which the program has been set up. The discussion that follows pertains to the data flow, flightpath generation, system geometry, flight dynamics, flight attitude perturbations, antenna gains, and power budget link margins. A sample application of the program and its output is also presented.

A.1 COMPUTER FACILITY

Using standard Fortran, the model code has been implemented on a PDP 11/70 interactive graphics system, which is shown in figure A-1. This system offers considerable input-output capability to the user. The special-purpose I/O peripherals that this particular application primarily employs are the Vector General CRT displays for two- and three-dimensional graphic display and the Remote Job Entry to EKS (CYBER System) for access to synthetically generated antenna pattern volumetric data. The storage disks are employed to store the antenna pattern data bases when they have been input to the system and the resultant channel model predictions for a given flight profile scenario.

A.2 DATA FLOW

Figure A-2 is a block diagram of the direct path channel computer code. As shown, the computer implementation consists of four main procedures: (1) algorithms to determine the airplane flight profile and dynamics with respect to time, (2) system geometry codes, (3) an attitude perturbation model, and (4) algorithms to derive the basic signal strength properties of the channel.

Waypoint descriptors and aircraft attributes are required input data to the "airplane flight profiles and dynamics" procedures, which produce, as a function of time, the profiles geographic location and nominal roll, pitch, and heading attitudes. These output data, together with information on the ground station position, are then employed in the "system geometry algorithm." Outputs from this algorithm provide a time history of the ground station-to-airplane range, local elevation and azimuth antenna look-angles at the transmitter (ELT and AZT), and the local elevation and azimuth antenna look-angles at the airplane receiver (ELR and AZR). Deviations about the nominal airplane attitude, which are known to be caused by conditions such as wind loading and flight technical errors, are derived as a function of the nominal attitude data and a set of input data describing the bounds on the roll, pitch, and heading variations. The output from this algorithm consists of a family of perturbed local airplane-to-ground station antenna look-angles for each point on the flight track.

Using the majority of the output data generated by the other three program procedures, the "systems performance algorithms" require additional ground and airborne station parameters and data arrays (i.e., antenna patterns, cable losses, transmitted power, etc.) to predict the power received by the airborne unit. If the airplane system employs two or

more MLS receive antennas, this routine also provides information pertaining to the particular airborne antenna unit selected, as a function of time and position.

As previously mentioned, the PDP 11/70 interactive graphic system has both two- and three-dimensional software and hardware support facilities. This capability allows any two of the designated program output parameters to be plotted against each other (2-D) or against another parameter in the ensemble (3-D).

A.3 FLIGHTPATH GENERATION

In generating the flightpath scenarios, an x-y-z coordinate system is centered at the threshold of the runway (see fig. A-3) with the x axis lying along the runway centerline and projecting away from the airport. The flight scenario is initiated by specifying the starting points (x, y, z) position; a waypoint is also established at this location. In turn, each waypoint defines the track taken between itself and the following waypoint. The following descriptions are employed at each waypoint.

a. Leg type (straight line, curved, flare approach)
b. Descent rate
c. Leg length—straight line leg
d. Heading change—curved leg
e. Radius of curvature in x-y plane—curved leg
f. Radius of curvature in x-z plane—flare approach
g. True airspeed
h. Airplane weight
i. Flap setting

A.4 SYSTEM GEOMETRY

To determine the signal strength attributes of the MLS-to-aircraft link, it is necessary to know the range between the transmitter and receiver and the local antenna elevation and azimuth look-angles at each terminal. These parameters are illustrated in figure A-3, where a primed x-y-z coordinate system has been established at the MLS element location with the x axis being aligned to the airport runway's centerline.

The range parameter is, of course, necessary to calculate the free space path loss, whereas ELT and AZT are required for determination of the ground station antenna gain. Similarly, ELR and AZR are employed in the derivation of the airborne systems antenna gain. Basic trigonometric relationships are used to derive these five parameters.

A.5 FLIGHT DYNAMICS

To properly include the receivers antenna pattern data in the link budget calculations, one must account for airplane roll, pitch, and heading orientation along the prescribed flightpath. The heading parameter is one of the inputs required to describe the flight profile plan view, whereas roll and pitch data are derived for straight-line segments, coordinated turns, and flare maneuvers through the following procedures.

A.5.1 Nomenclature (See figs. A-4 and A-5)

C_L coefficient of lift, nondimensional

h_{cg} height of aircraft cg above touchdown elevation, m (ft)

h'_{cg} height of aircraft cg above ground reference line, m (ft)

n load factor

R radius of curvature in the x-y plane, m (ft)

R_f flare radius of curvature in the x-z plane, m (ft)

S wing area, m^2 (ft^2)

V_g groundspeed, m/s (kn)

V_t true airspeed, m/s (kn)

W aircraft weight, kg (lb)

X_{cg} x coordinate of cg location, m (ft)

Z_{cg} z coordinate of cg location, m (ft)

α_o flare flightpath angle, rad

α_{FP} flightpath angle, rad

α_w wing angle of attack, rad

α_i wing angle of incidence, rad

β bank angle, rad

θ body angle, rad

A.5.2 Bank Angle

Under nominal flight conditions, airplane roll attitude (β) is derived from the following relationships:

a. Straight line-constant descent segments $\beta = 0$

b. Flare approach $\beta = 0$

c. Coordinated turn $\beta = 0$ $\qquad \tan^{-1}\left\{\dfrac{V_t^2}{11.26\ R}\right\}$

A.5.3 Pitch Attitude

Pitch attitude (θ) is related to airplane flightpath angle (α_{FP}), wing angle of attack (α_w), and wing angle of incidence (α_i) through the following expression:

$$\theta = \alpha_{FP} + (\alpha_w - \alpha_i)$$

For the 737-100, α_i is equal to approximately 1^o, whereas α_{FP} is obtained from program input data for the constant descent rate segment or is derived internally for the flare landing phase. Airplane angle of attack is obtained from figure A-4 where C_L and α_w are plotted for a family of wing flap positions. (Similar data arrays are stored for the other Boeing jets.) Flap settings are part of the input data used to describe each segment; the coefficient of lift is obtained from—

$$C_L = \frac{295.4\,Wn}{V_t^2 S \cos \beta}$$

where for constant descent segments n = 1; for the 737-100 the wing area (S) is on the order of 91.04 m^2 (980 ft^2) and the weight (W) is typically 40 823 kg (90 000) lb on approach for the 737-100 and 213 188 kg (470 000 lb) for the 747.

The flare approach portion of the landing phase is characterized by a nonunity load factor, a 0^o bank angle, and a continuously varying flightpath angle. Load factor is a parameter of arbitrary value indicating the sharpness of the flare maneuver. A higher load factor will result in a shorter flare radius of curvature and sharper flare, while a lower load factor produces a longer radius and more gradual flare. Although the "Jet Transport Performance Manual" states that n = 1.2 is a normal flare value, it is felt that more realistic results are obtained using a value of 1.1. Figure A-6 illustrates the relative geometries associated with the 1.1 and 1.2 load factor values for a conventional 3^o 737-100 approach at 66.9 m/s (130 kn).

A discontinuity in body angle will result at the initiation of flare if the load factor is treated as a step function jumping from 1.0 prior to flare to a higher value immediately after flare begins. This condition is remedied by allowing n to linearly increase in time as—

$$n = 1 + \frac{(n_{flare}-1)t}{\Delta t} \qquad t < t'$$

$$n = n_{flare} \qquad t \geq t'$$

where t' is the elapsed time from flare initiation and Δt is taken to be 0.5 sec.

During the flare maneuver, the flightpath angle is continuously changing. This parameter, in addition to the airplane x-z point pair relationship, is characterized by assuming that the flare approach describes a circular arc whose radius in the x-z plane is given by—

$$R_f = \frac{0.088466}{n-1} V_g^2$$

The intercept point between the final straight line segment and the flare segment is defined as that position where α_{FP} is equal to α_o, as shown in figure A-5. Using small angle approximations, the x,z intercepts, the (x_{cg}, z_{cg}) flare functional relationship, and the α_{FP} relationship are expressed as—

$$x_{intercept} = R_f \alpha_o$$

$$z_{intercept} = R_f \alpha_o^2/2$$

$$z_{cg} = R_f - (R_f^2 - x_{cg}^2)^{1/2}$$

$$\alpha_{FP} = x(R_f^2 - x_{cg}^2)^{-1/2}$$

A.6 FLIGHT ATTITUDE PERTURBATIONS

The perturbation model accounts for the fact that, in practice, airplane attitude will not exactly follow the specified nominal roll, pitch, and heading values but will undergo a certain amount of deviation. Such deviations are commonly caused by wind conditions and flight technical errors. Including a perturbation model places bounds on the airplane antenna gains and resulting power levels that are predicted for the flightpath. For each spatial point on the flight track, the model derives the airplane antenna gains associated with the nominal value and all combinations of the perturbed attitude values. The maximum, nominal, and minimum values are subsequently used to characterize antenna attributes over the flight track. Figure A-7 is a block diagram illustrating this operation.

In determining the perturbed receivers elevation and azimuth look-angles, geometrical relationships (shown in fig. A-8) are employed. Subscripts g and a refer to coordinates centered on the ground-based and aircraft-based axes, respectively. As previously stated, the ground-based coordinate system is located at the runway threshold with the x-y plane lying in the horizontal plane; the aircraft coordinate system is taken to be located at the airplane center of gravity with the x axis running the length of the fuselage toward the nose and the z axis projecting through the airplane top centerline.

To determine the look-angles from the receiver location to the transmitter station, the airplane coordinate system must be shifted to the receiver location and the transmitter coordinates must be expressed in terms of the shifted airplane coordinate system (i.e., $X_{R,T}$, $Y_{R,T}$, $Z_{R,T}$). Allowing for airplane roll, pitch, and yaw deviation, this series of operations may be written as—

$$\begin{bmatrix} X_{R,T} \\ Y_{R,T} \\ Z_{R,T} \end{bmatrix} = \begin{bmatrix} 1 & 0 & 0 \\ 0 & \cos R & \sin R \\ 0 & \sin R & \cos R \end{bmatrix} \begin{bmatrix} \cos P & 0 & -\sin P \\ 0 & 1 & 0 \\ \sin P & 0 & \cos P \end{bmatrix} \begin{bmatrix} \cos H & \sin H \\ -\sin H & \cos H \\ 0 & 0 \end{bmatrix} \begin{bmatrix} 0 & X_T - X_A \\ 0 & Y_T - Y_A \\ 1 & Z_T - Z_A \end{bmatrix}_g + \begin{bmatrix} X_R \\ Y_R \\ Z_R \end{bmatrix}_a$$

where

$R = R_o + \Delta R$

R_o = nominal airplane roll angle

ΔR = roll perturbation

$P = P_o + \Delta P$

P_o = nominal airplane pitch angle

ΔP = pitch perturbation

$H = H_o + \Delta Y$

H_o = nominal airplane heading

ΔY = yaw perturbation

From $X_{R,T}$, $Y_{R,T}$, and $Z_{R,T}$, the airplane antenna look-angles are determined as—

$$ELR = \tan^{-1} \left\{ \frac{Z_{R,T}}{(X_{R,T}^2 + Y_{R,T}^2)\ 1/2} \right\}$$

$$AZR = \tan^{-1} \left\{ \frac{X_{R,T}}{Y_{R,T}} \right\}$$

A.7 ANTENNA GAINS

A.7.1 Airborne Unit

The airborne antenna installation is considered to consist of one or more antenna units. When two or more elements are involved, a single radiation distribution is constructed through the following formulation:

$$G_c(ELR,AZR) = MAX \left\{ G_1(ELR,AZR) + E_1,\ G_2(ELR,AZR) + E_2,\ \text{----},\ G_n(ELR,AZR) + E_n \right\}$$

where

$G_c(ELR,AZR)$ = composite antenna pattern gain including the receive system efficiencies and line losses, dB

$G_n(ELR,AZR)$ = gain of the nth antenna, dB

E_n = efficiency of the nth antenna including all losses between the receive antenna output and the MLS airborne unit (a negative value), dB

$MAX\{A,B,C\}$ = an operation to select the maximum value of quantities A, B, C, etc.

ELR,AZR = elevation and azimuth antenna look-angles (see fig. A-3)

The above selection procedure is carried out for all combinations of the ELR and AZR arrays to form a new antenna data base. This base is then employed in the link budget calculations as if it were the sole airplane antenna unit.

A.7.2 Ground Station Antenna Gains

Apart from the distance measuring equipment (DME) link, which is not covered in this report, three MLS ground station antennas are considered part of the basic MLS complement: the azimuth and elevation guidance elements and the differential phase shift keying (DPSK) sector coverage antenna. Within the program these antennas have their gain attributes determined through use of experimentally derived data sets coupled with the following relationship, based upon the separation of variables:

$$G_T(ELT,AZT) = G_o + G_1(ELT) + G_2(AZT)$$

where

$G_T(ELT,AZT)$	=	gain of the respective transmitter antenna, dB
G_o	=	antenna peak gain, dB
$G_1(ELT)$	=	normalized elevation look-angle gain distribution, dB
$G_2(AZT)$	=	normalized azimuth look-angle gain distribution, dB
ELT, AZT	=	antenna's elevation and azimuth look-angles (see fig. A-3)

Parameter G_o depends upon the particular MLS element under analysis and its efficiency. Recent All-Weather Operations Panel (AWOP) power budget specifications (ref. A-1) call for the following G_o values:

a. AZ 3^o beamwidth, 14.4 dB
b. AZ 2^o beamwidth, 16.3 dB
c. EL2^o beamwidth, 14.1 dB
d. DPSK sector coverage, 7.3 dB

For the DPSK sector coverage system, $G_1(ELT)$ and $G_2(AZT)$ are derived from table look-up routine implementations of the data illustrated in figures A-9(a) and A-10, respectively.

It is assumed that the MLS receiver operates in a region centered about the peak of the guidance scanning beam. Thus for the elevation guidance system, $G_1(ELT)$ is approximately equal to 0 dB (neglecting a slight beam peak degradation) and $G_2(AZT)$ is obtained from the data of figure A-9(b). Similarly for the azimuth guidance system, $G_2(AZT)$ is set equal to 0 dB and its elevation look-angle distribution $G_1(ELT)$ is derived from figure A-9(a).

A.8 RECEIVED SIGNALS LEVELS

Received power levels at the input to the MLS airborne receivers are calculated as a function of the characteristics of the ground station element under analysis, the propagation channel, and the airborne antenna unit, including cable and connector losses. The following relationships are used to derive the received power level:

$$P_{rcvd} = P_t + G_t + G_r - L_{fs} - E - M$$

where

P_{rcvd}	=	received power, dBm
P_t	=	transmitted power, dBm
G_t	=	transmitter antenna gain, dB
G_r	=	receiver antenna gain, dB
L_{fs}	=	free space path loss, dB
E	=	system inefficiencies, dB
M	=	miscellaneous losses, dB

Both G_t and G_r are obtained from tabulated data as a function of the local elevation and azimuth angle (see sec. A.7). System inefficiencies include component losses such as connectors, cables, and age degradation; the miscellaneous loss term incorporates factors such as multipath signal loss and atmospheric attenuation. Free space path loss is a function of distance and frequency and is derived from:

$$L_{fs} = 32.45 + 20 \log D + 20 \log F$$

where D is the distance between transmitter and receiver in kilometers and F is the frequency of operation in megahertz.

A.9 PROGRAM APPLICATIONS

A sample case will be presented to illustrate (1) the program's basic features and (2) airplane antenna system influences upon performance. Prior to discussing these results, a brief description of the aircraft antenna employed in the application will be given.

A.9.1 Modeled Aircraft Antenna Patterns

Two aircraft antennas were modeled for the program applications. These antenna data are not included in the body of the program but are accessed from input data arrays of the requisite format. Both antenna data sets were obtained from NASA Langley Research Center (LRC) and represent total volumetric coverage radiation distributions every 2° in azimuth and elevation. These data were gathered on the LRC scale model antenna range using a frequency of 35 GHz and a 1/11-scale representation of the Boeing 737 airplane (ref. A-2).

Both antennas are vertically polarized monopoles. To a first order, a monopole antenna mounted on or near the airplane's centerline has a near-omnidirectional azimuth pattern and a fairly narrow elevation pattern that peaks close to the horizon. This donut-shaped distribution is, of course, influenced by aircraft body curvature, wings, tail components, etc.

One of the antennas was located at body station 239 near the top forward fuselage, slightly off center. The other was a rear-mounted unit at station 950 on the bottom centerline. Principal plane pattern distributions (roll, pitch, and azimuth) are given for these antennas in figures A-11 through A-16. Peak directivity of the front antenna was determined to be 7.5 dB, and the total loss/efficiency between the antenna and receiver input port was set to 3.0 dB (i.e., roughly a 0.5-dB coupling loss and a 2.5-dB cable loss for a 7.6m (25-ft) run of FHJ4-50B type cable). For the rear antenna, a peak gain of 8.5 dB was computed and a total loss/efficiency of 7.5 dB was invoked (i.e., 21.3m (70 ft) of cable run and a 0.5-dB coupling loss).

A.9.2 Sample Program Run

This case has been designed to illustrate the major features of the model while at the same time dramatizing the advantages of a dual airplane antenna installation over that of a single antenna unit. The single system was assumed to consist of the front antenna only, whereas the dual system employs both the front and rear units in a switched mode that selects the antenna producing the strongest signal at the receiver.

Figure A-17 provides a flight-time referenced plan view and profile view of the flightpath which, in essence, corresponds to a 360° holding pattern turn centered 27.8 km (15 nmi) from the runway threshold at an altitude of 4.9 km 16 086 ft. Received power levels from

the elevation beam MLS element were derived for the one- and two-antenna airborne terminal solutions. The elevation beam was taken to be located at x = -243.8m (-800 ft), y = 76.2m (250) ft, z = 2.4m (8) ft.

Because the airplane is flying at a constant altitude and radius of curvature, its roll and pitch angles are fixed and equal to 21.5° and 5.6°, respectively. The local elevation and azimuth look-angle time histories for the transmitting and receiving antenna units are given in figures A-18 and A-19. As indicated, the transmitting unit local elevation look-angle (ELT) varies slightly about the 10° value and its local azimuth look-angle (AZT) ranges from approximately -6° to +6°. On the other hand, the receiving antenna local elevation look-angle (ELR) varies from -33° to +12° and its local azimuth look-angle (AZR) varies over the full 360°.

Removing the time variable between ELR and AZR and exercising the attitude perturbation model produces the (ELR, AZR) array shown in figure A-20. This plot represents the potentially active portion of the antenna for the flightpath under analysis.

Results pertaining to the single antenna solution (station 239, front top centerline) and the dual solution (station 239 and station 950 back bottom centerline; switched) will now be presented.

Time histories of the maximum (upper curve), minimum (lower curve), and nominal (middle curve) antenna gain-plus cable loss and received power levels for the single antenna situation are given in figure A-21. The perturbation model used to generate these three curves accounts for flight attitude deviations from the nominal; it assumed roll and pitch deviations up to $\pm 5^{\circ}$ and heading deviation up to $\pm 15^{\circ}$.

The antenna gain, plus cable loss, is seen to vary from a high of 4.5 dB to a low of approximately -43 dB. Comparing the time axis of figure A-21 to the time reference marks of figure A-17 indicates that, as expected, the high antenna gains occur when the airplane is heading toward the transmitter (i.e., t = 120 sec) and that the low antenna gains result from conditions where the airplane is heading away from the transmitter (i.e., t = 45 sec). Figure A-21 also shows that the received power levels and antenna gains vary in concert. This condition occurs because the airplane distance to the transmitter, and the transmitter antenna look-angles, undergo minimal changes during the airplane's 360° maneuver. Thus, from the expression in section A-8, L_{fs} and G_t are essentially constant. It should also be noted that on the beam center the effective radiated power was specified as 54.1 dBm and, in accordance with the April 1979 AWOP power budget subgroup M (ref. A-1), the miscellaneous system loss was set equal to 5 dB. From the AWOP report, the full-capability elevation guidance receiver portion sensitivity is specified as -98.5 dBm (referenced to the receiver input). Thus, from figure A-21, one observes that for a substantial portion of the flight profile the required signal level is not met.

For the dual-antenna installation case, the corresponding antenna gain and received power level time histories are presented in figures A-22 and A-23, respectively. In both data sets, the nominal (middle curve), maximum (upper curve), and minimum (lower curve) perturbation values are illustrated. In addition to the airplane antenna gain data, which are observed to vary from a high of 4.5 dB to a low of -10 dB, figure A-22 also presents information pertaining to the antenna selected by the receiver. The solid squares correspond to rear antenna selection, and the open circles represent conditions where the front antenna system provided the maximum signal level.

Comparing figure A-23 to figure A-22, we again observe that the antenna gain and received power level time histories vary in concert. It is also noted that for the entire flight profile the minimum received signal power does not fall below 95.0 dBm, thus providing at least a 3-dB required signal power excess.

A.10 REFERENCES

A.1 "Report of Power Budget Subgroup." All Weather Operations Panel—Working Group M, Montreal, Quebec, April 1979.

A.2 Gilreath, M. C.: Airborne Antenna Polarization Study for the Microwave Landing System, NASA LRC Technical Memorandum TMX-73952, July 1976.

APPENDIX B

MLS ANTENNA PATTERNS

The MLS antenna radiation patterns were stored on a computer file in a matrix of gain as a function of elevation and azimuth angles. The MLS simulation programs used these data files directly. However, the performance of the antennas is most easily seen by looking at the principal radiation patterns.

Figures B-1 through B-12 show the pitch plane radiation patterns of the top and bottom MLS antennas that were used for this study. These patterns show that the top antennas have maximum forward directivity near the horizon, while the aft coverage peaks above the horizon. The bottom antenna has good coverage at the horizon aft of the airplane. The coverage forward is maximum well below the horizon.

REFERENCES

1 Yu, C. L.; and Burnside, W. D.: "Volumetric Pattern Analysis of Fuselage-Mounted Airborne Antennas." Ohio State University ElectroScience Laboratory, Report 2902-24, April 1976.

2 Chu, T. T.; and Mielke, R. R.: "A Study of Antenna Locations on Commercial Aircraft To Meet the Microwave Landing System Requirements." Old Dominion University, September 1977.

3 Gilreath, M. C.: "Airborne Antenna Polarization Study for the Microwave Landing System." NASA TM X-73952, July 12, 1976.

4 "Microwave Landing System Signal Format and System Level Functional Requirements." FAA-ER-700-08C, May 10, 1979, including Change 1, May 16, 1980, FAA/DOT Engineering Requirement, Tables 14 and 16.

5 MLS Airborne Antenna/Radome Study Contract DOT FA72WA-3010. Boeing Commercial Airplane Company, June 30, 1975.

6 "Flight Control Computer System." ARINC Characteristic 701, March 1, 1979, p. 5.

*Table 1. Antenna Percentage Coverage**

Percent of sector area that directivity exceeds 0 dBi for elevation angles 25 deg above the horizon to 40 deg below the horizon			
Airplane and related figures	Top antenna—for azimuth angles ±90 deg from nose	Bottom antenna—for azimuth angles ±90 deg from tail	Combined coverage—for all azimuth angles
707 (6,7,8)	63	76	99
727 (9,10,11)	65	72	97
737 (12,13,14)	66	68	87
747 (15,16,17)	50	75	100
757 (18,19,20)	62	73	98
767 (21,22,23)	63	74	98

*The combined coverage does not represent actual operational capability.

129044-1

Table 2. MLS DPSK Link Budget—Frequency = 5 GHz

Transmitter power	42.6 dBm
Ground antenna gain, peak	7.3 dBi
Horizontal and vertical coverage loss	1.0 dB
Free space path loss, 37 km (20 nmi)	138.7 dB
Miscellaneous losses	5.2 dB
Aircraft antenna gain	0 dBi
Aircraft cable loss	5.0 dB
Received signal at MLS input	-100.0 dBm
Receiver noise figure	11.0 dB
Noise bandwidth	150.0 kHz
Signal-to-noise ratio	11.24 dB

129044-2

Table 3. Cable Characteristics

Cable type	Attenuation, dB/100m (dB/100 ft)	Weight, kg/100m (lb/100 ft)
RG 214	91.9 (28.0)	18.8 (12.6)
RG 393	68.9 (21.0)	24.6 (16.5)
FHJ4-50B	31.2 (9.5)	26.8 (18.0)

129044-3

Table 4. MLS Coaxial Cable Parameters—Top Centerline Antenna Location

Aircraft	Cable length, m (ft)	RG 214		RG 393		FHJ4-50B	
		W_1, kg (lb)	α_1, dB	W_1, kg (lb)	α_1, dB	W_1, kg (lb)	α_1, dB
707	6.4 (21)	1.18 (2.6)	5.9	1.59 (3.5)	4.4	1.72 (3.8)	2.0
727	7.3 (24)	1.36 (3.0)	6.7	1.81 (4.0)	5.0	1.95 (4.3)	2.3
737	5.8 (19)	1.09 (2.4)	5.3	1.41 (3.1)	4.0	1.54 (3.4)	1.8
747	13.1 (43)	2.45 (5.4)	12.0	3.22 (7.1)	9.0	3.49 (7.7)	4.1
757	10.7 (35)	1.99 (4.4)	9.8	2.63 (5.8)	7.4	2.86 (6.3)	3.3
767	9.1 (30)	1.72 (3.8)	8.4	2.27 (5.0)	6.3	2.45 (5.4)	2.9

129044-4

Table 5. MLS Coaxial Cable Parameters—Bottom Centerline Antenna Location

Aircraft	Cable length, m (ft)	RG 214		RG 393		FHJ4-50B	
		W_2, kg (lb)	α_2, dB	W_2, kg (lb)	α_2, dB	W_2, kg (lb)	α_2, dB
707	29.87 (98)	5.58 (12.3)	27.4	7.39 (16.2)	20.6	7.98 (17.6)	9.3
727	29.26 (96)	5.49 (12.1)	26.9	7.17 (15.8)	20.2	7.85 (17.3)	9.1
737	20.11 (66)	3.76 (8.3)	18.5	4.94 (10.9)	13.9	5.40 (11.9)	6.3
747	44.80 (147)	8.39 (18.5)	41.2	11.02 (24.3)	30.9	12.02 (26.5)	14.0
757	35.05 (115)	6.58 (14.5)	32.2	8.62 (19.0)	24.2	9.39 (20.7)	10.9
767	36.58 (120)	6.85 (15.1)	33.6	8.98 (19.8)	25.3	9.80 (21.6)	11.4

129044-5

Table 6. Antenna System Performance Cross-Reference

Aircraft	Antenna system	Below threshold, sec	Figure number
707	Forward	33	29
707	Dual	0	30
727	Forward	34	31
727	Dual	0	32
737	Forward	0	33
737	Dual	0	34
747	Forward	32	35
747	Dual	0	36
757	Forward	36	37
757	Dual	0	38
767	Forward	36	39
767	Dual	0	40

129044-6

Table 7. MLS Roles Versus AFS Modes

MLS role	AFS mode
MLS directly substitutes for ILS	Heading/altitude select (transitioning to) MLS/ILS capture (transitioning to) Autoland
MLS allows limited selection of interception with final approach to landing.	LNAV/VNAV (with transition to) MLS/DME gate (transitioning to) Autoland
MLS serves as a principal guidance sensor for complex curved approaches.	LNAV/VNAV (transitioning to) MLS-AZ/EL select (transitioning to) Autoland (modified)

129044-7

Table 8. Summary of MLS-Associated Mode Effects on AFS

MLS-associated mode	Effects			Other comments
	FMCS	FCCS	TCCS	
MLS/ILS capture and autoland	Slight effect	Slight effect	No effect	
MLS/DME gate	Moderately complex new guidance logic; slight increase in processing capacity	No effect	No effect	
Autoland	Slight effect	Slight effect	No effect	
MLS-AZ/EL select	Complex new guidance logic; expanded data base; increased processing capacity	No effect	No effect	
Autoland (modified)	New logic	Slight effect	No effect	Extensive certification testing

129044-8

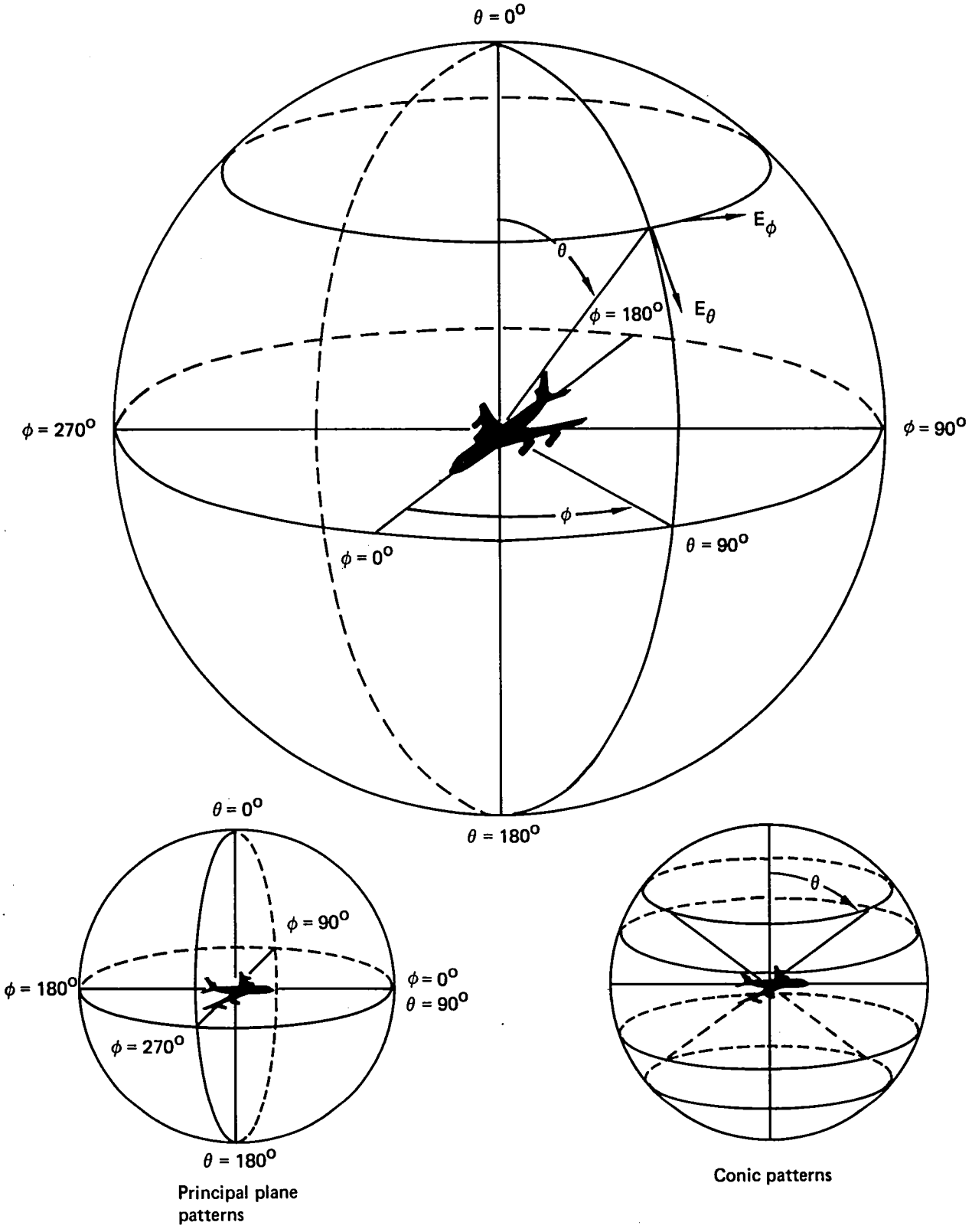

Figure 1. Antenna Radiation Pattern Coordinate System

129044-9

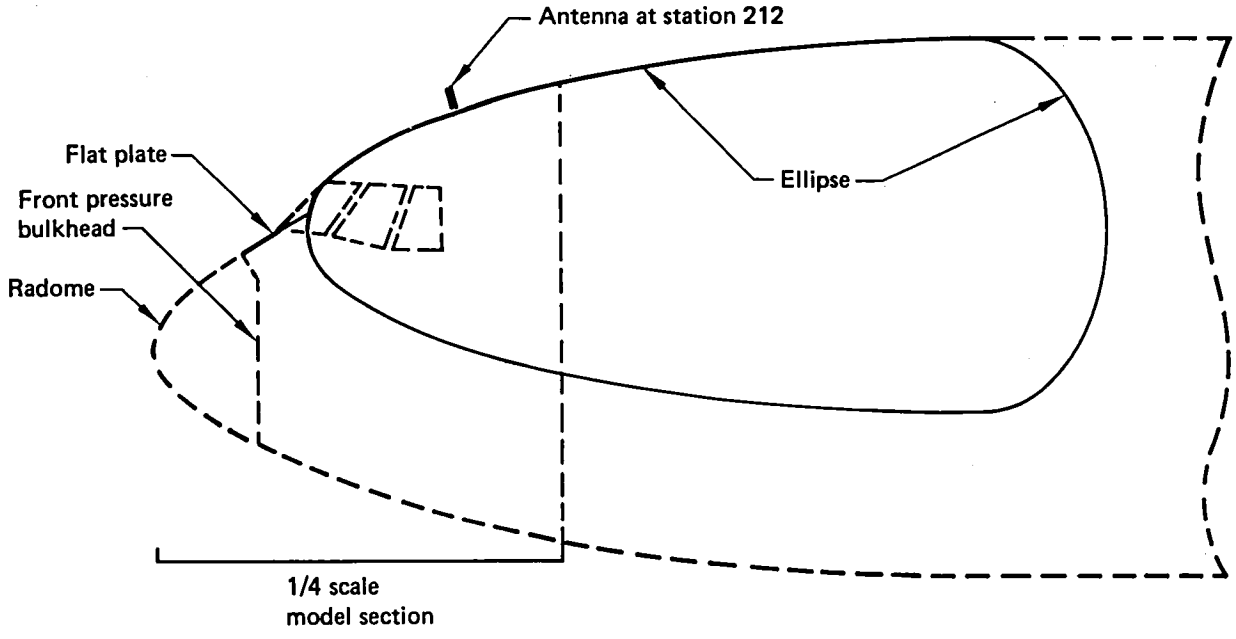

Figure 2. 767 GTD Model Compared to Scale Model

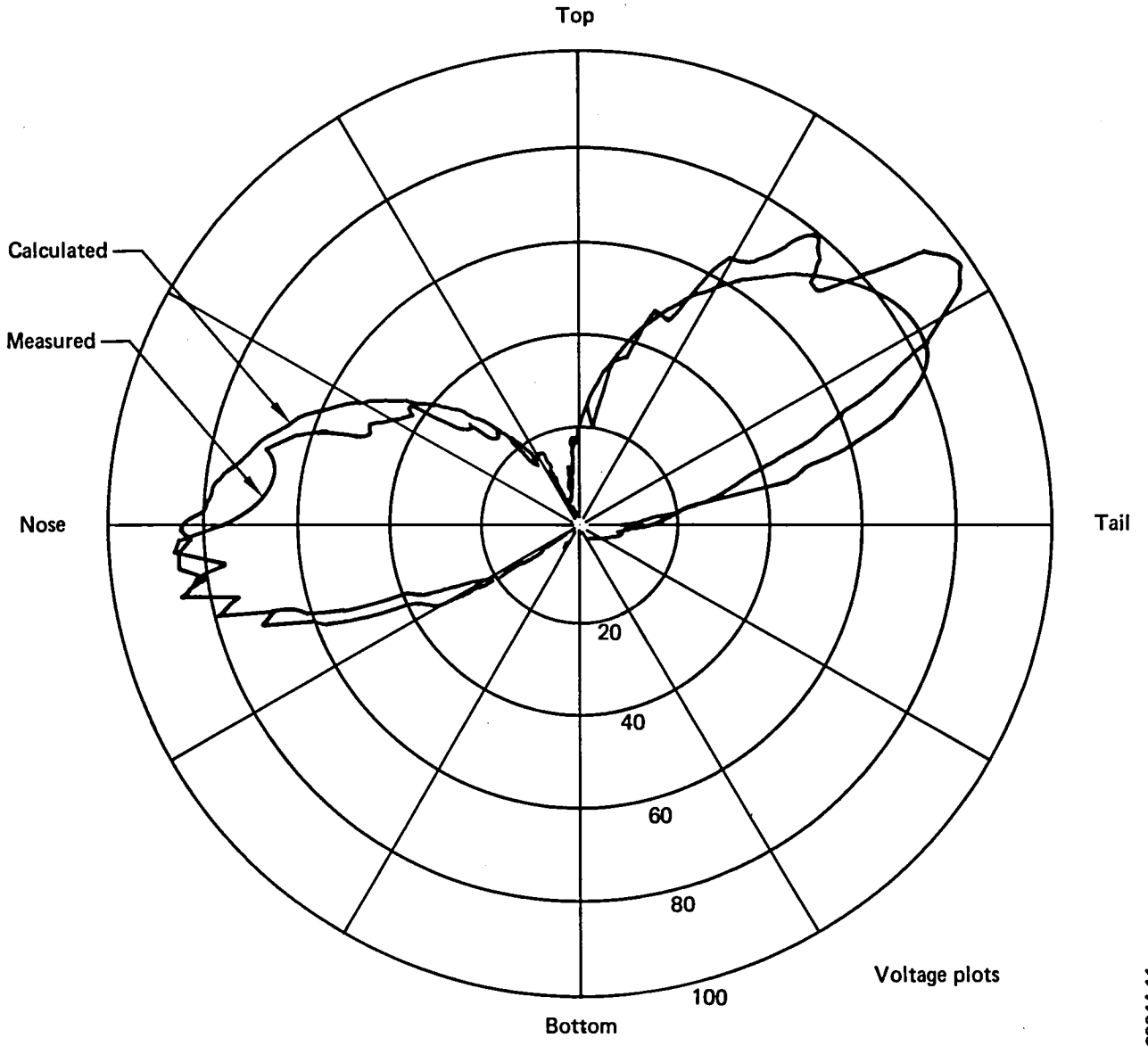

Figure 3. 767 MLS Antenna Pitch-Plane Pattern

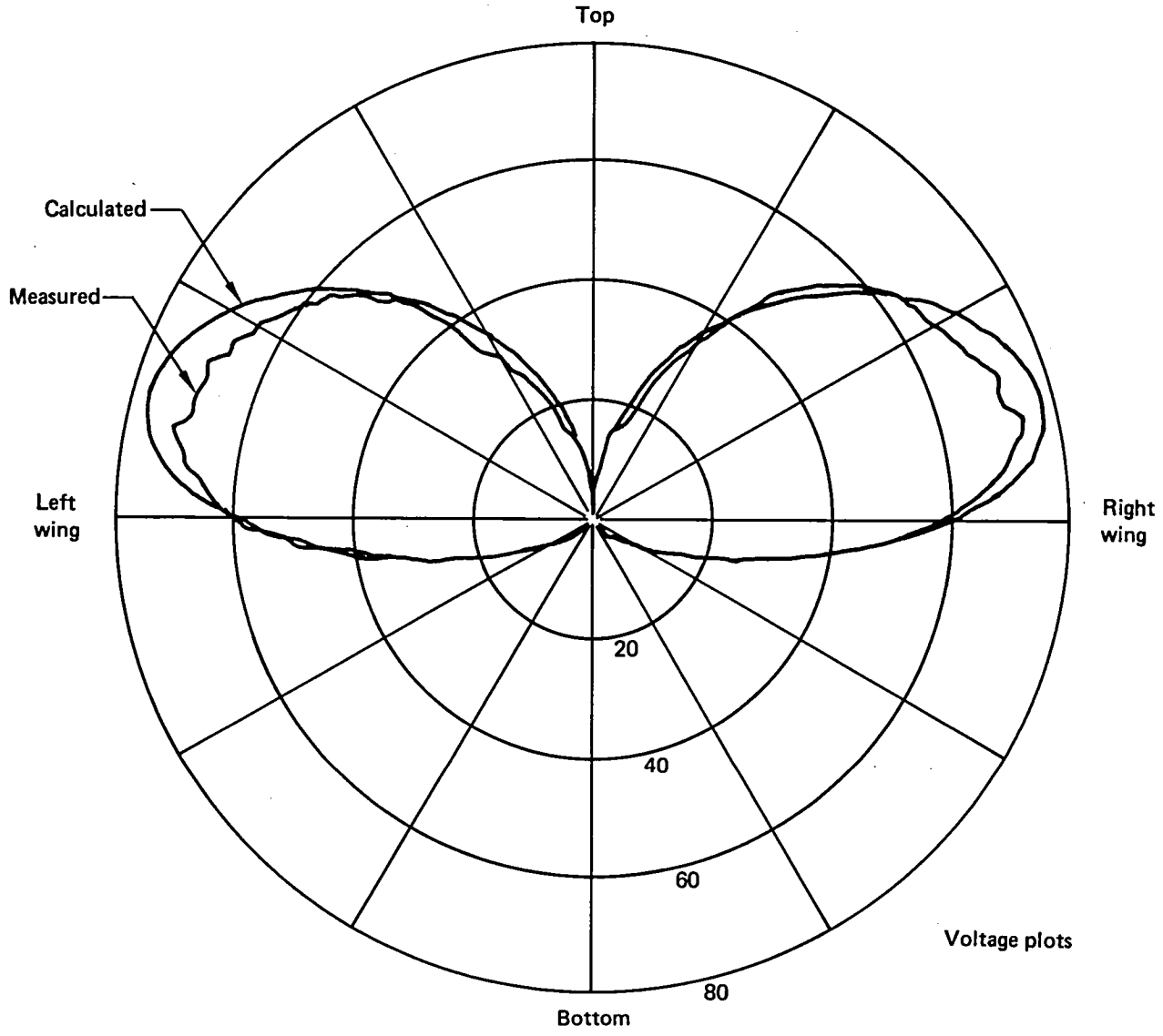

Figure 4. 767 MLS Antenna Roll-Plane Pattern

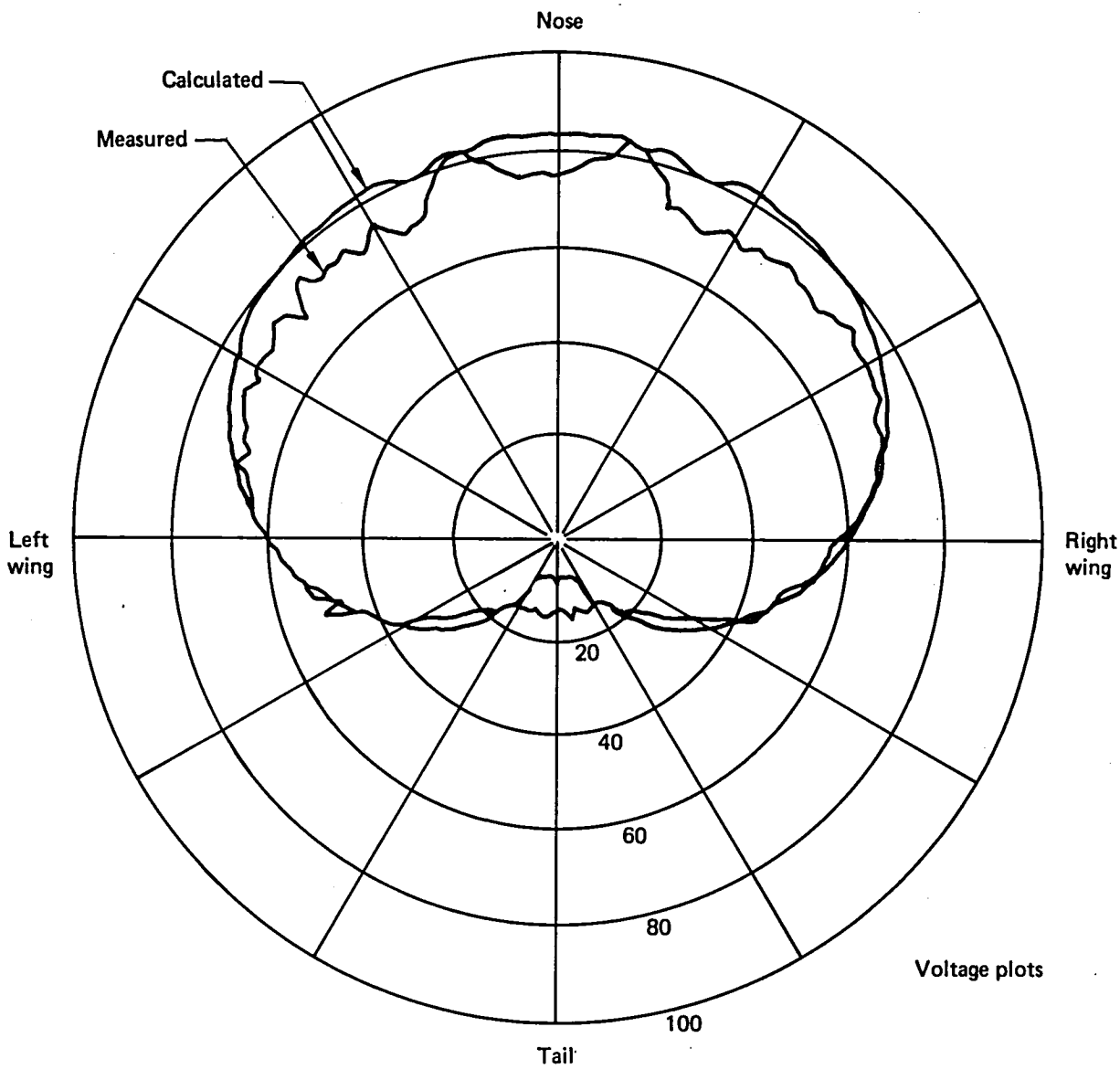

Figure 5. 767 MLS Antenna 90° Conic Pattern

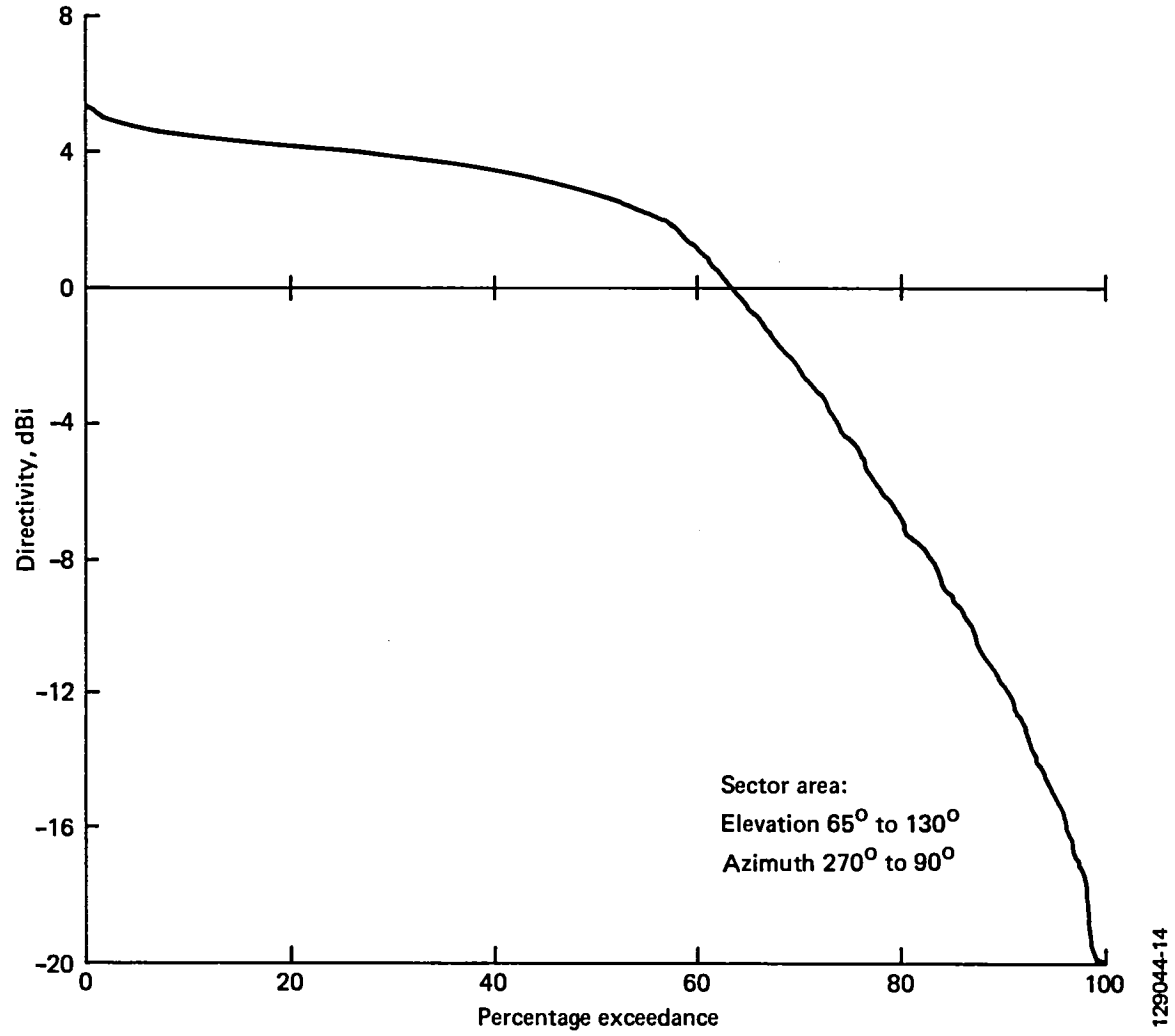

Figure 6. 707 Percentage Coverage—Top Antenna

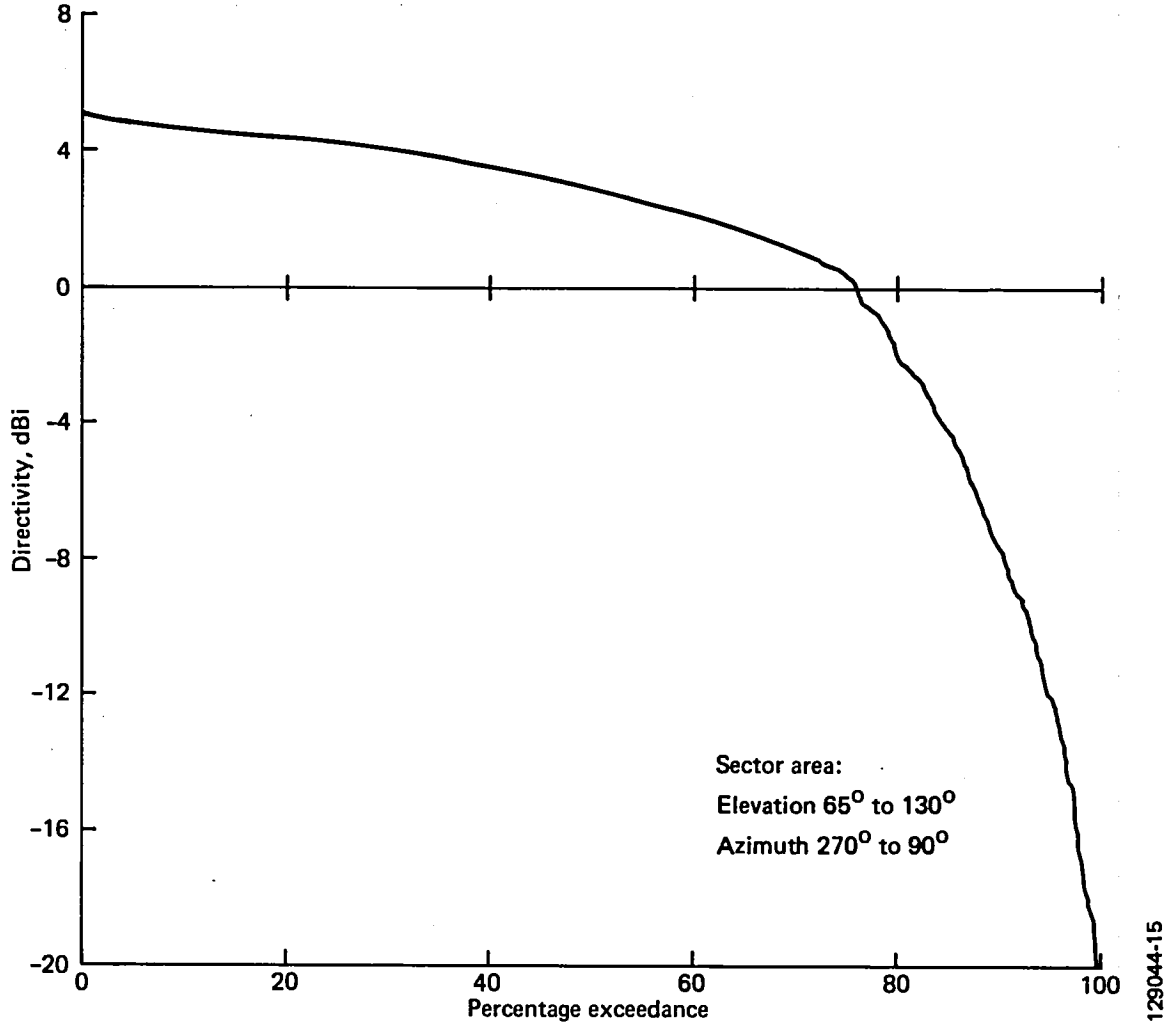

Figure 7. 707 Percentage Coverage—Bottom Antenna

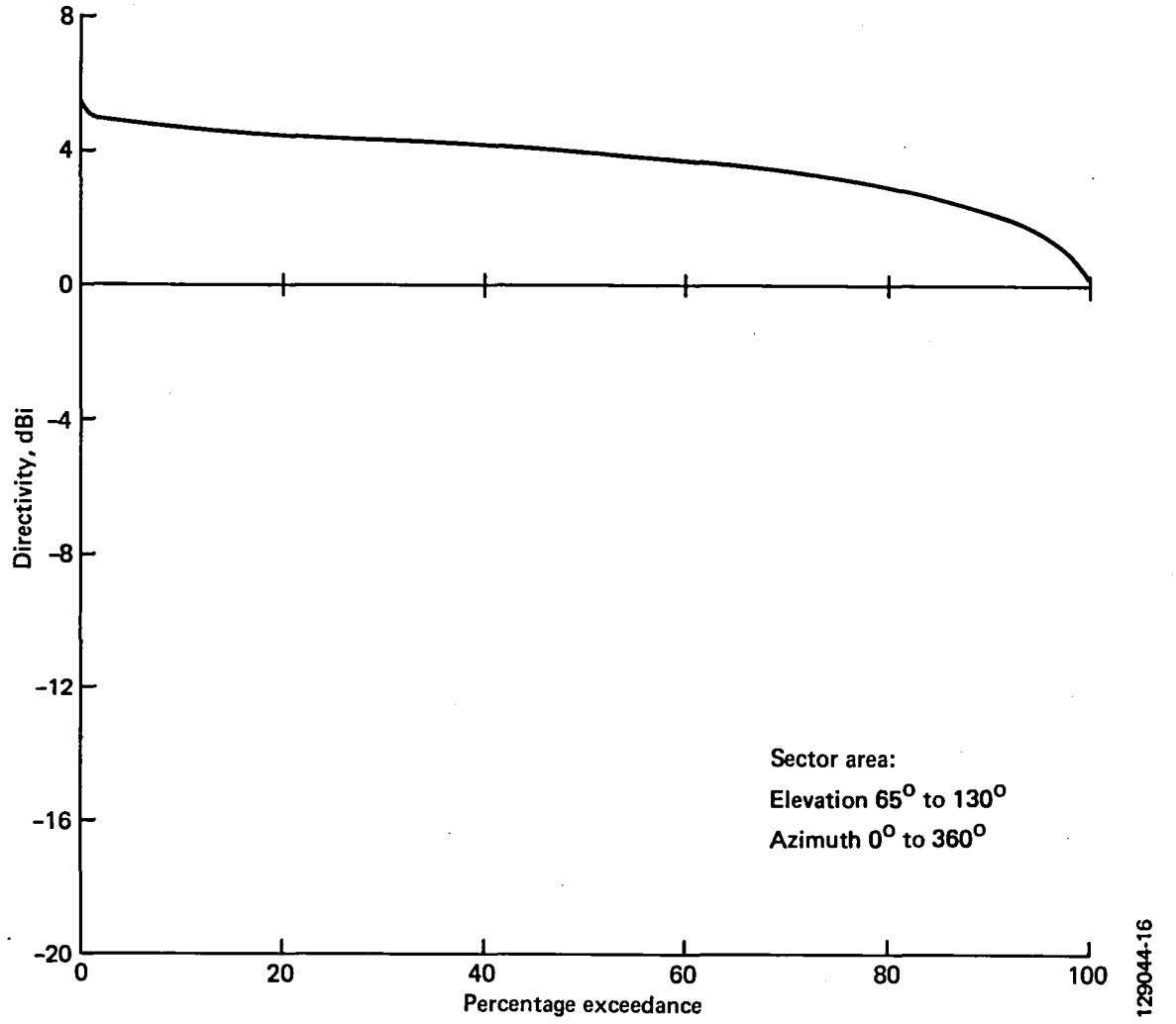

*Assuming identical element line losses, etc.

Figure 8. 707 Percentage Coverage—Combined Radiation Pattern*

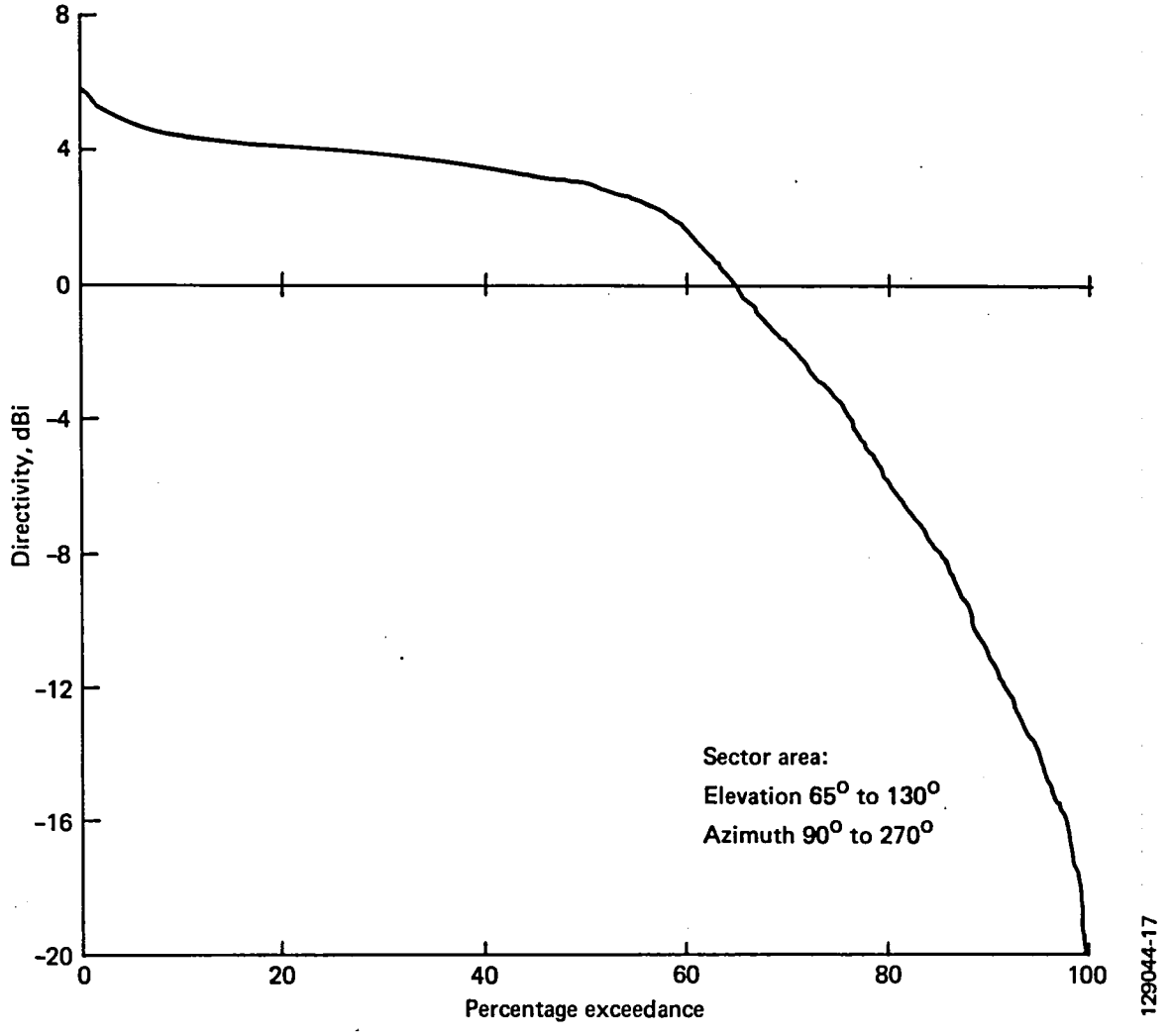

Figure 9. 727 Percentage Coverage—Top Antenna

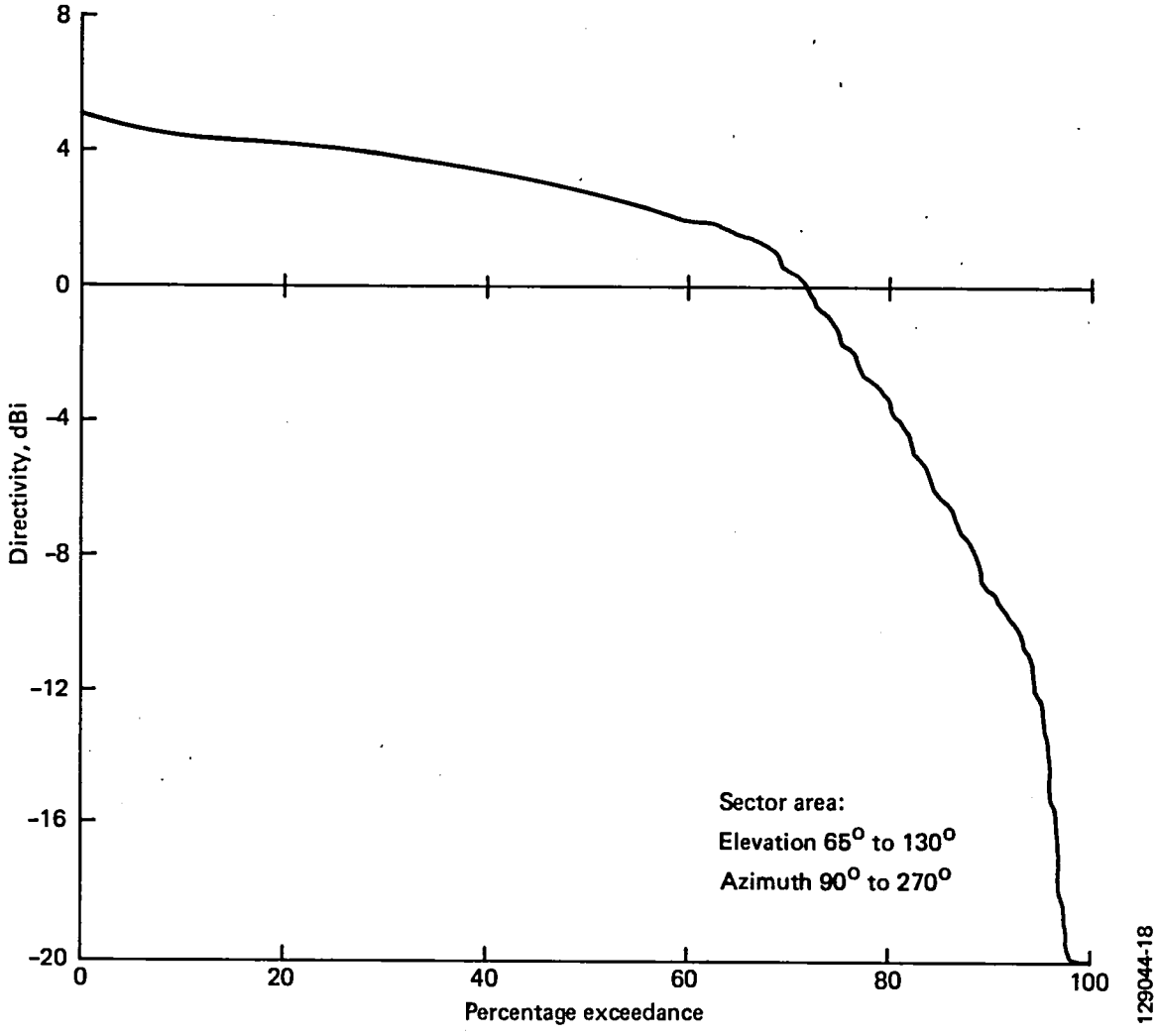

Figure 10. 727 Percentage Coverage—Bottom Antenna

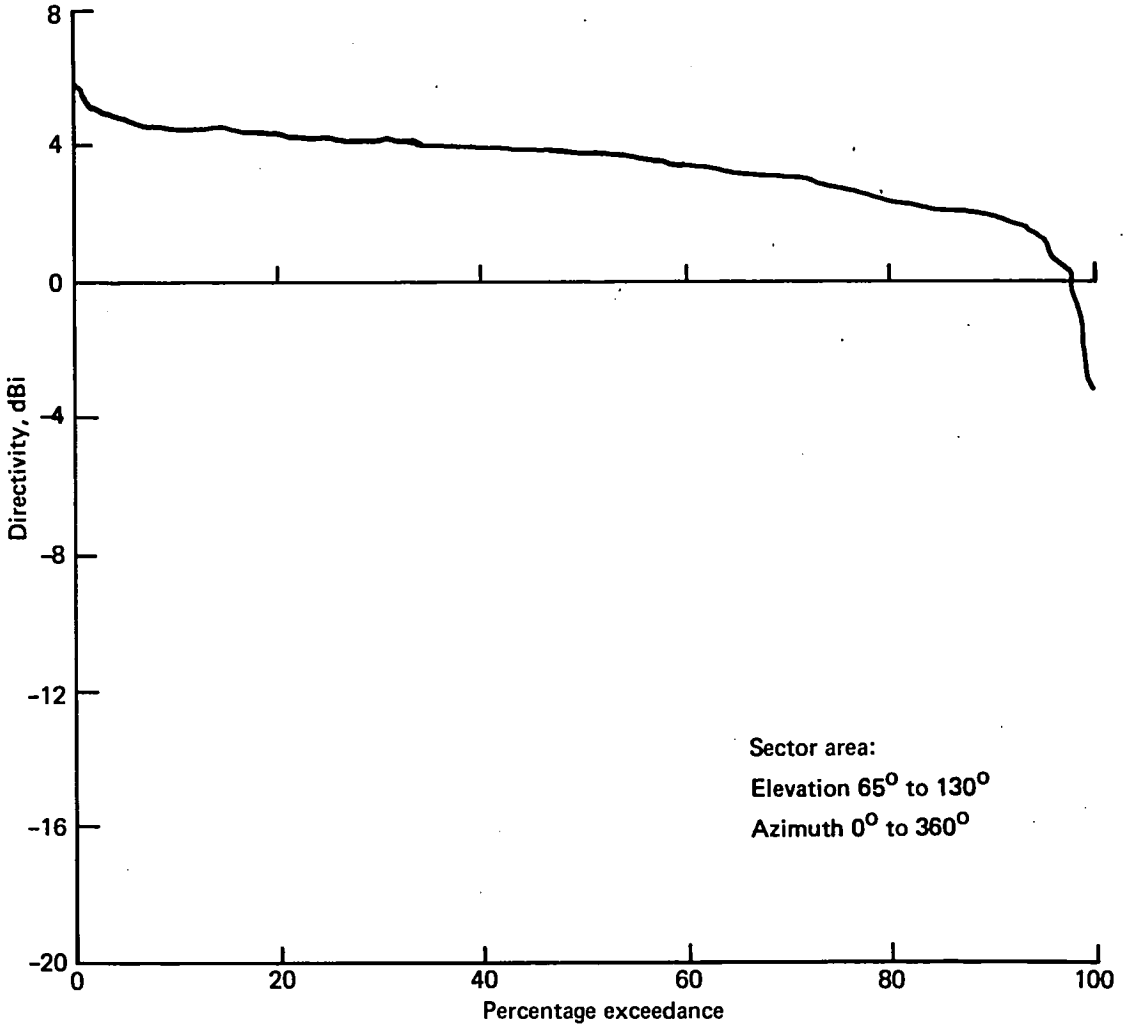

Figure 11. 727 Percentage Covered—Combined Radiation Pattern*

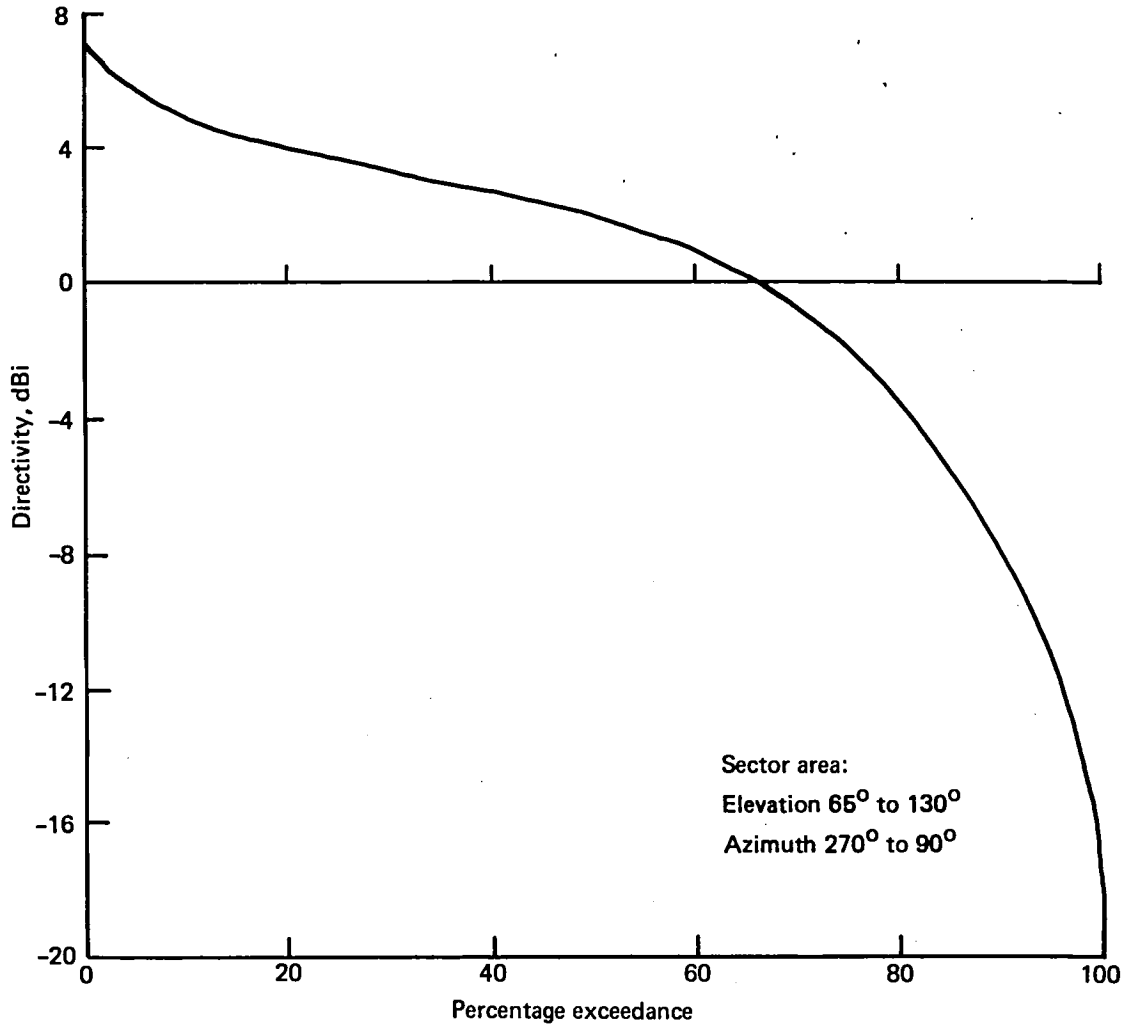

Figure 12. 737 Percentage Coverage—Top Antenna

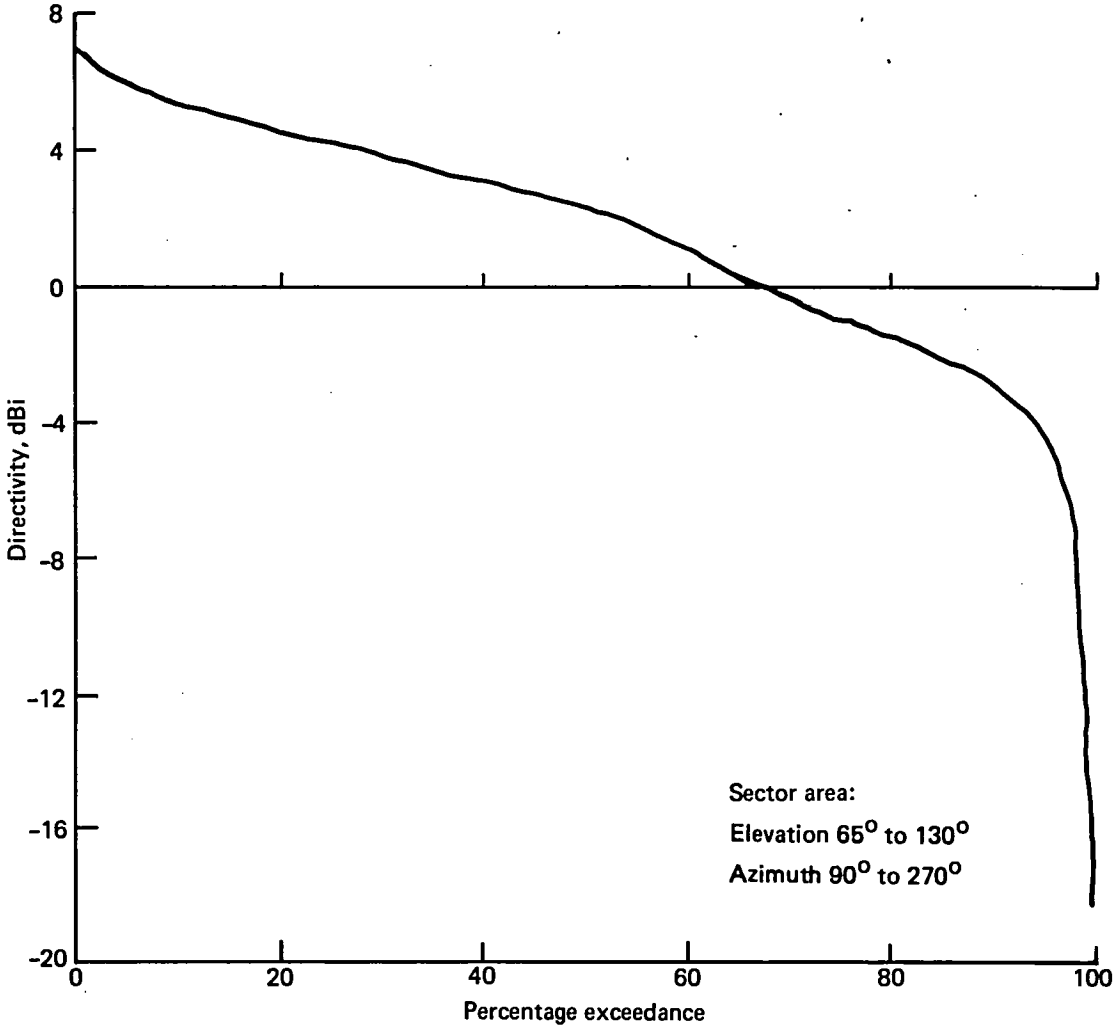

Figure 13. 737 Percentage Coverage—Bottom Antenna

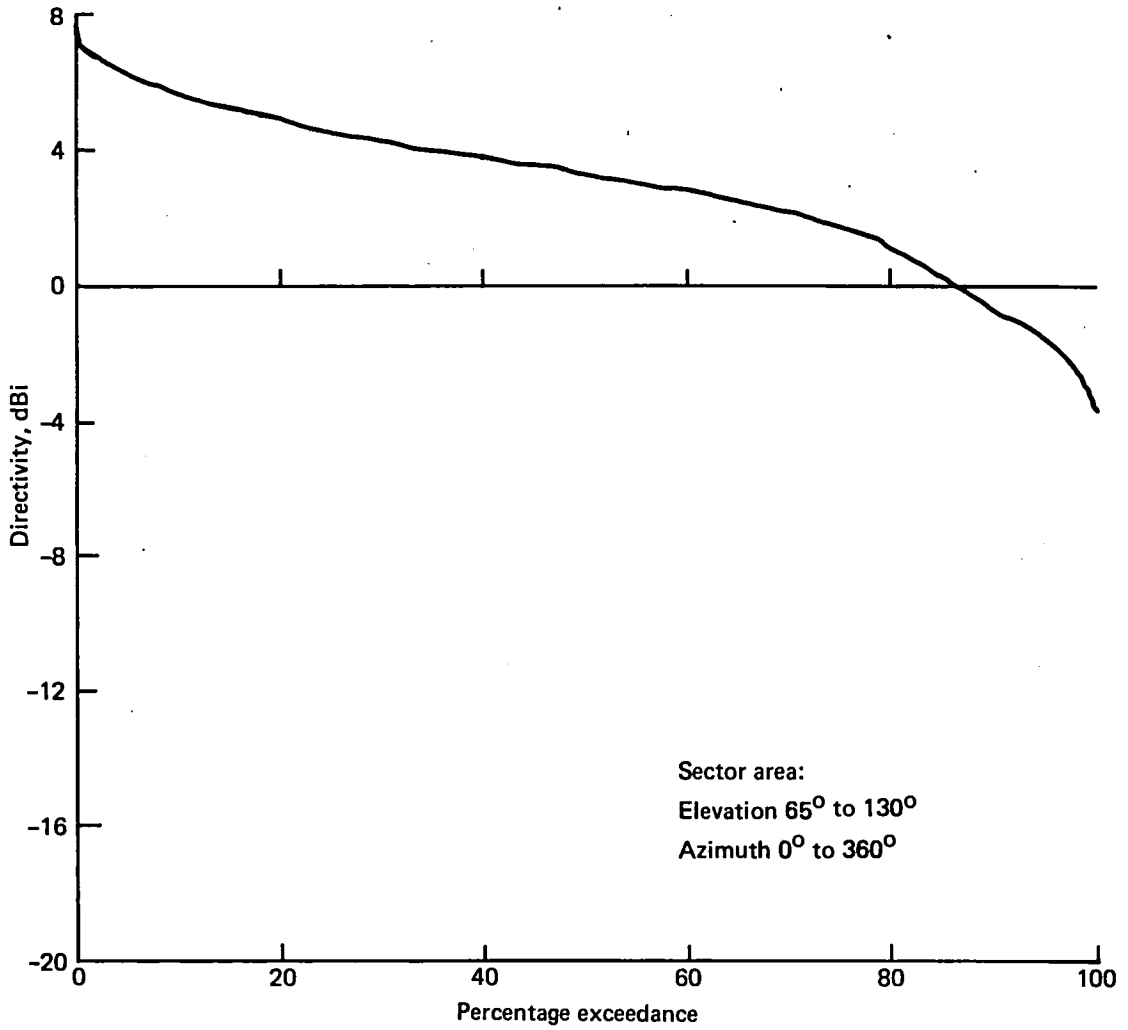

*Assuming identical element line losses, etc.

Figure 14. 737 Percentage Coverage—Combined Radiation Pattern*

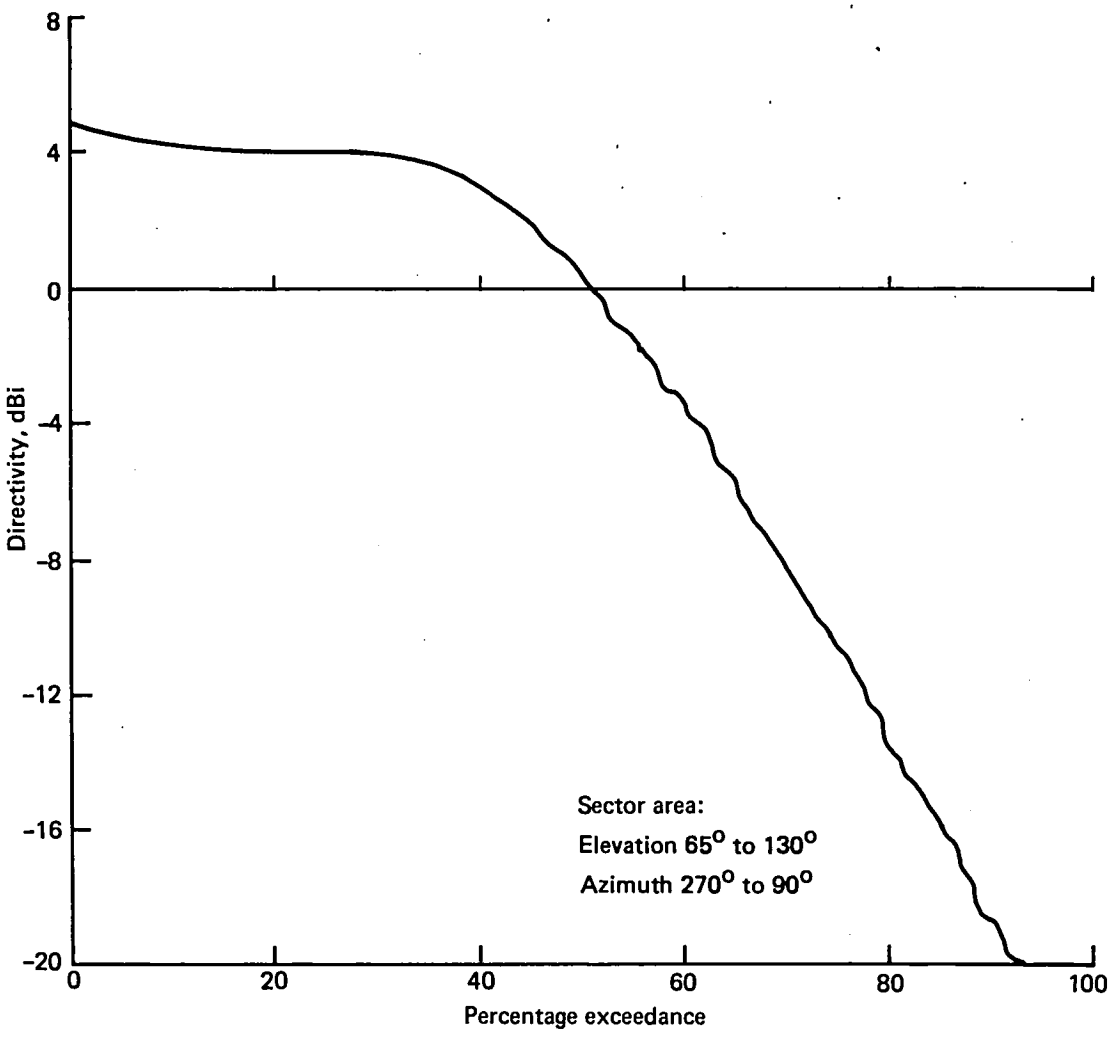

129044-23

Figure 15. 747 Percentage Coverage—Top Antenna

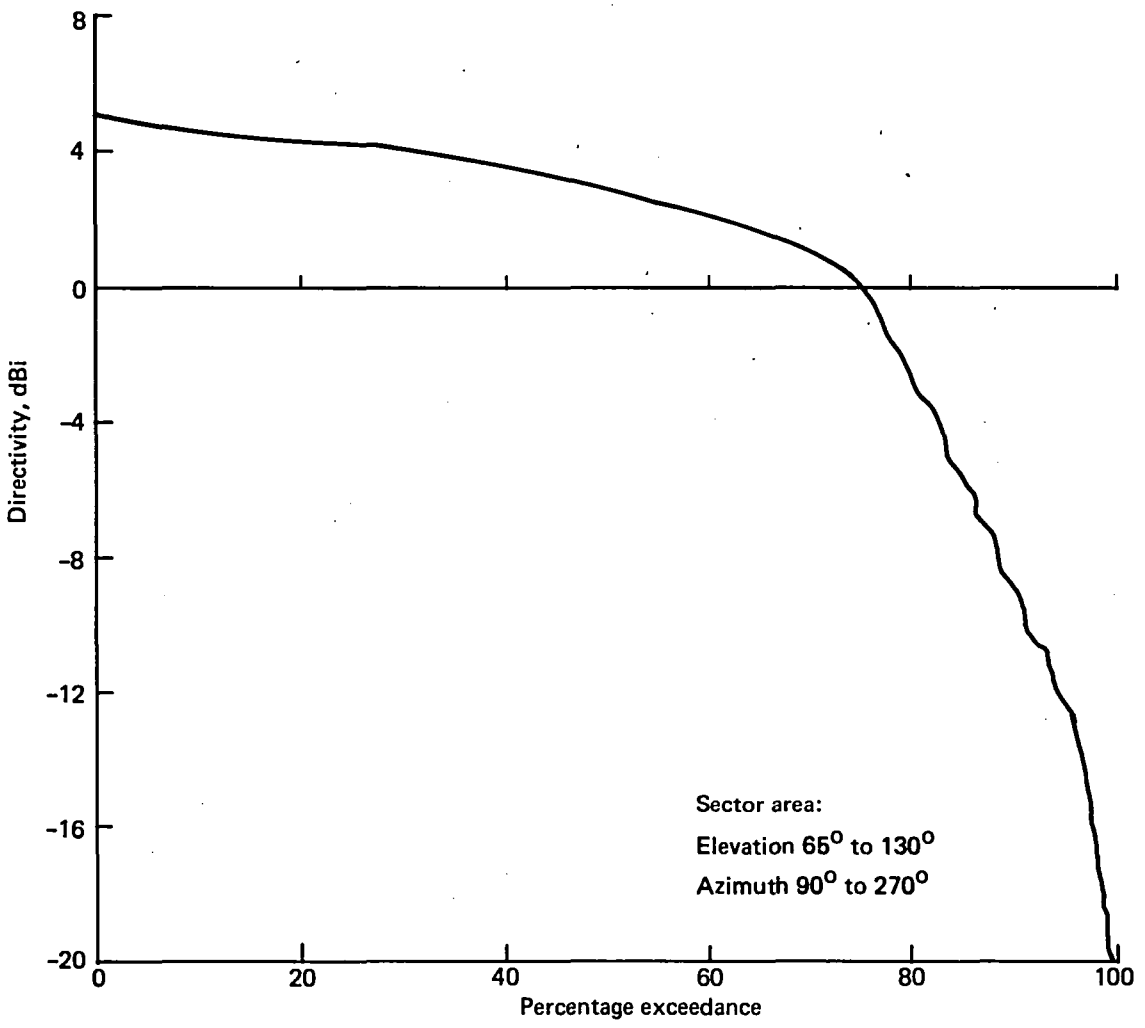

Figure 16. 747 Percentage Coverage—Bottom Antenna

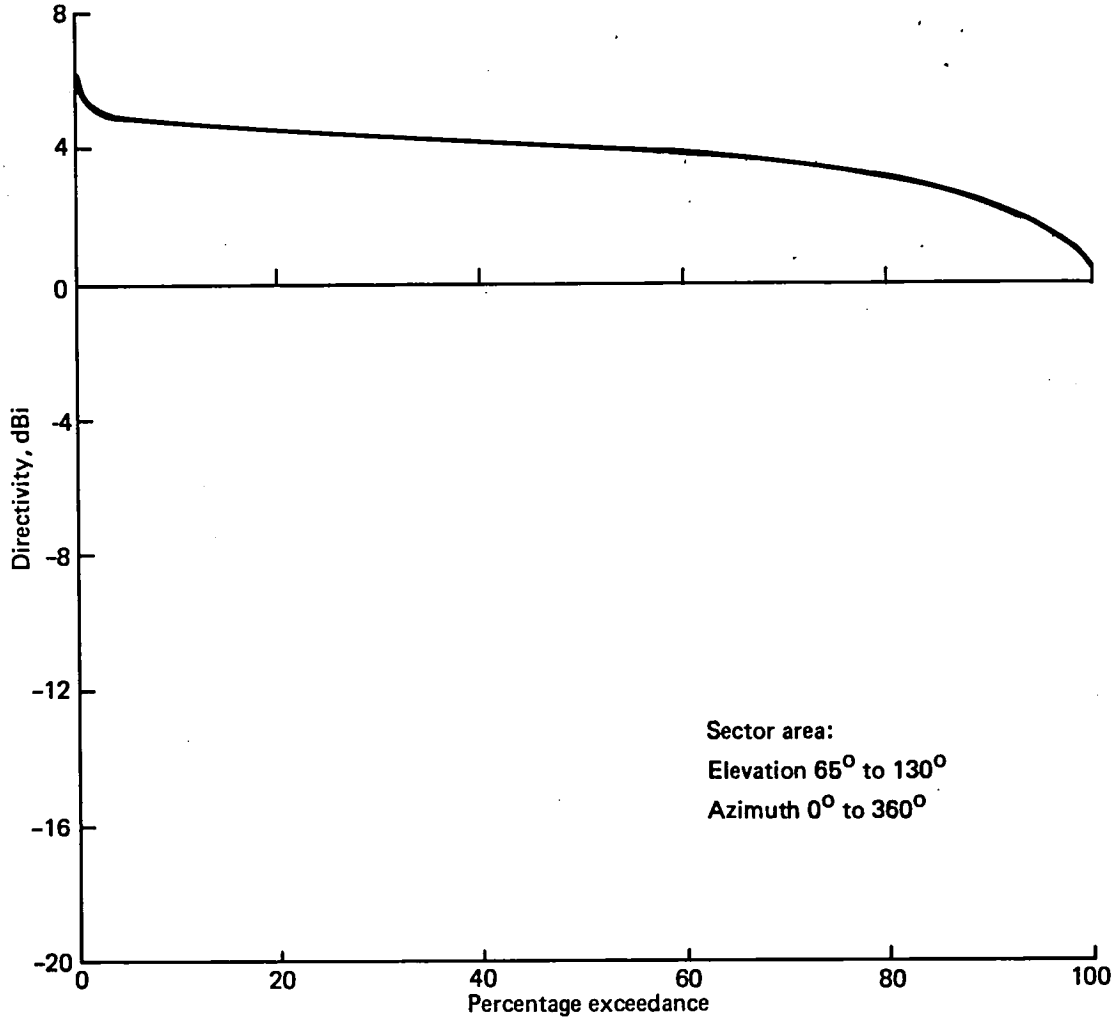

*Assuming identical element line losses, etc.

129044-25

Figure 17. 747 Percentage Coverage—Combined Radiation Pattern*

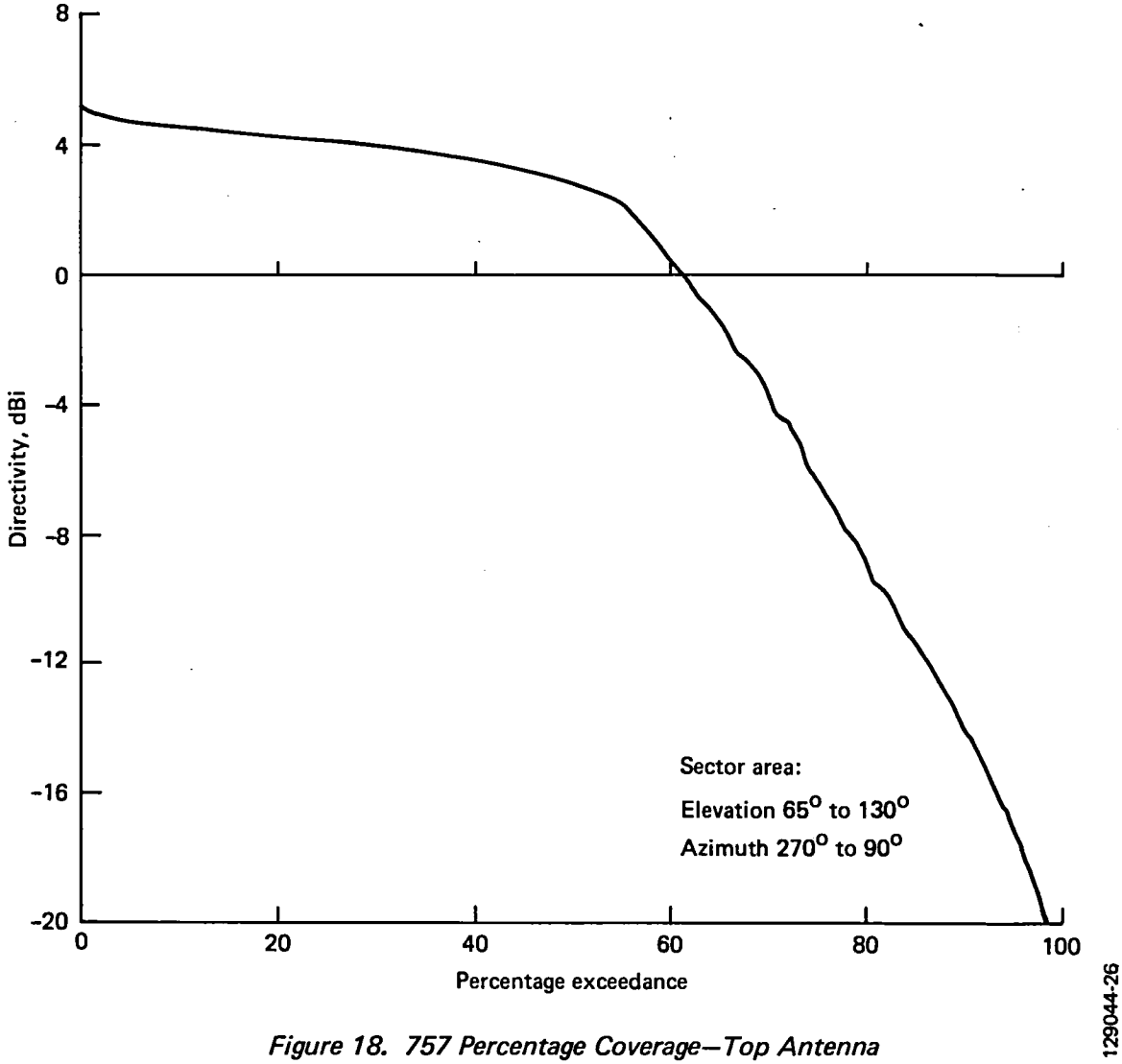

Figure 18. 757 Percentage Coverage—Top Antenna

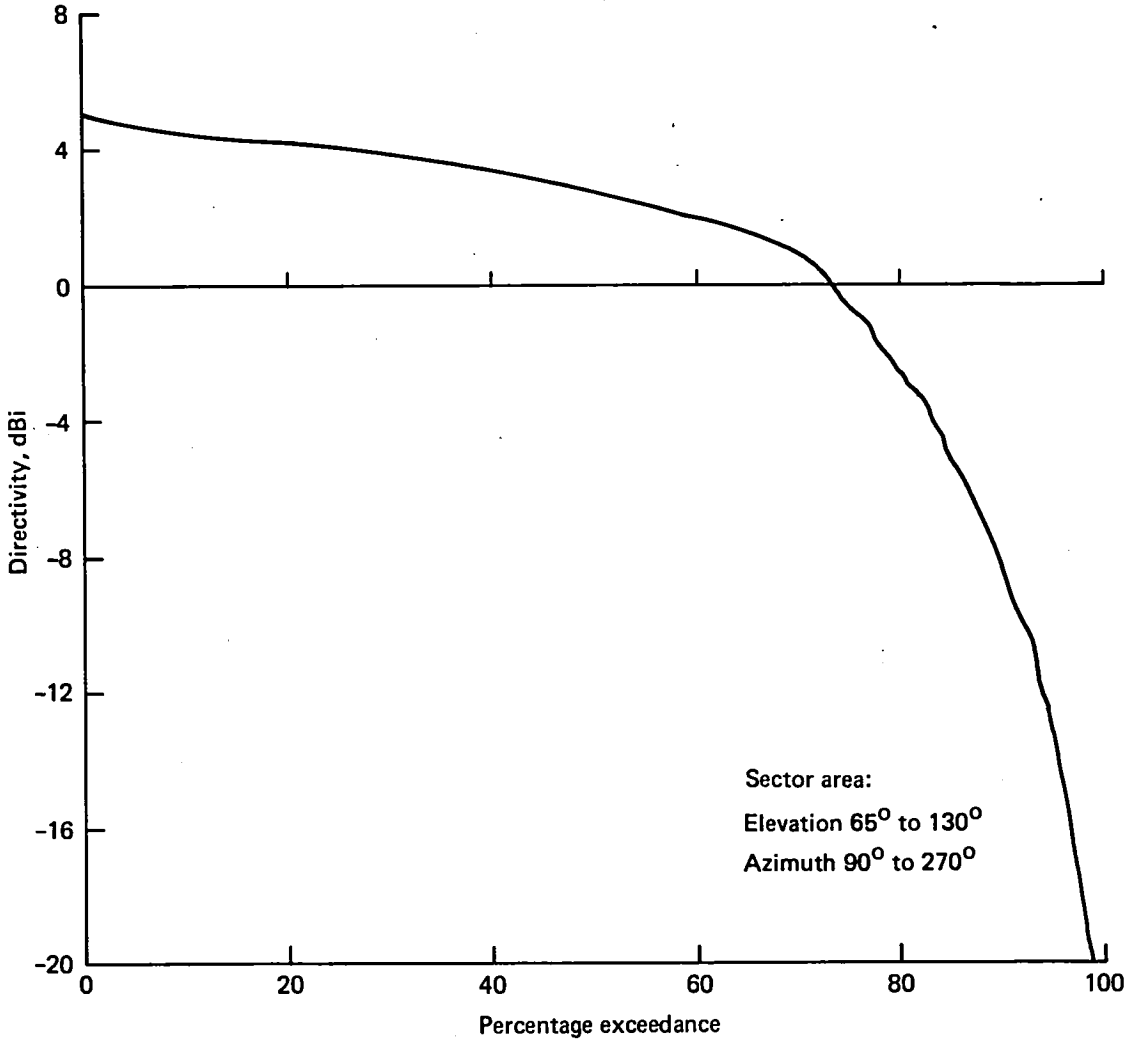

Figure 19. 757 Percentage Coverage—Bottom Antenna

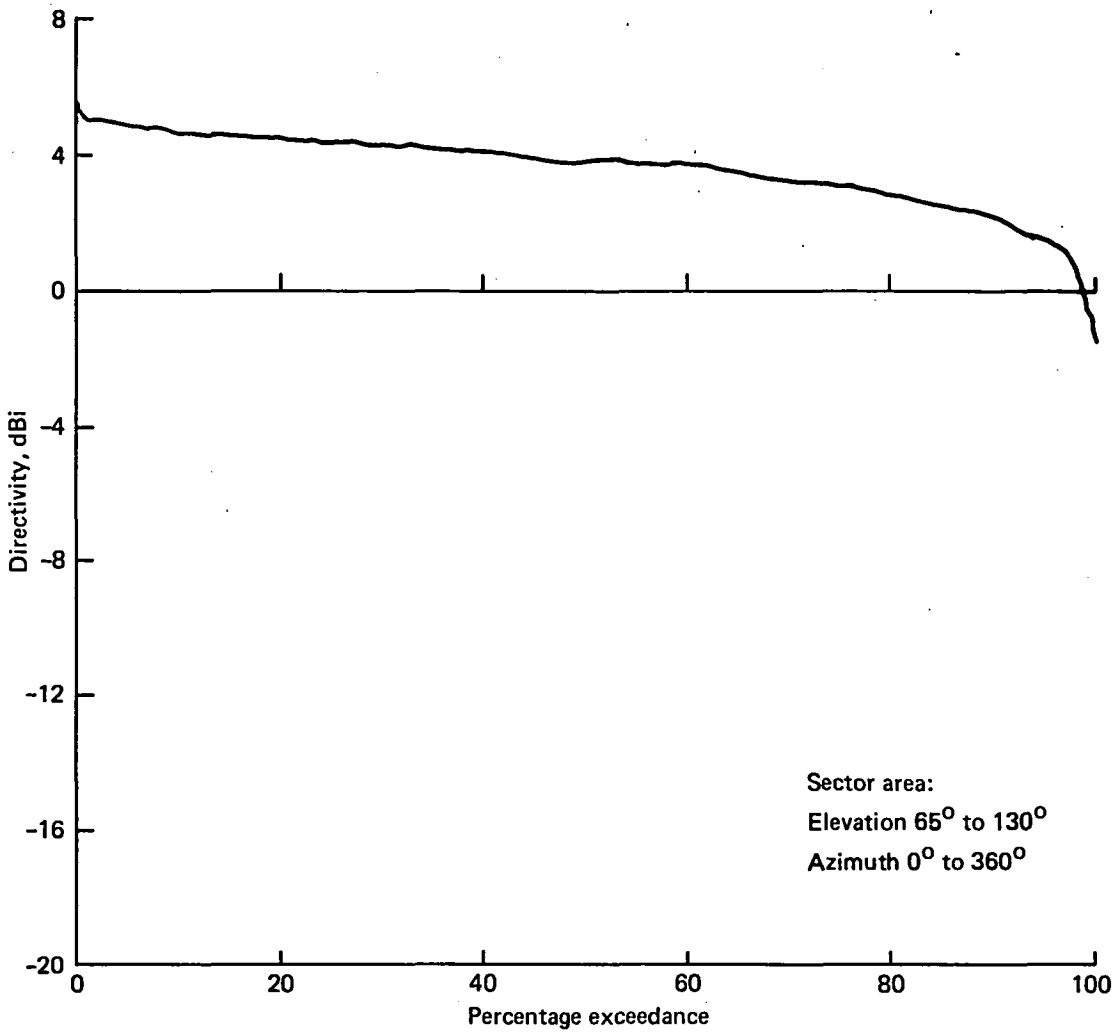

*Assuming identical element line losses, etc.

129044-28

Figure 20. 757 Percentage Coverage—Combined Radiation Pattern*

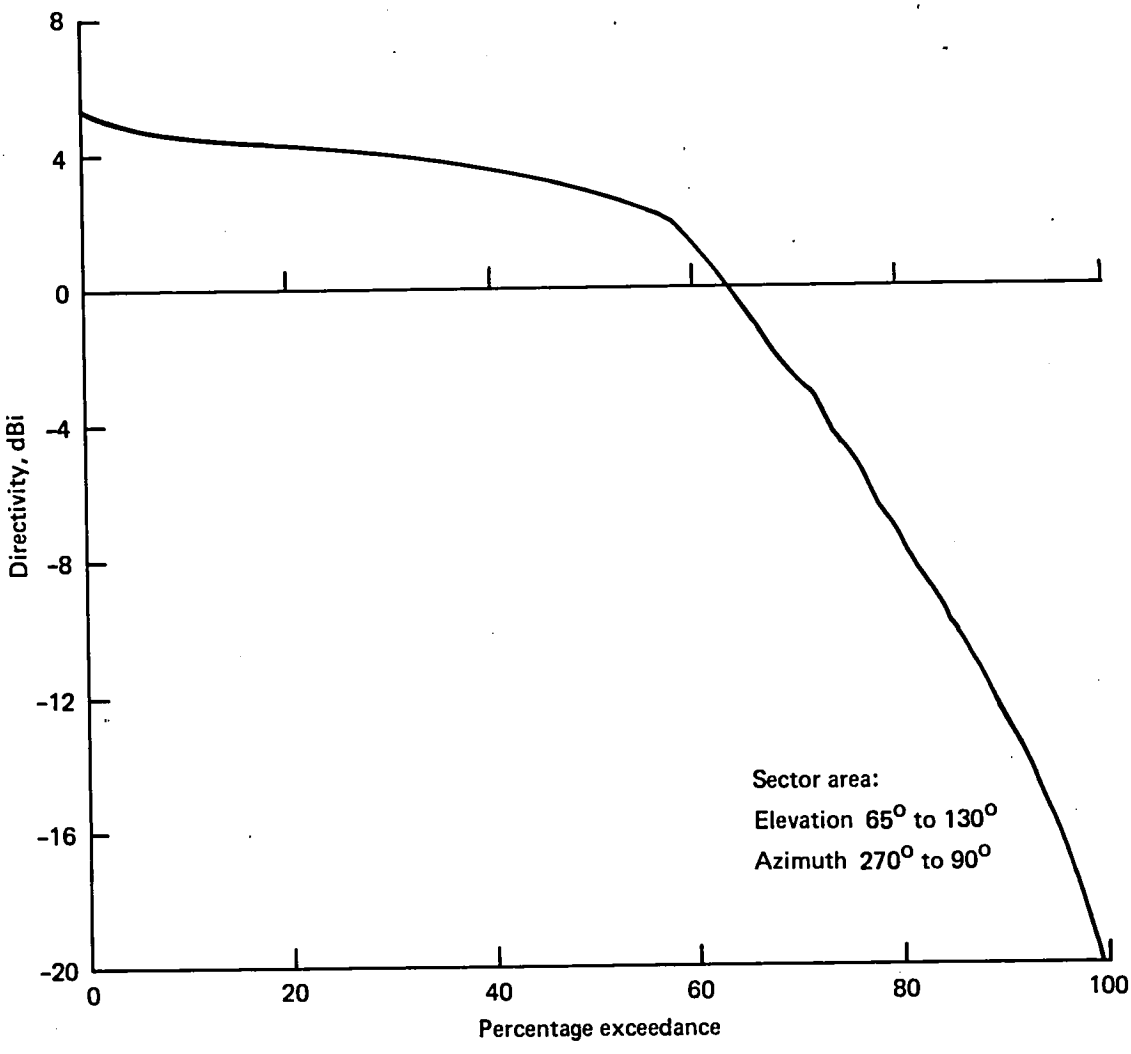

129044-29

Figure 21. 767 Percentage Coverage—Top Antenna

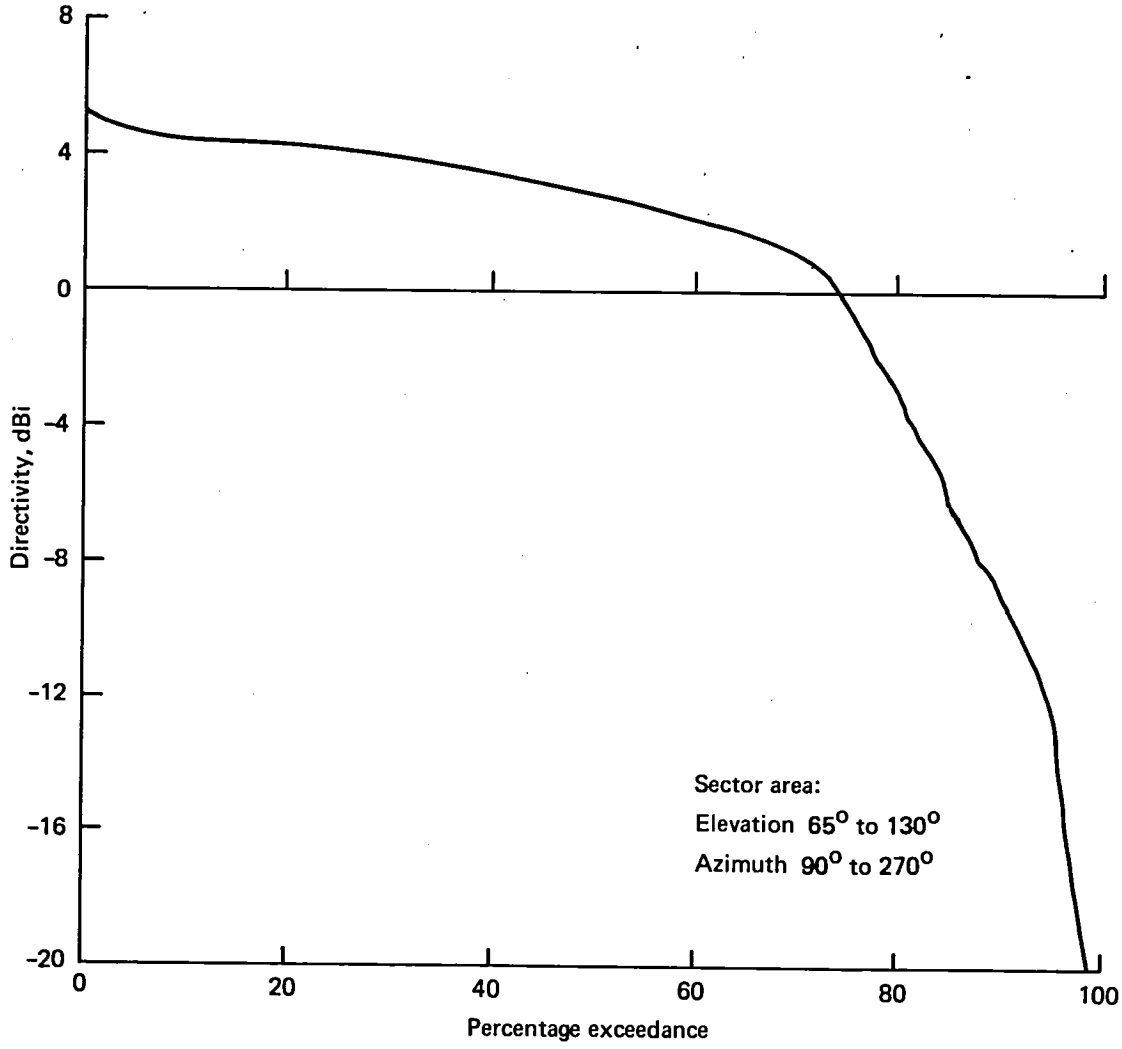

Figure 22. 767 Percentage Coverage—Bottom Antenna

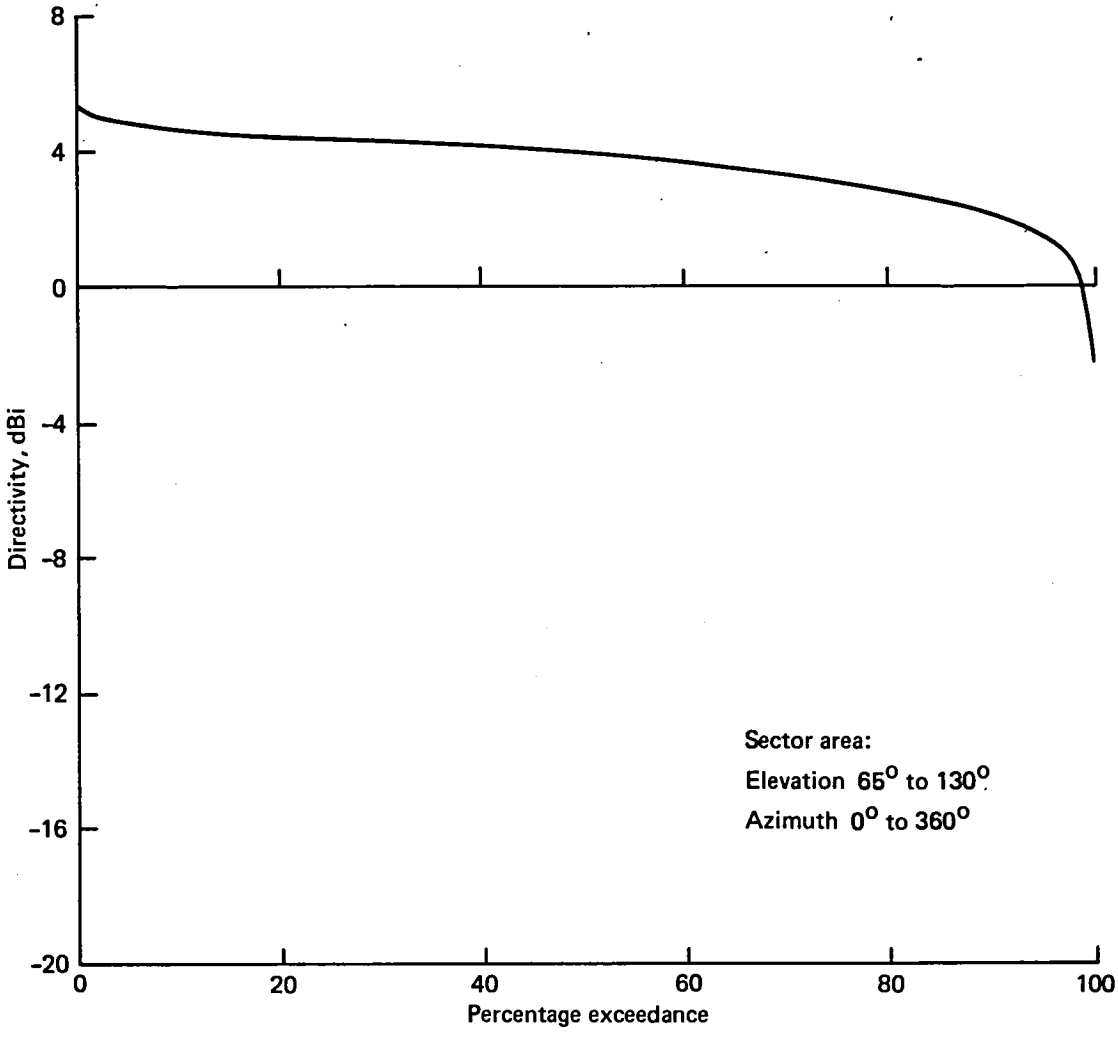

*Assuming identical element line losses, etc.

Figure 23. 767 Percentage Coverage—Combined Radiation Pattern*

129044-31

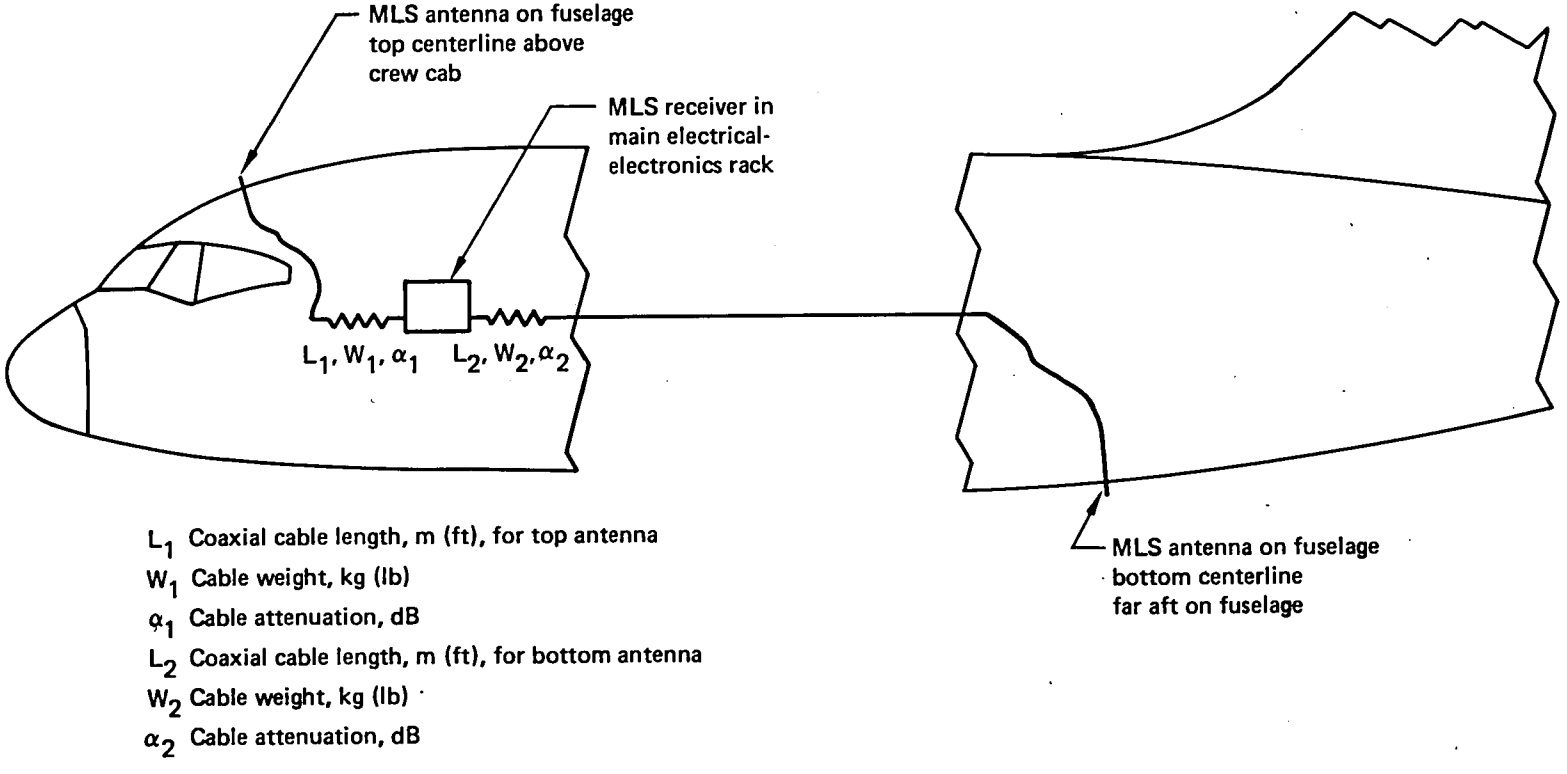

Figure 24. Generic MLS Installation

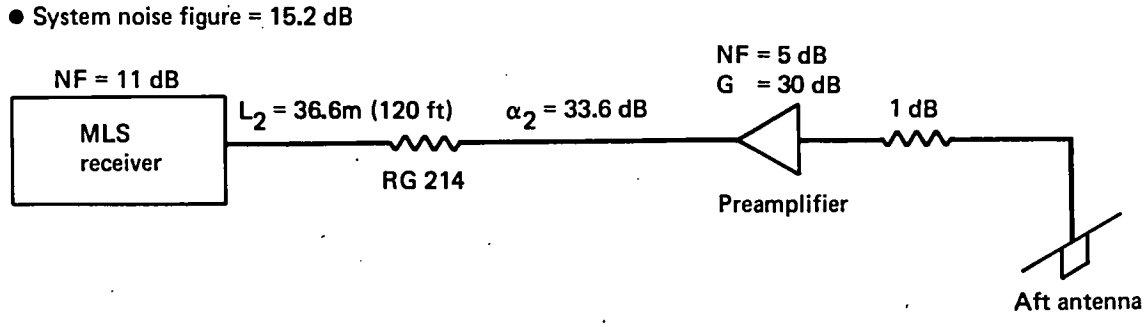

129044-33

Figure 25. System Configuration—767 Aft Antenna

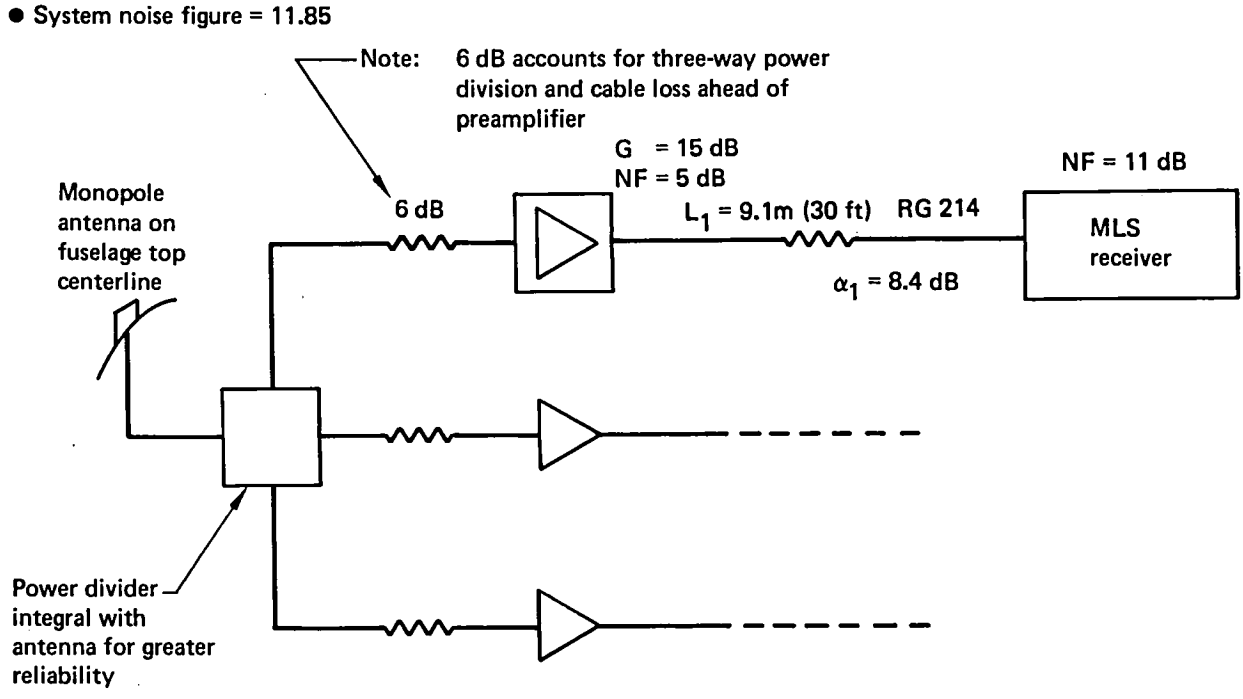

129044-34

Figure 26. Triple-Redundant MLS Installation—767 Aircraft

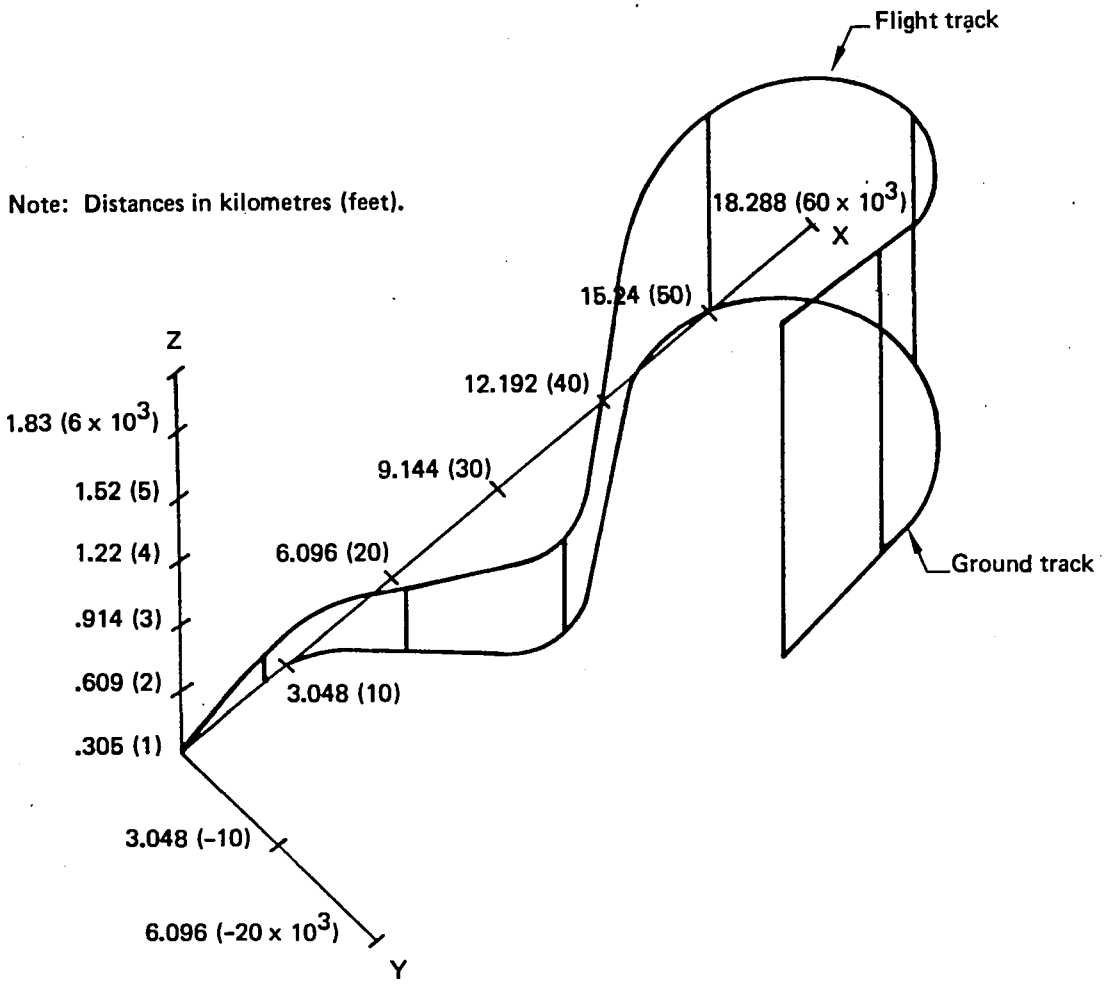

Figure 27. STAR DORA5 Flight Track

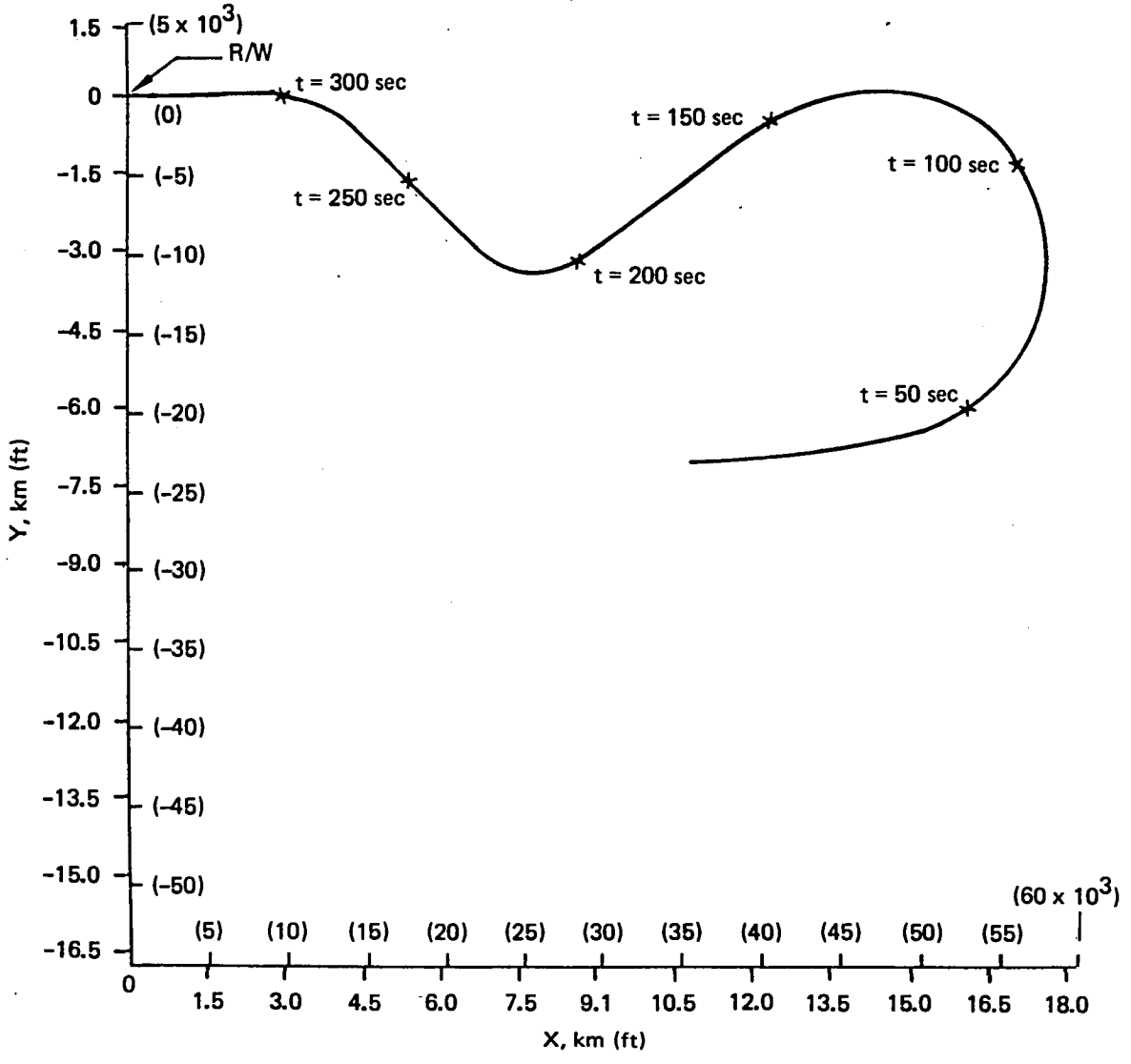

Figure 28. STAR DORA5 Track Profile

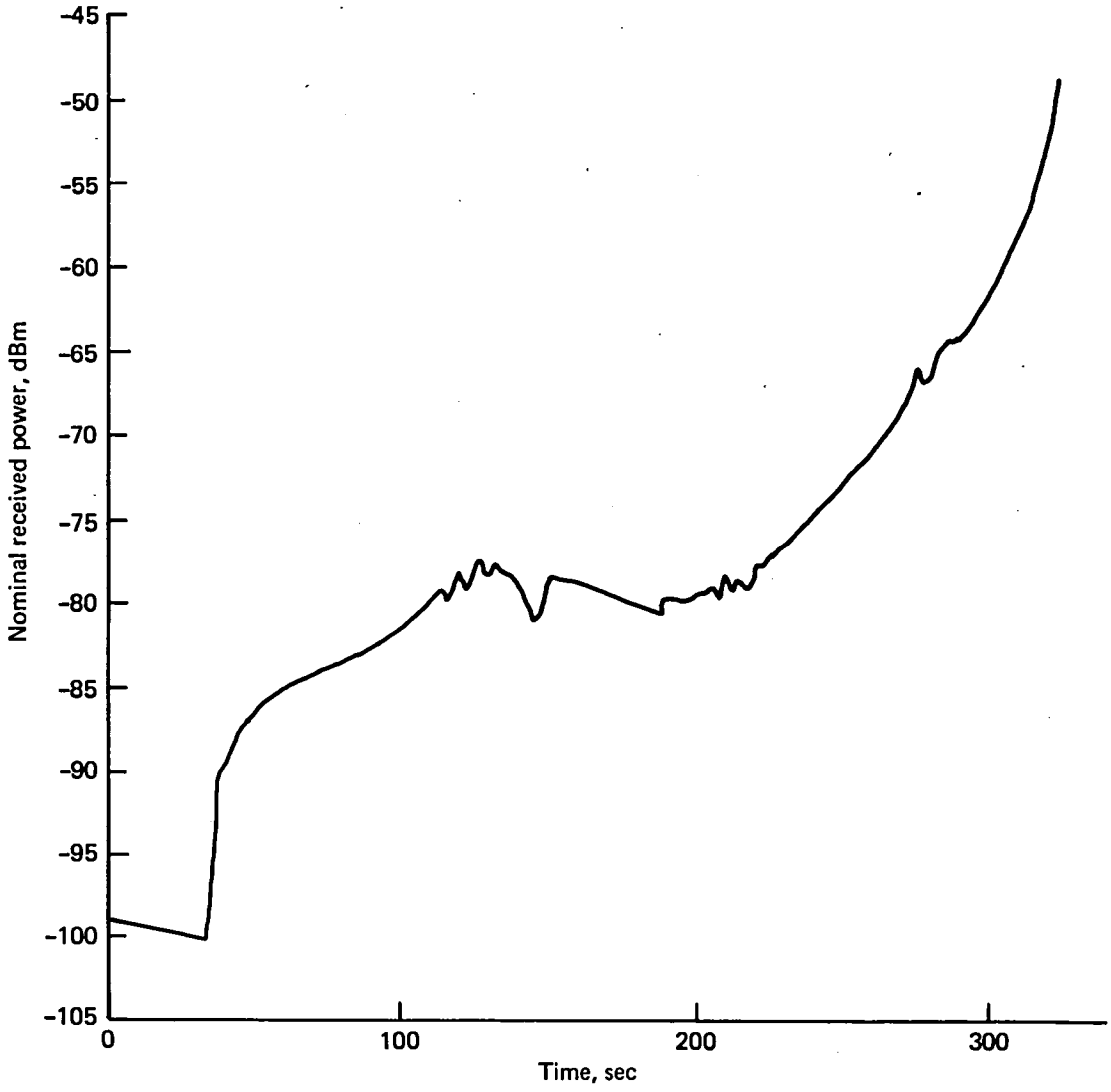

Figure 29. Antenna System Performance—707 Single Antenna System

129044-37

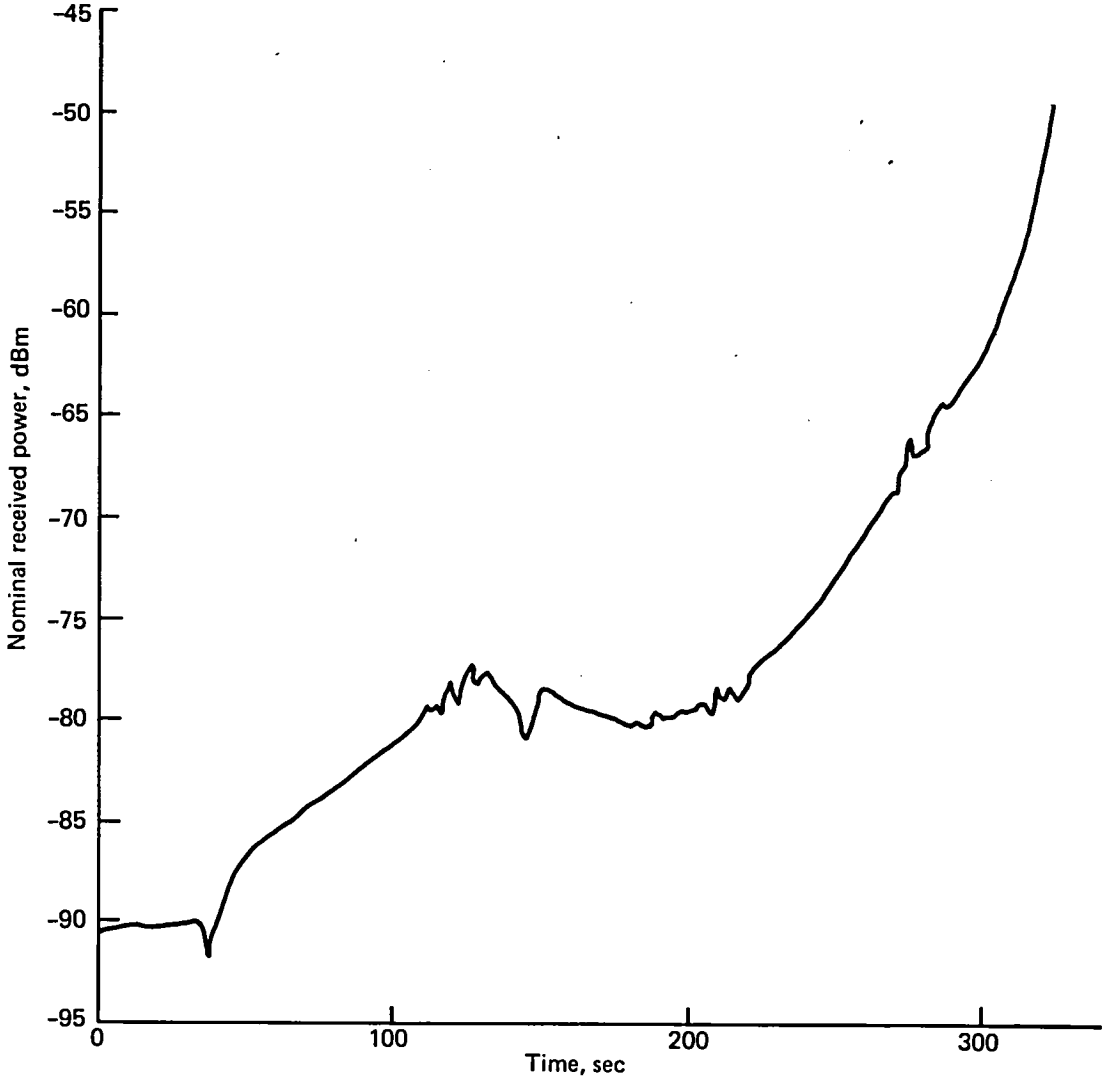

129044-38

Figure 30. Antenna System Performance—707 Dual Antenna System

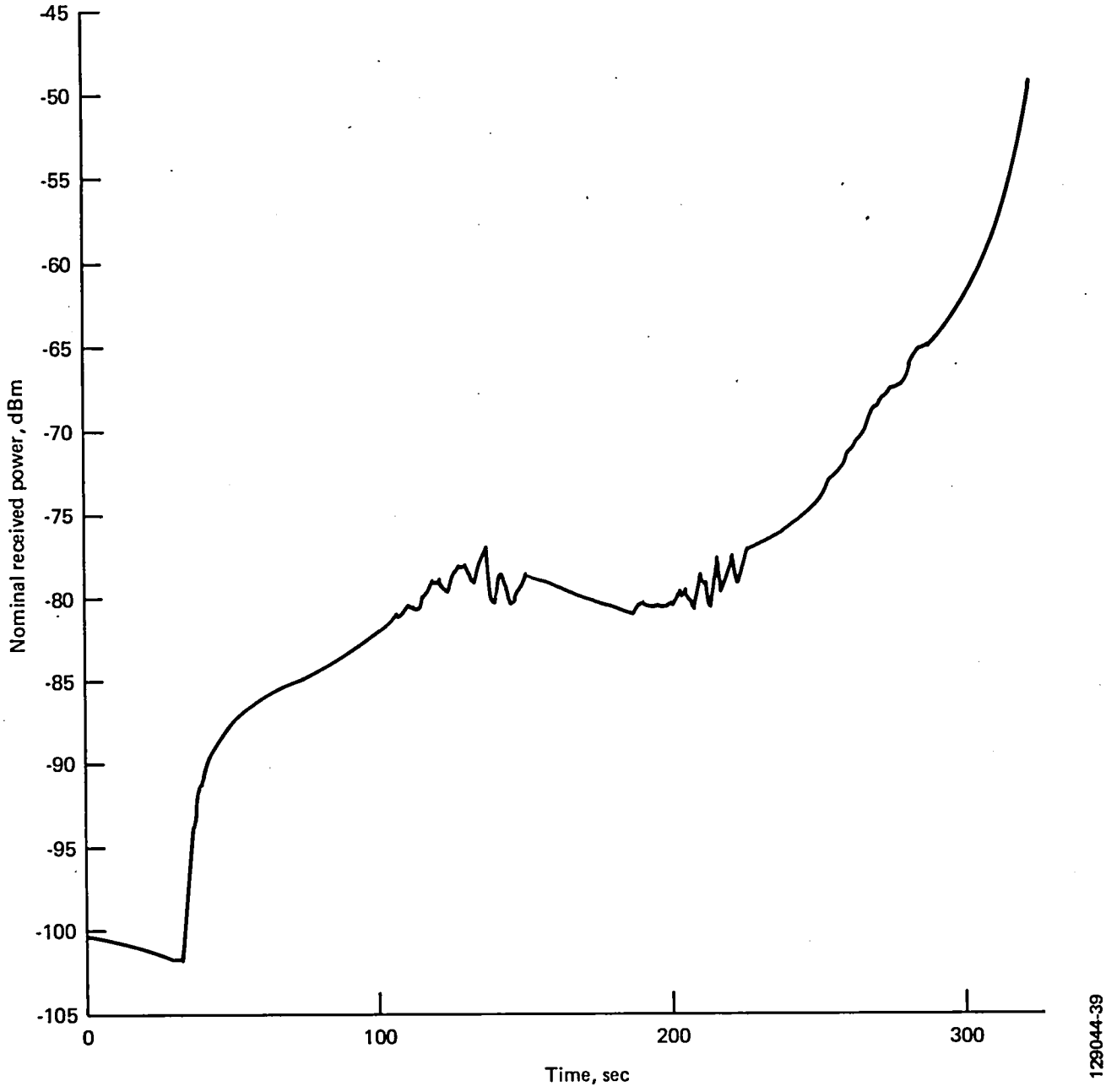

Figure 31. Antenna System Performance—727 Single Antenna System

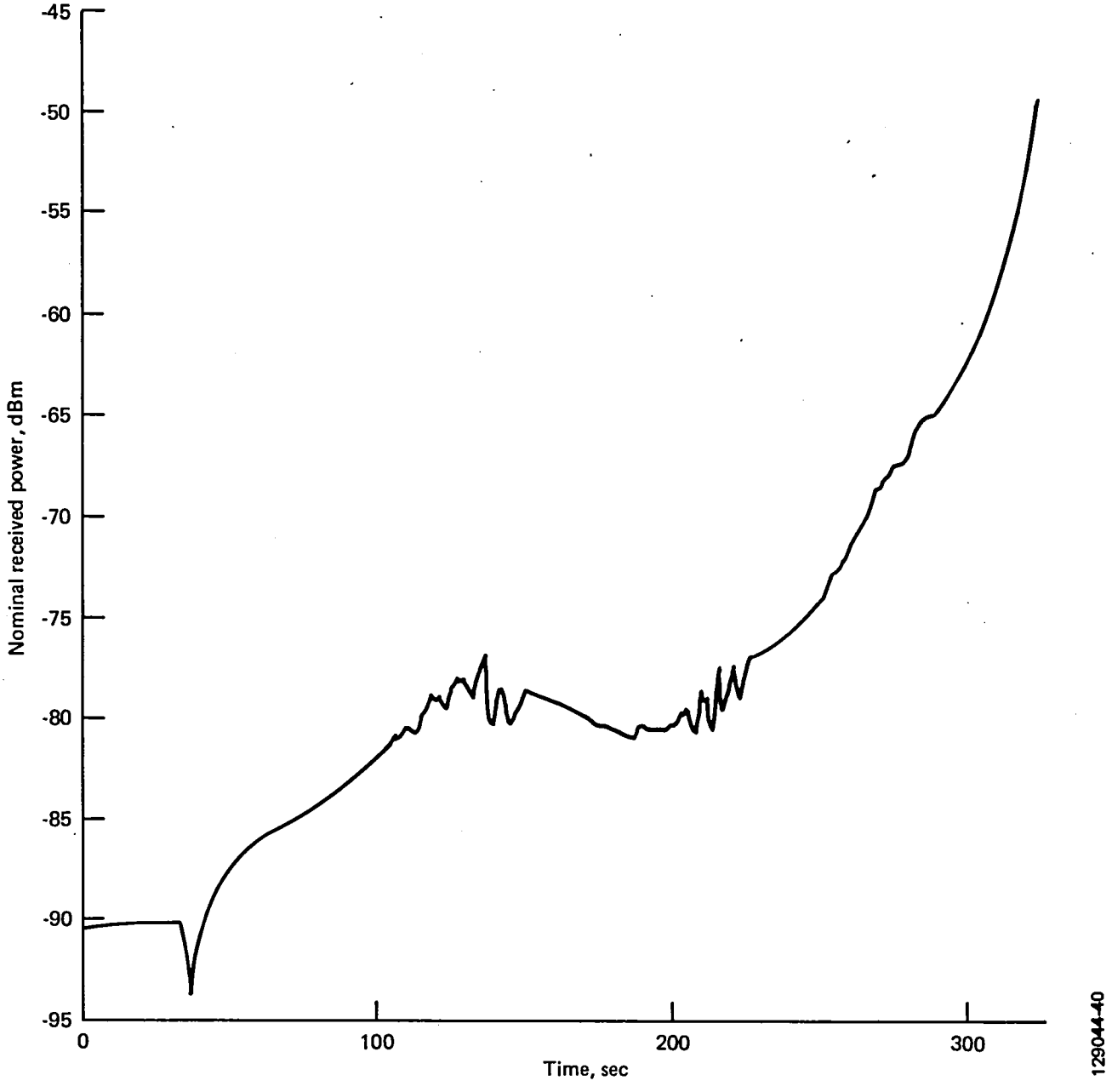

Figure 32. Antenna System Performance—727 Dual Antenna System

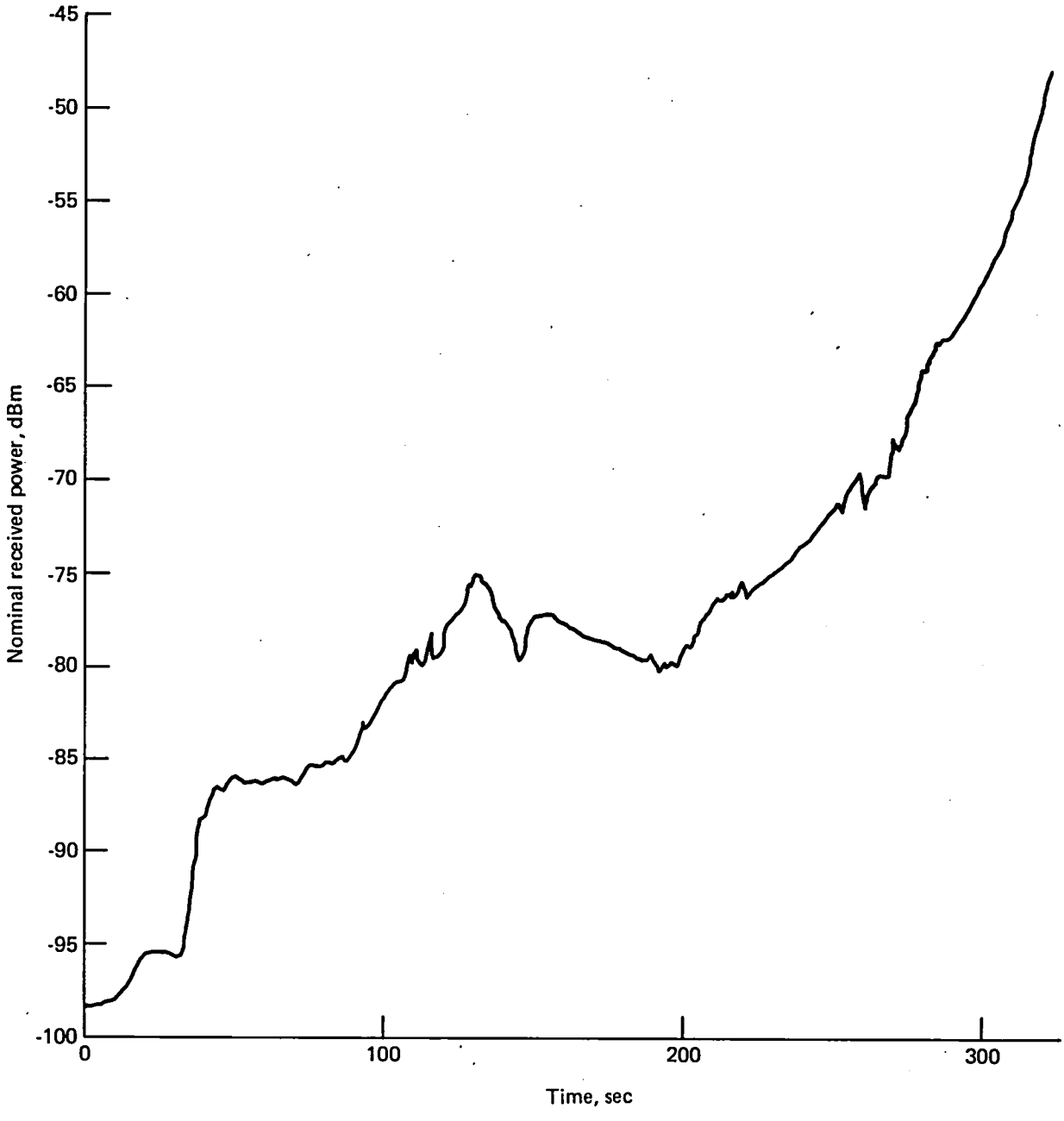

Figure 33. Antenna System Performance—737 Single Antenna System

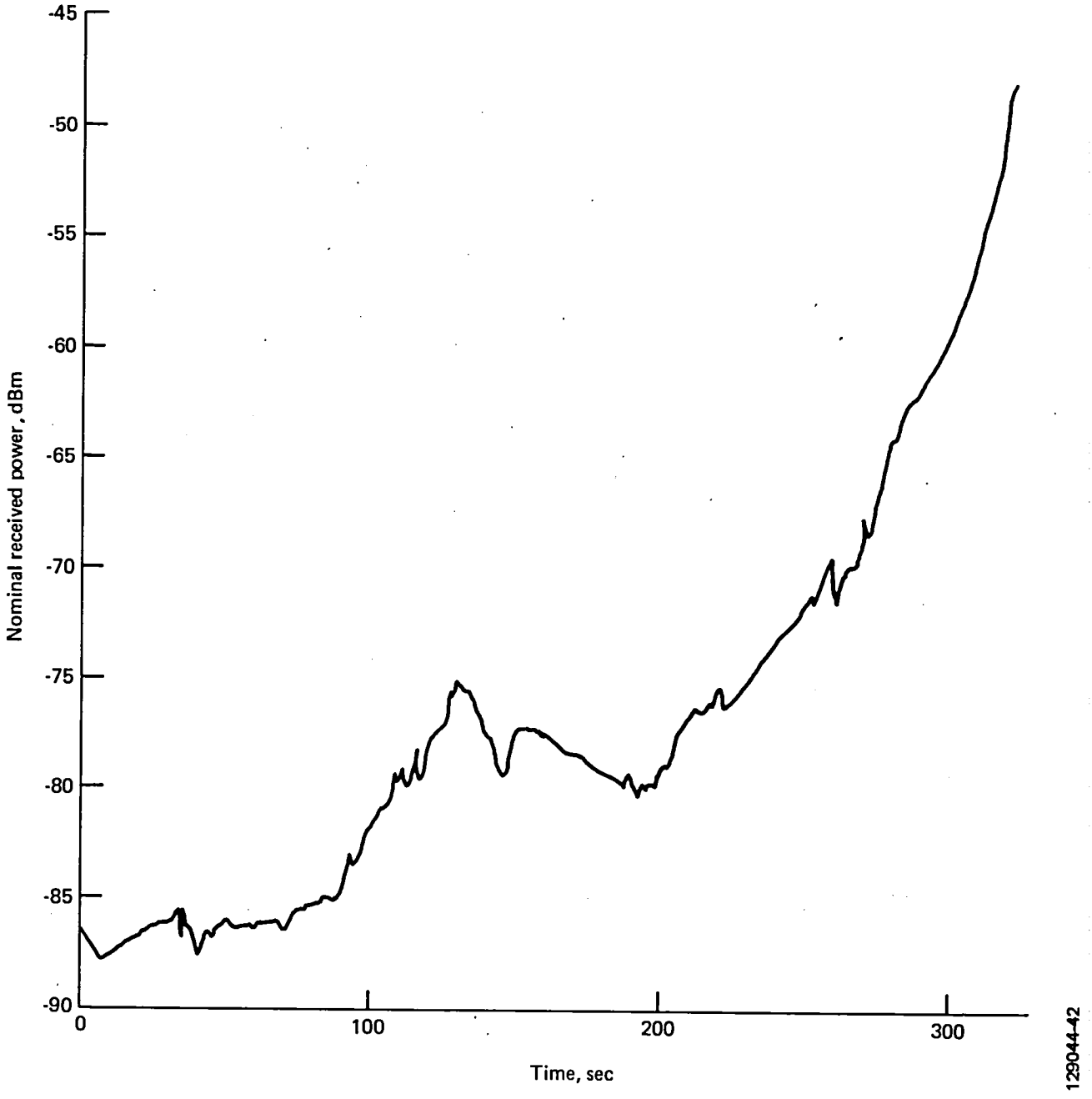

Figure 34. Antenna System Performance—737 Dual Antenna System

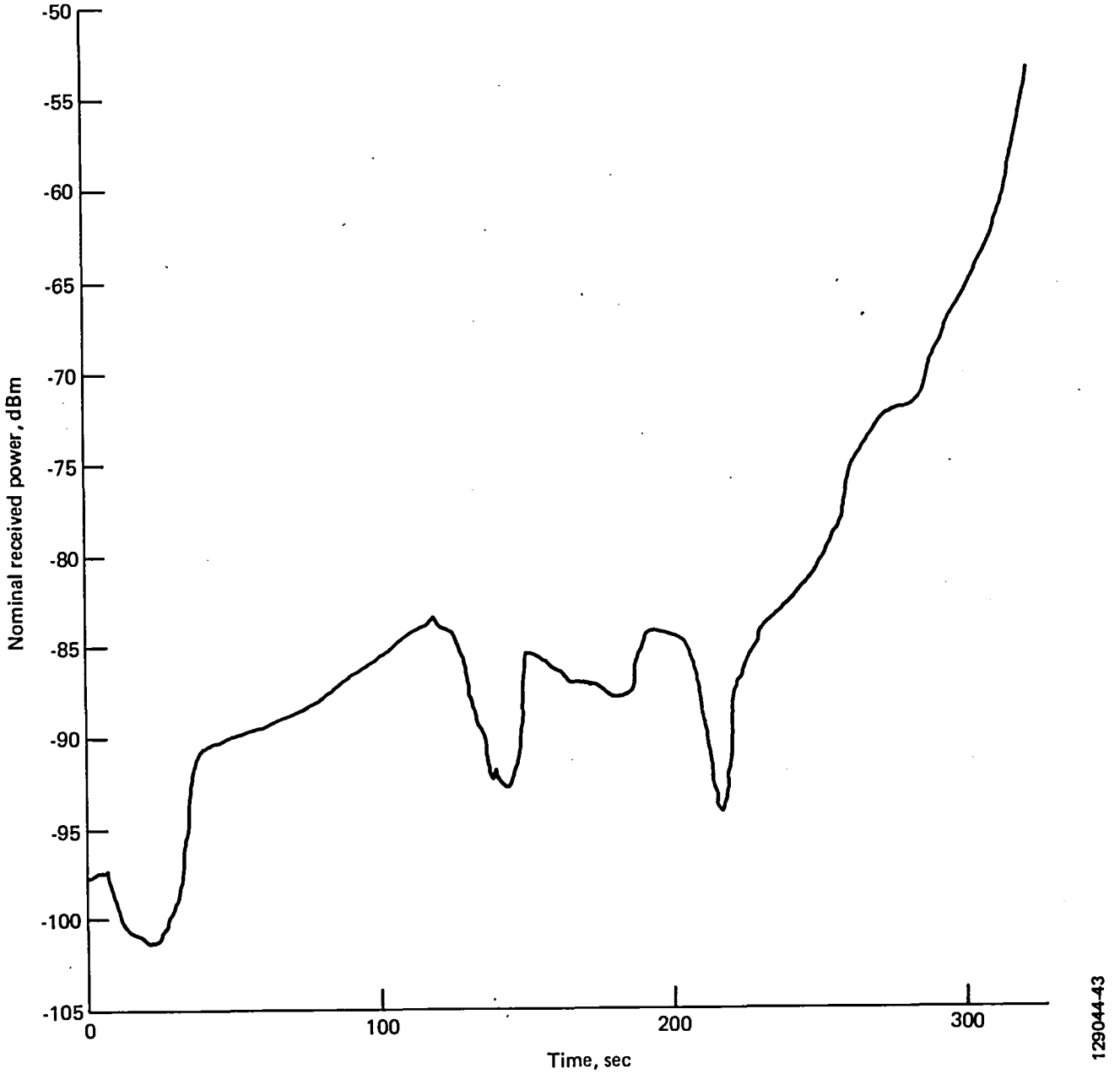

Figure 35. Antenna System Performance—747 Single Antenna System

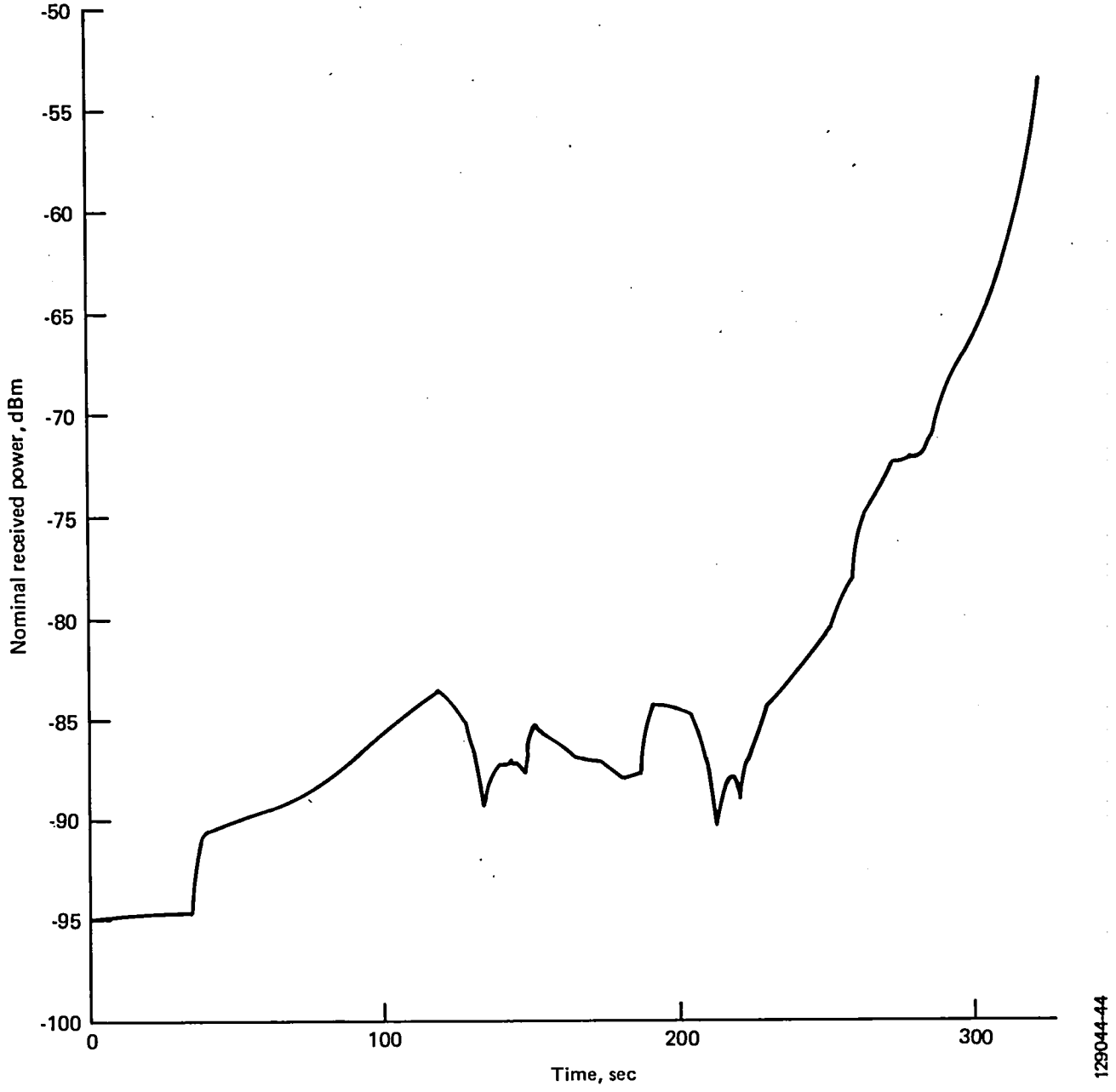

Figure 36. Antenna System Performance—747 Dual Antenna System

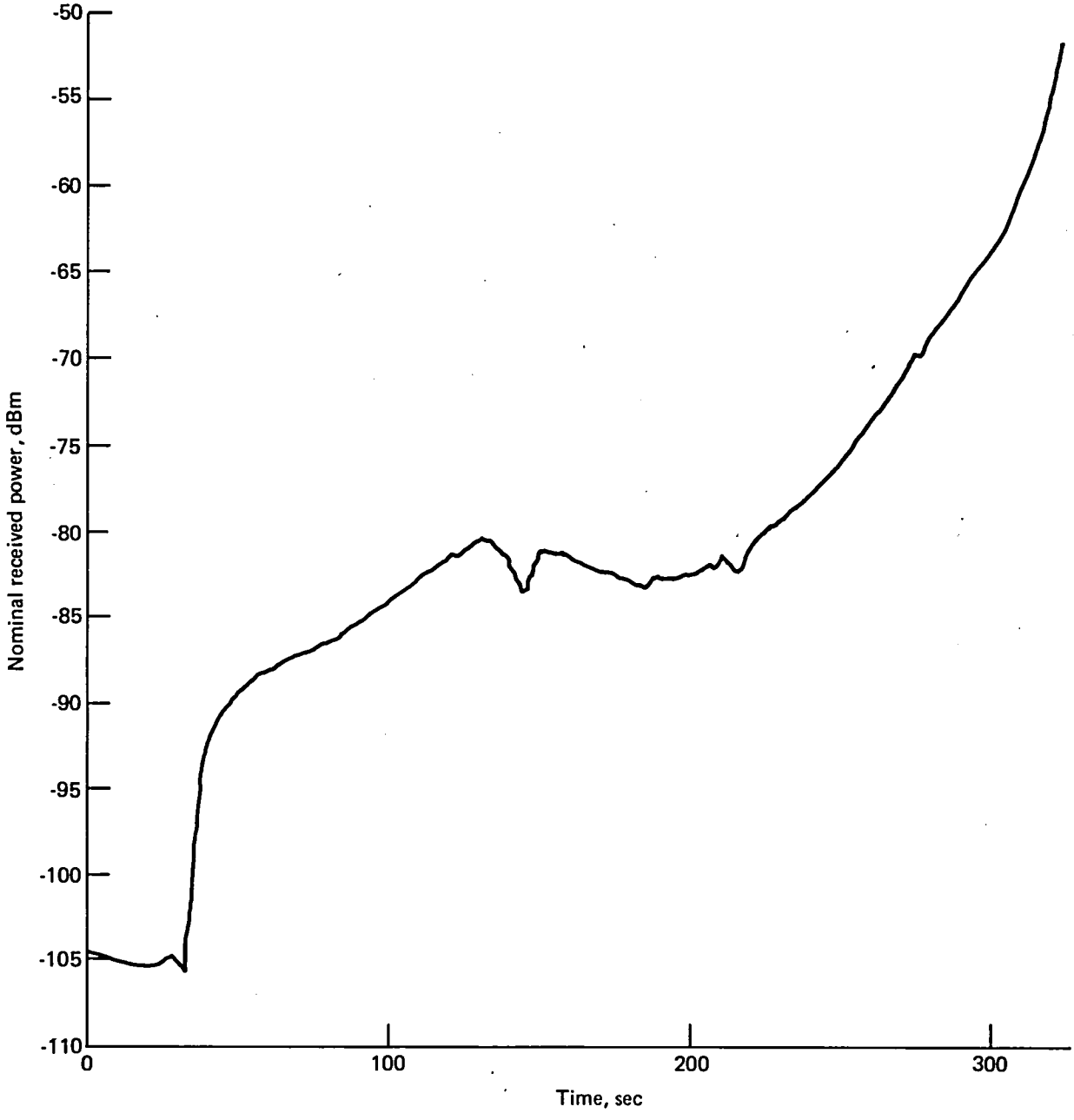

Figure 37. Antenna System Performance—757 Single Antenna System

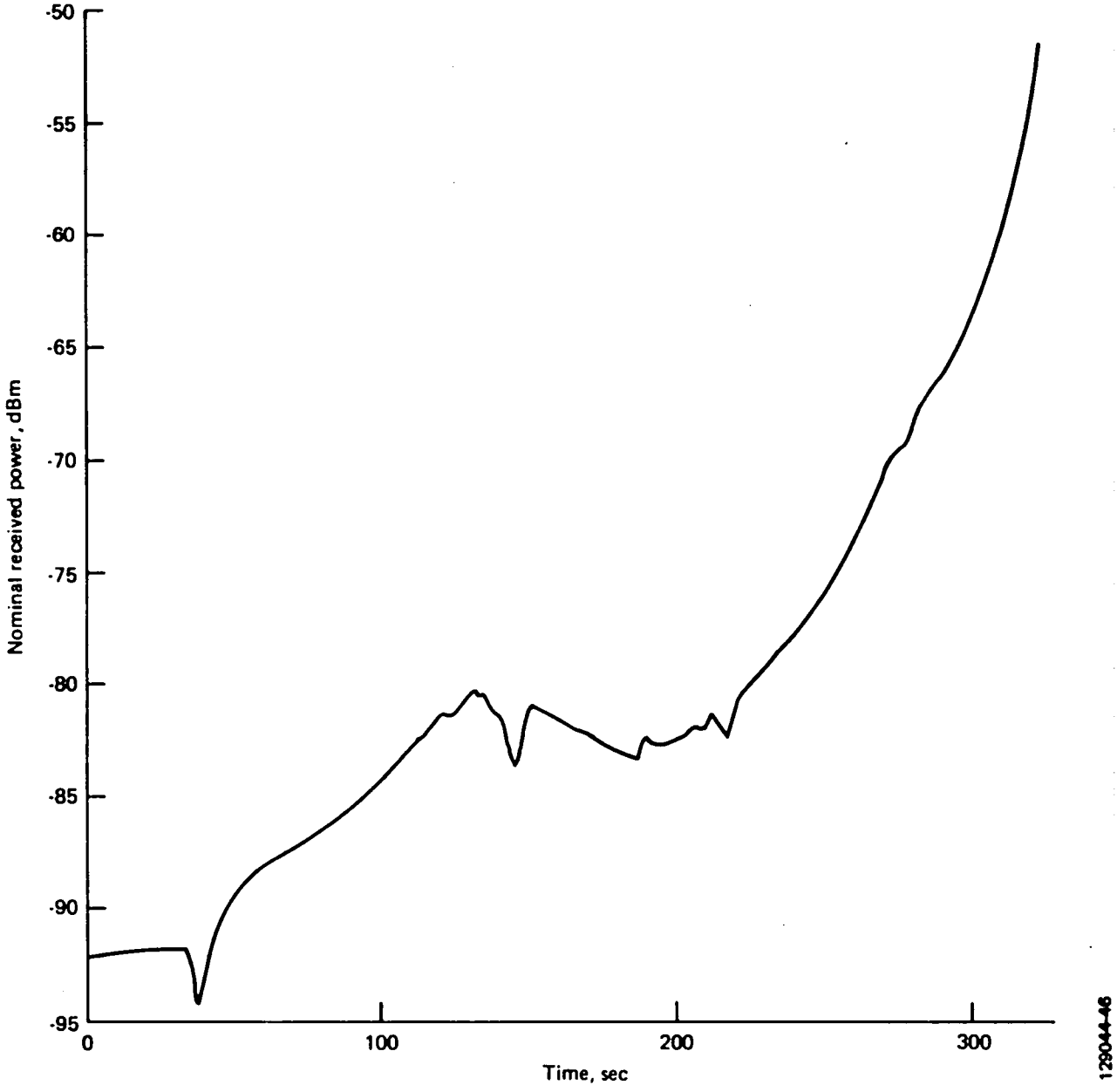

Figure 38. Antenna System Performance—757 Dual Antenna System

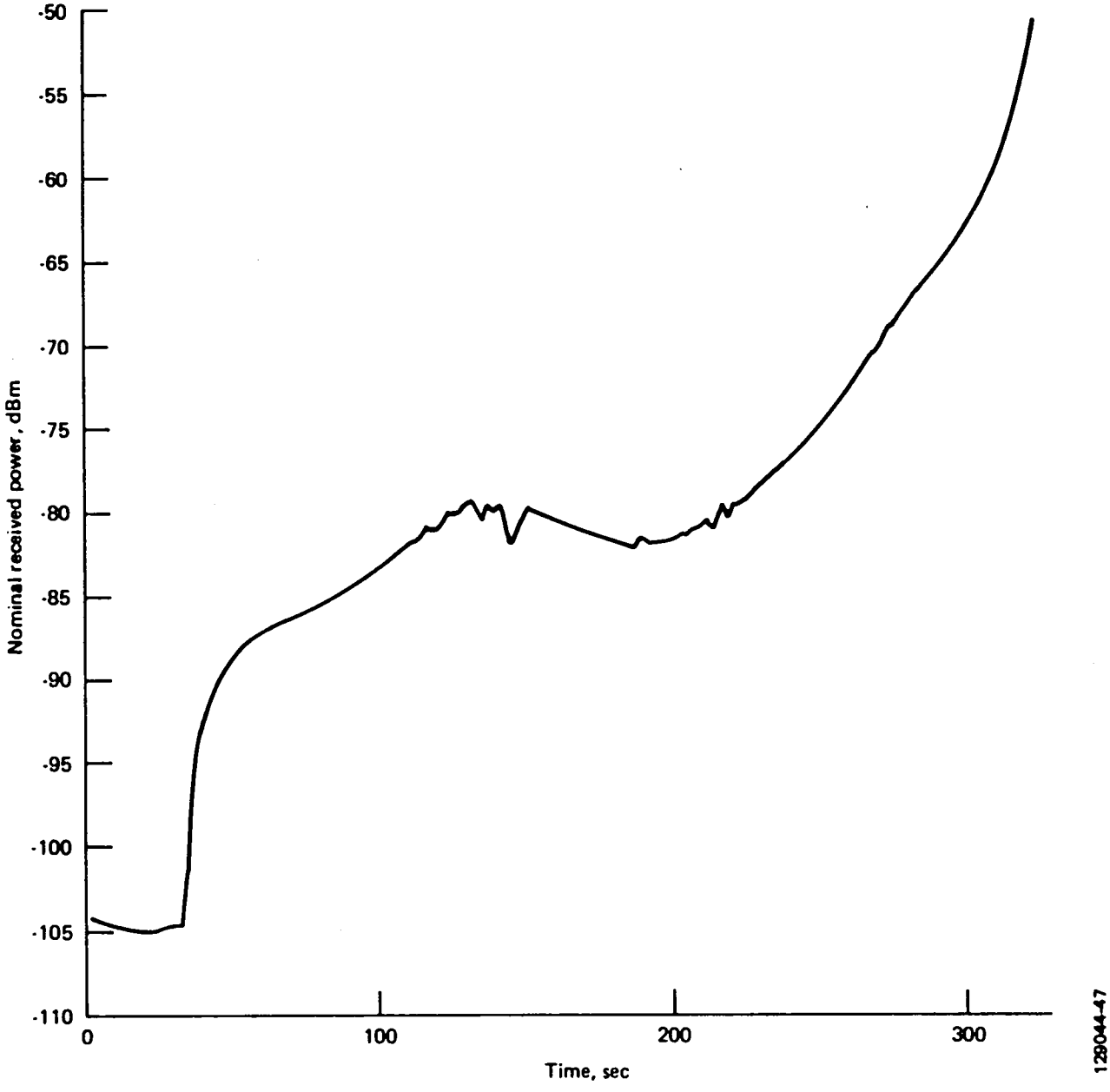

Figure 39. Antenna System Performance—767 Single Antenna System

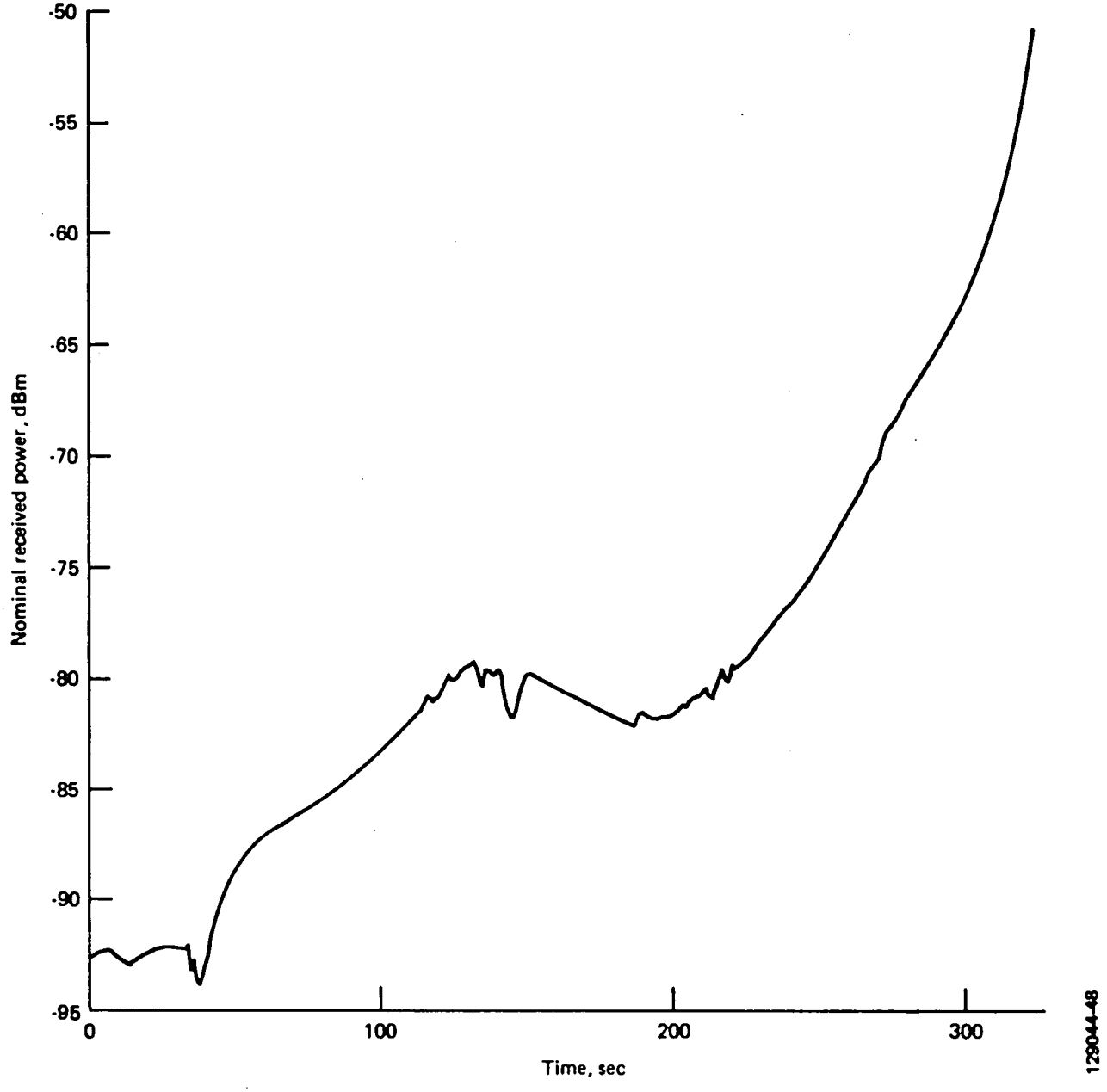

Figure 40. Antenna System Performance—767 Dual Antenna System

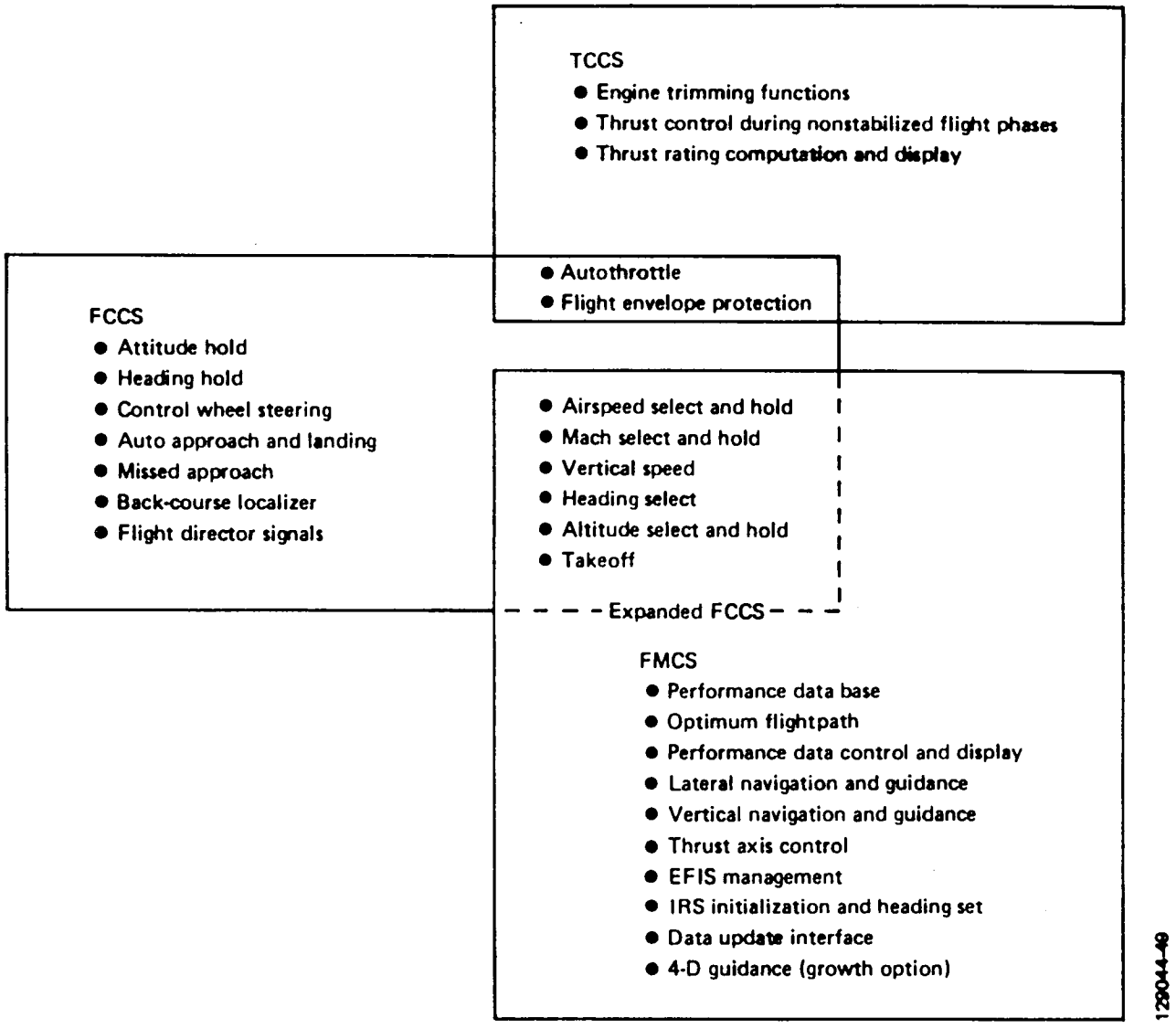

Figure 41. ARINC-Defined AFS Subsystem Functional Partitioning

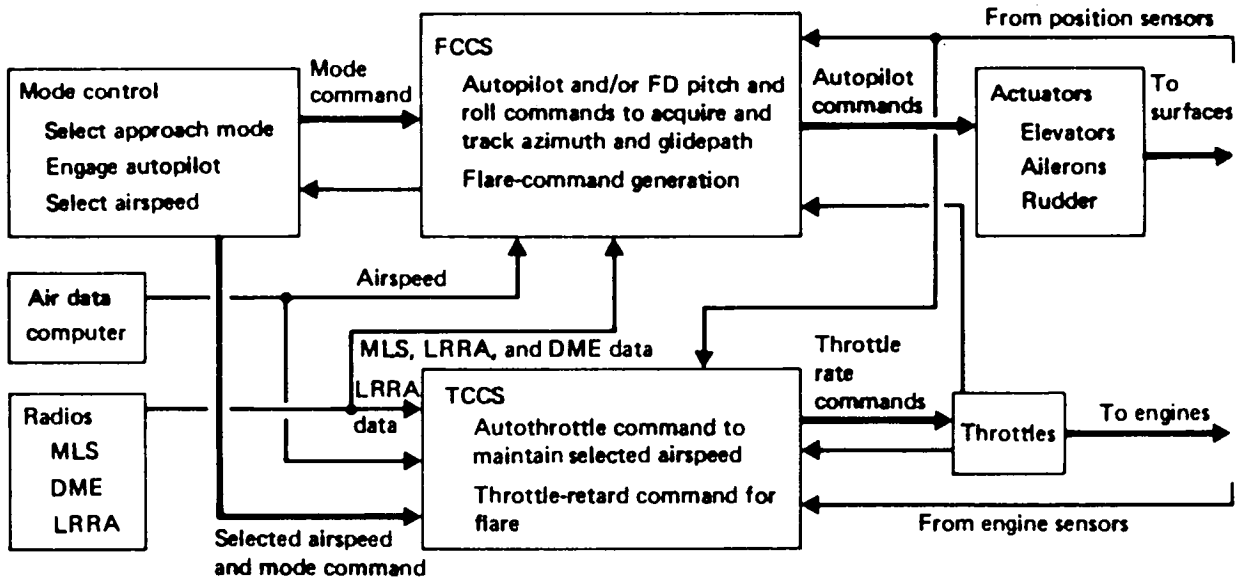

Figure 42. Functional Diagram of AFS With MLS Directly Substituting for ILS

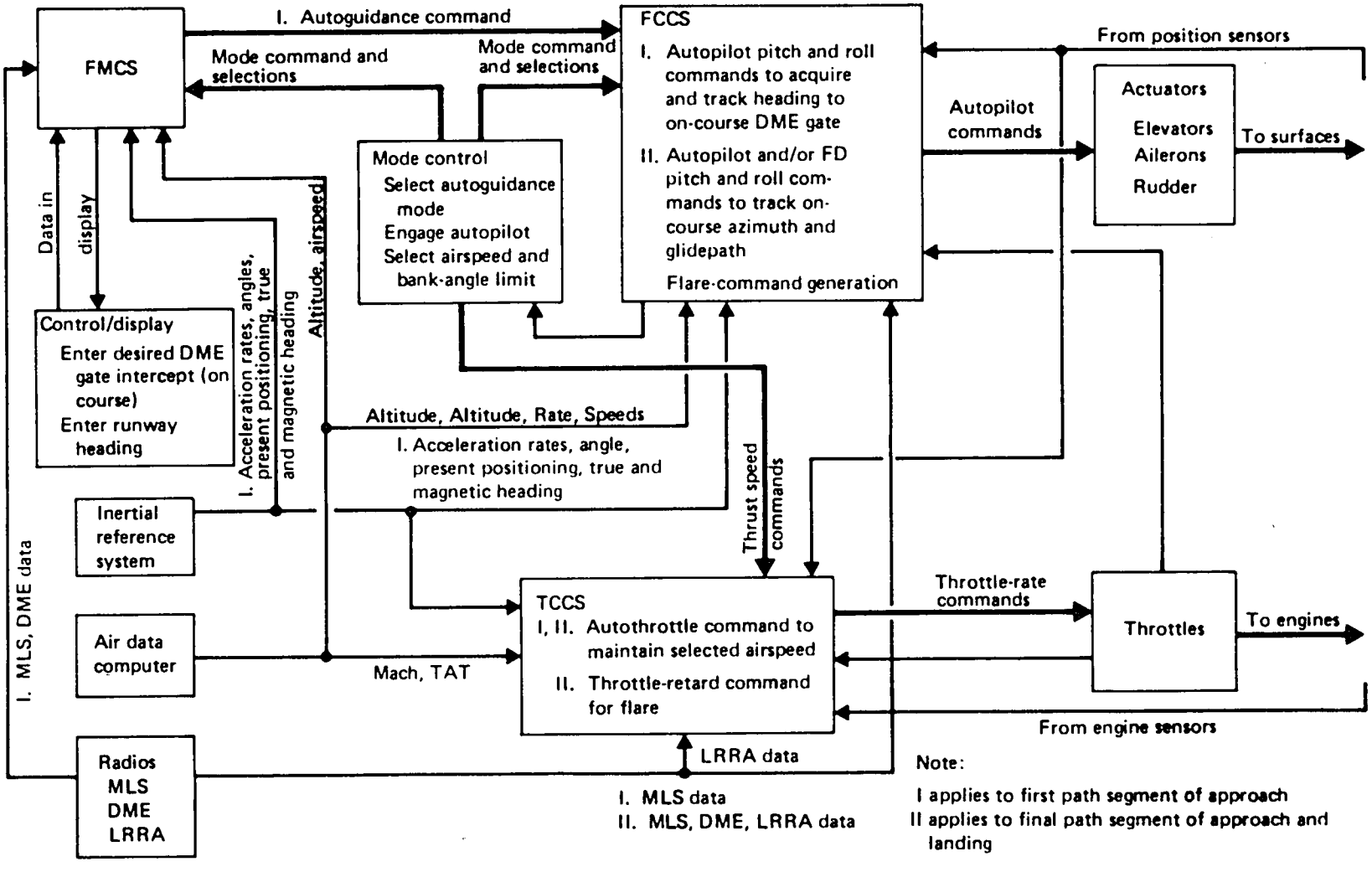

1290461

Figure 43. Functional Diagram of AFS With MLS Permitting Limited Selection of Interception Angle With Final Approach Course

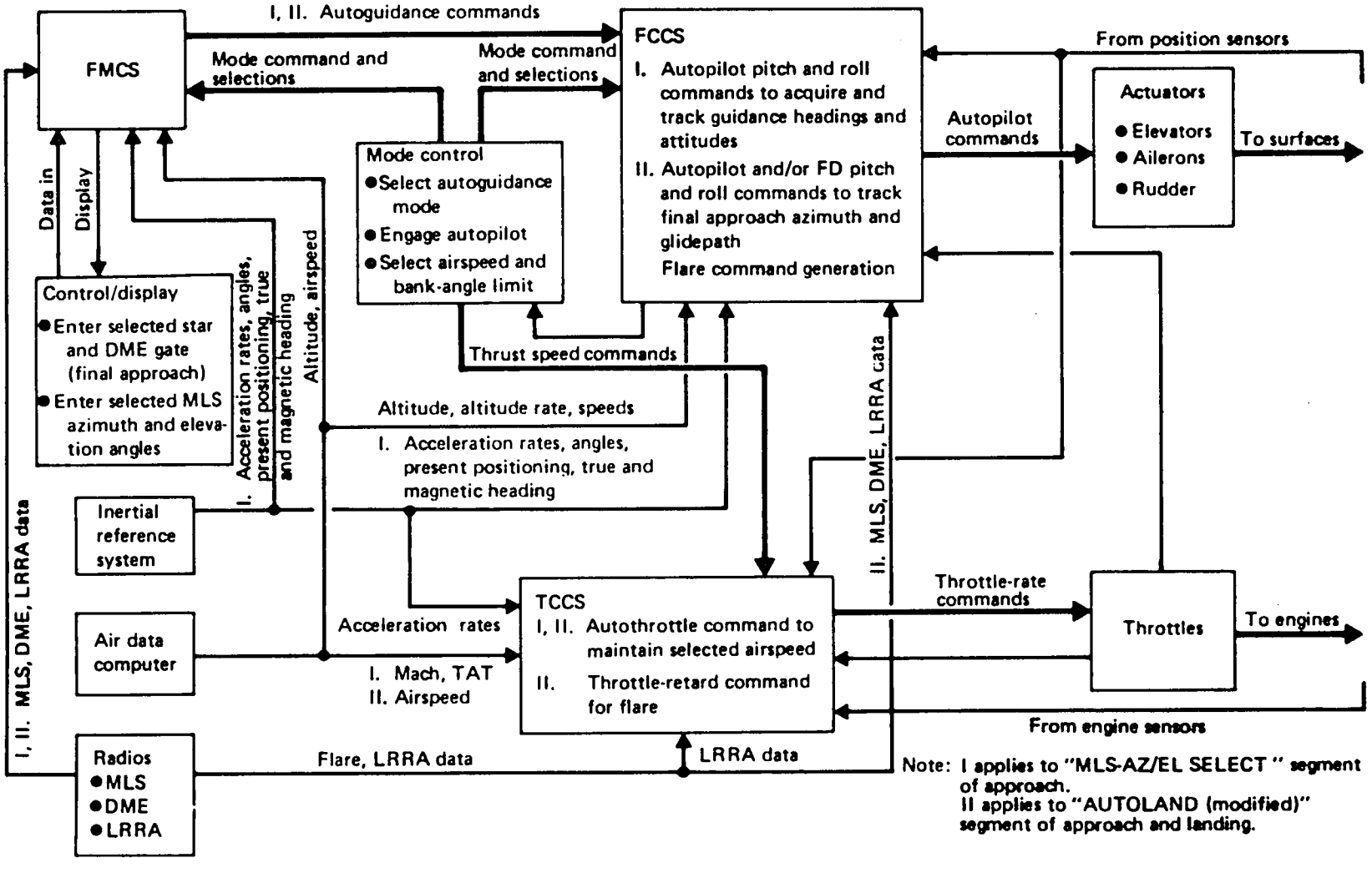

Figure 44. Functional Diagram of AFS With MLS as a Principal Guidance Sensor for Complex Curved Approaches

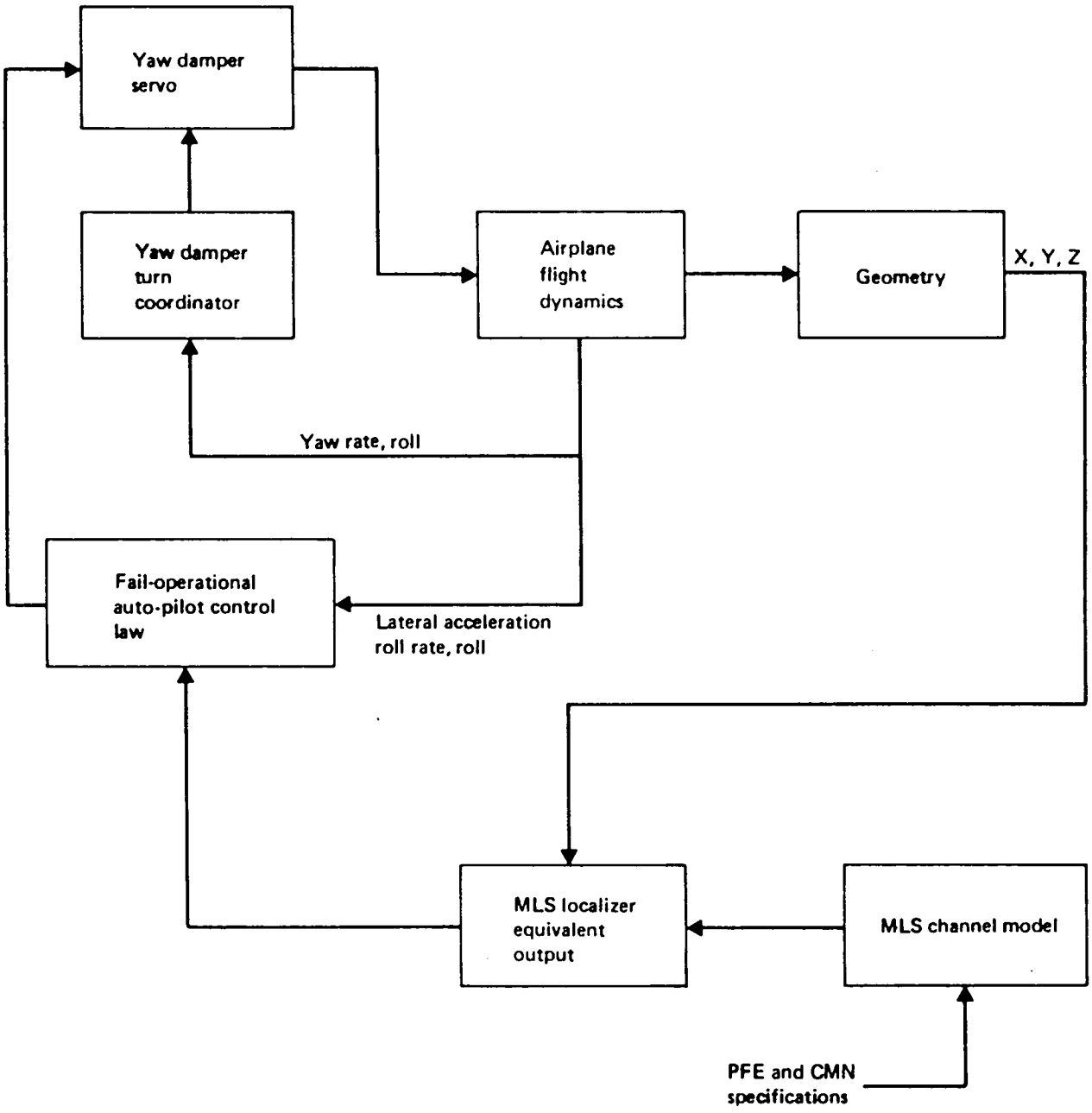

Figure 45. FY 1980 MLS/AFCS Simulation (Lateral Channel)

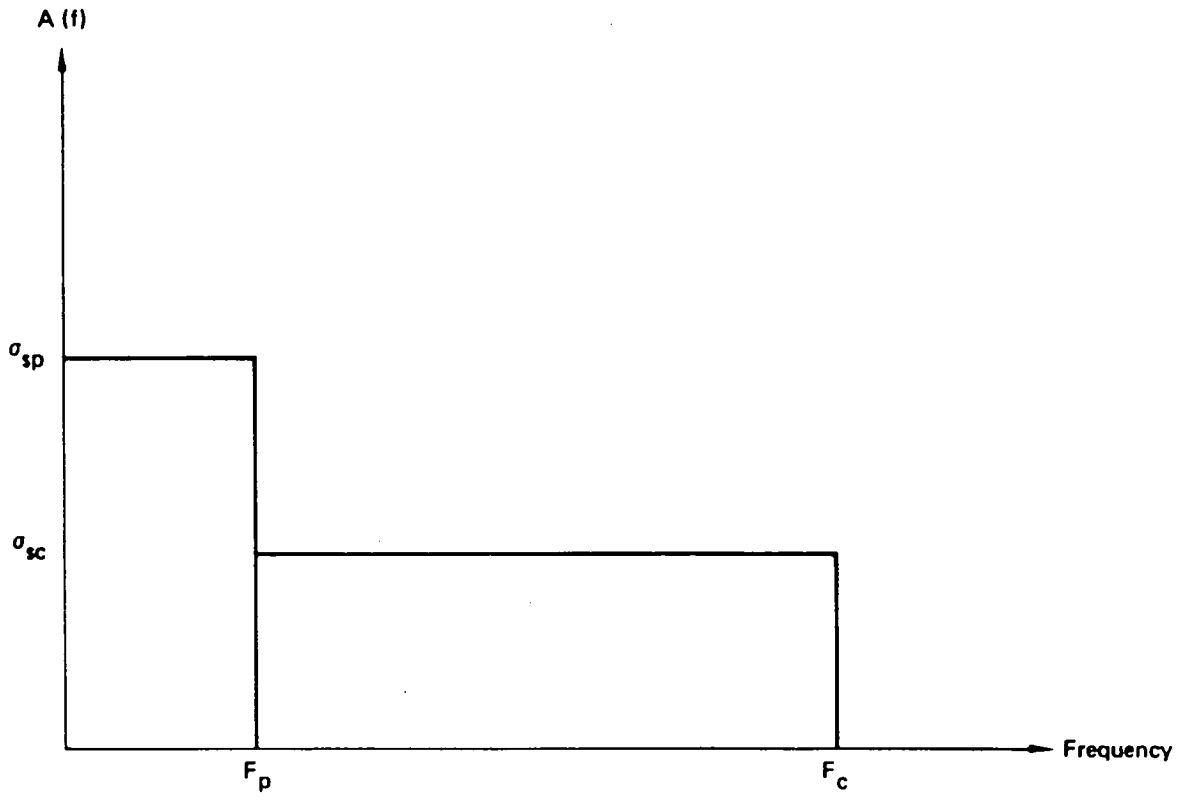

Figure 46. PFE and CMN Spectra Definitions

$$Ixx * \frac{\delta P_B}{\delta t} - IxZ * \frac{\delta R_B}{\delta t} - Q * S * B * C_l + Q * S * B * \sin(\alpha) * Cn = 0$$

$$-Ixz * \frac{\delta P_B}{\delta t} + Izz * \frac{\delta R_B}{\delta t} - Q * S * B * \sin(\alpha) * C_l - Q * S * B * \cos(\alpha) * Cn = 0$$

$$-W_{Bo} * P_B + U_{Bo} * R_B + \frac{V_B}{} - \frac{Q * S}{m} * Cy - g * \cos(\alpha) * \Phi = 0$$

$$C_l - C_{l\beta} * \beta - \frac{B}{2*V_p} * C_{lp} * P_s - \frac{B}{2*V_p} * C_{lr} * R_s - C_{l\delta R} * \delta R - C_{l\delta A} * \delta A = 0$$

$$C_n - C_{n\beta} * \beta - \frac{\delta\beta}{\delta t} - \frac{B}{2*V_p} * C_{np} * P_s - \frac{B}{2*V_p} * C_{nr} * R_s - C_{n\delta R} * R - C_{n\delta A} * \delta A = 0$$

$$C_y - C_{y\beta} * \beta - \frac{B}{2*V_p} * C_{yp} * P_s - \frac{B}{2*V_p} * C_{yzr} * R_s - C_{y\delta R} * \delta R = 0$$

129044-55

Figure 47. Mathematics of Airplane Dynamics

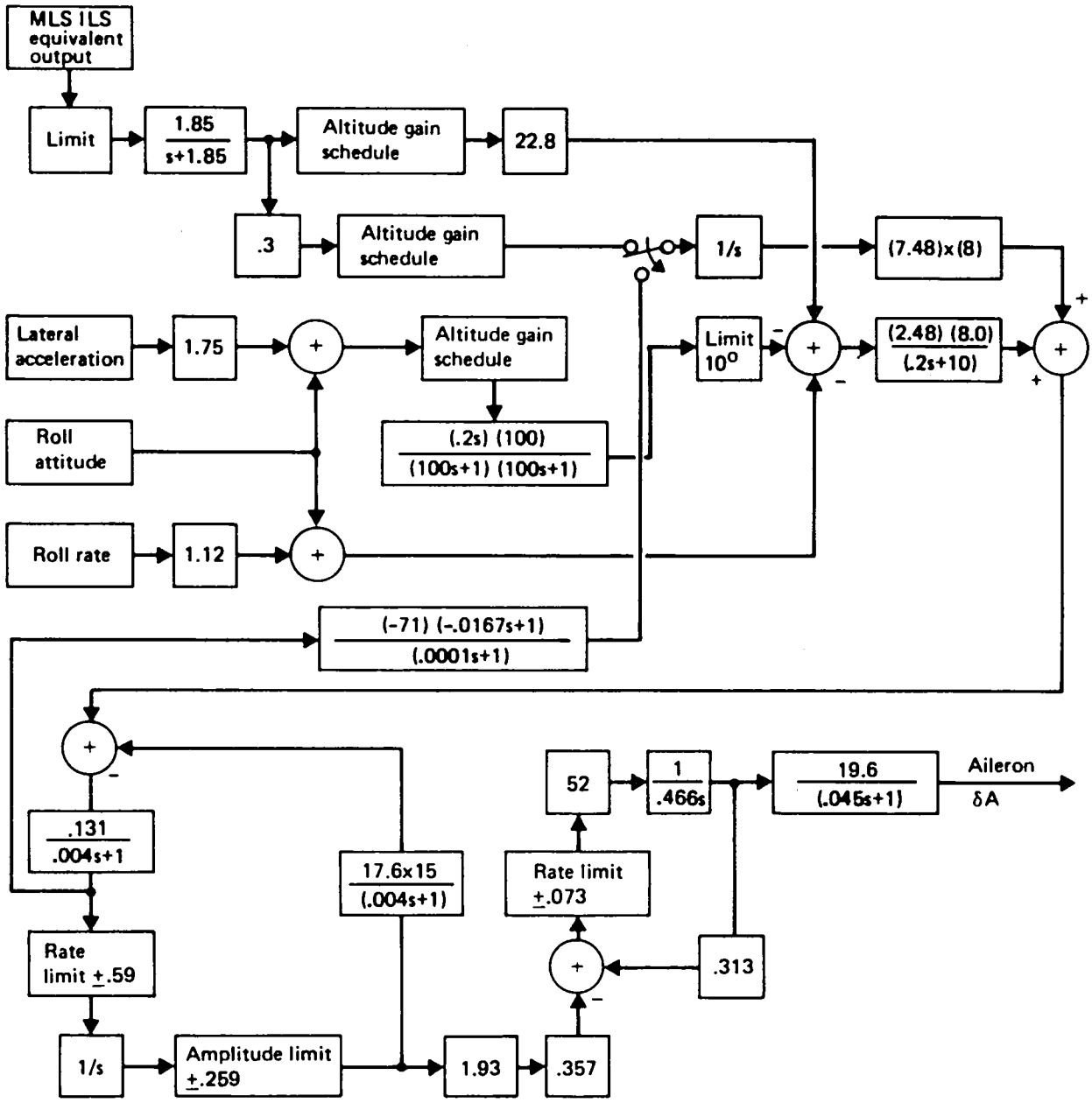

Figure 48. 747 Fail-Operational Autopilot

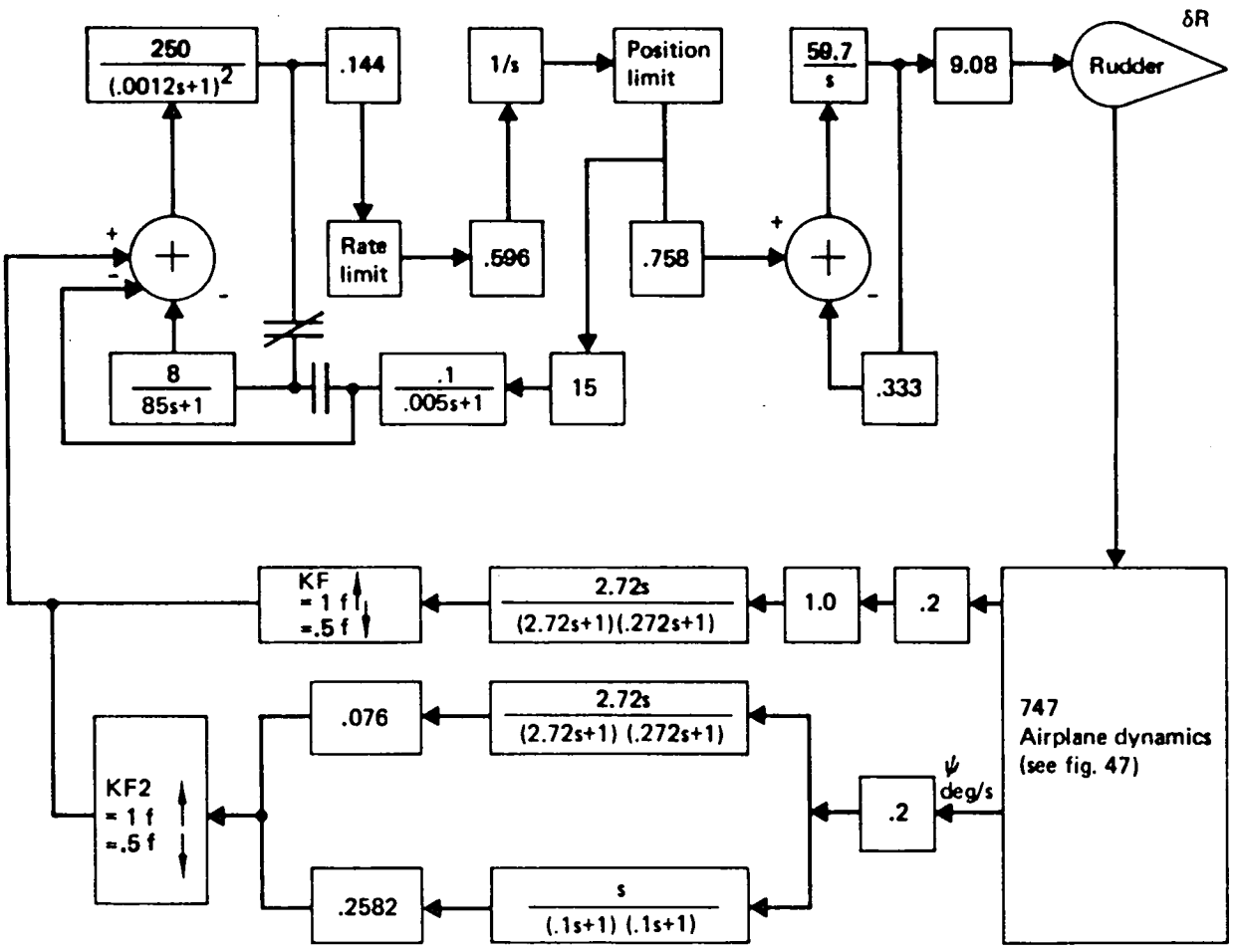

Figure 49. 747 Yaw Damper and Turn Coordinator Mathematical Model

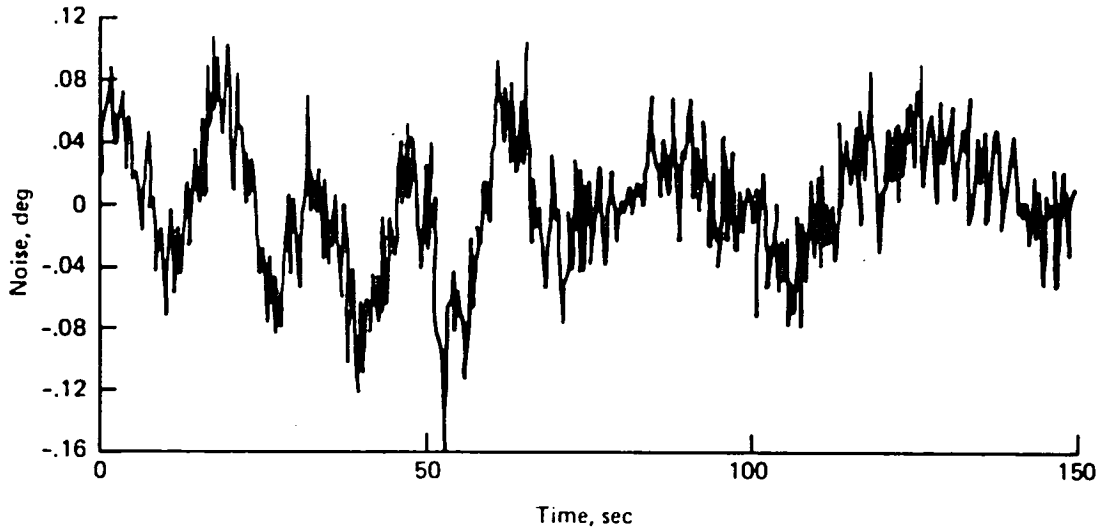

Figure 50. MLS Channel Noise

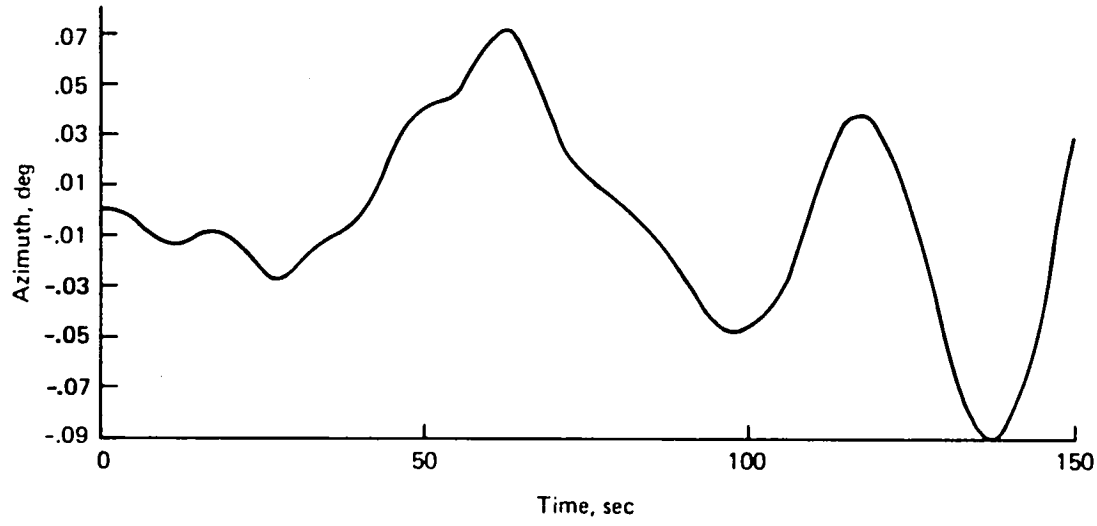

Figure 51. Exact Azimuth Angle

129044-59

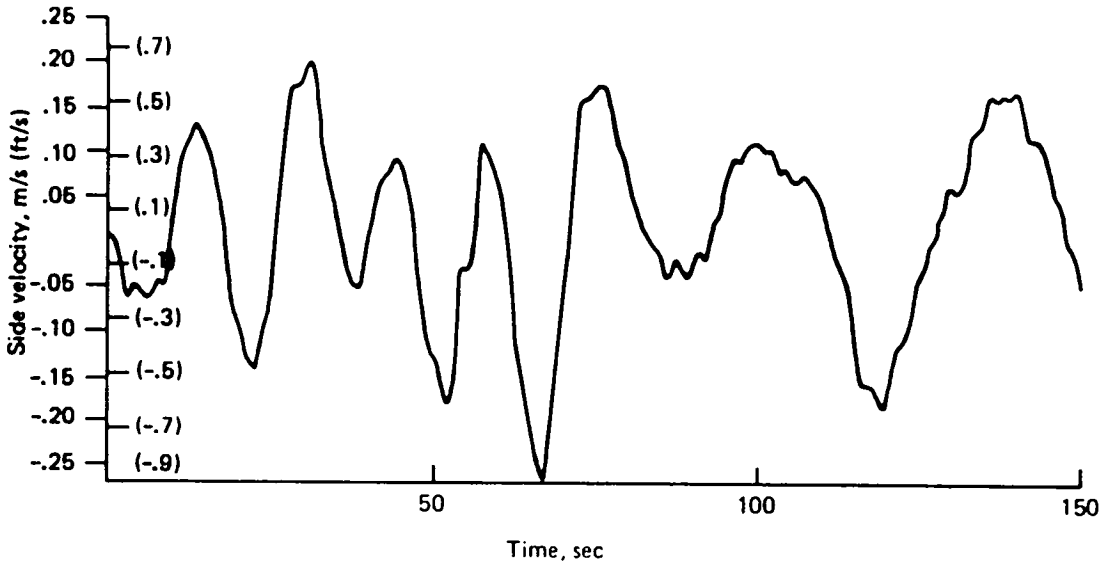

Figure 52. Airplane Side Velocity

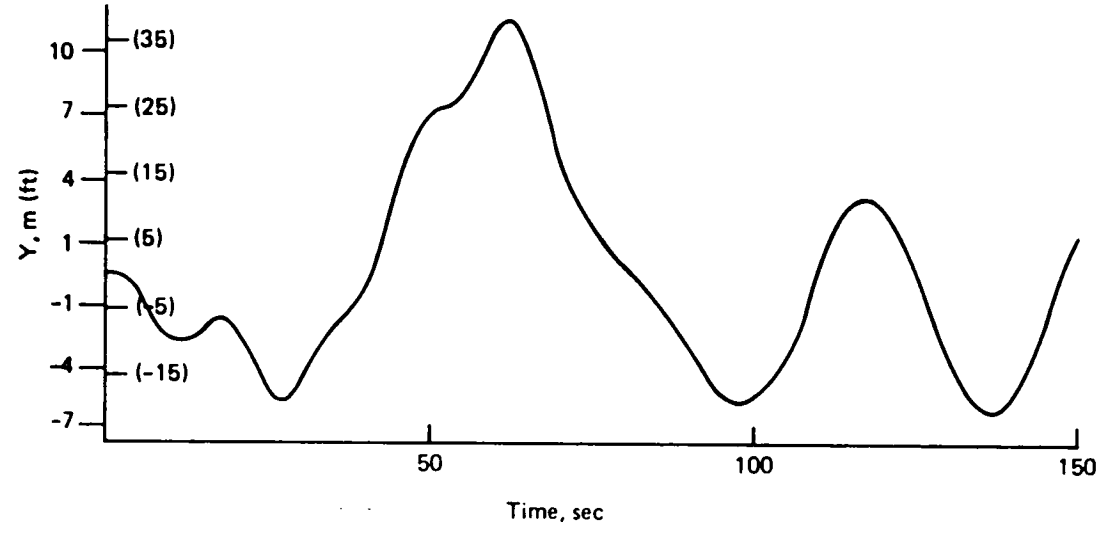

Figure 53. Airplane Lateral Displacement

129044-60

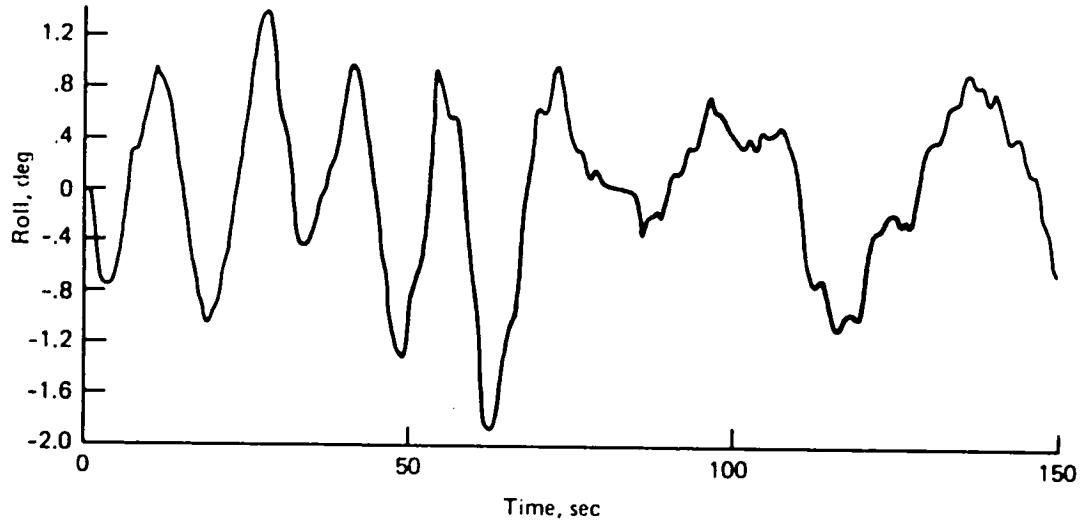

Figure 54. Roll Angle

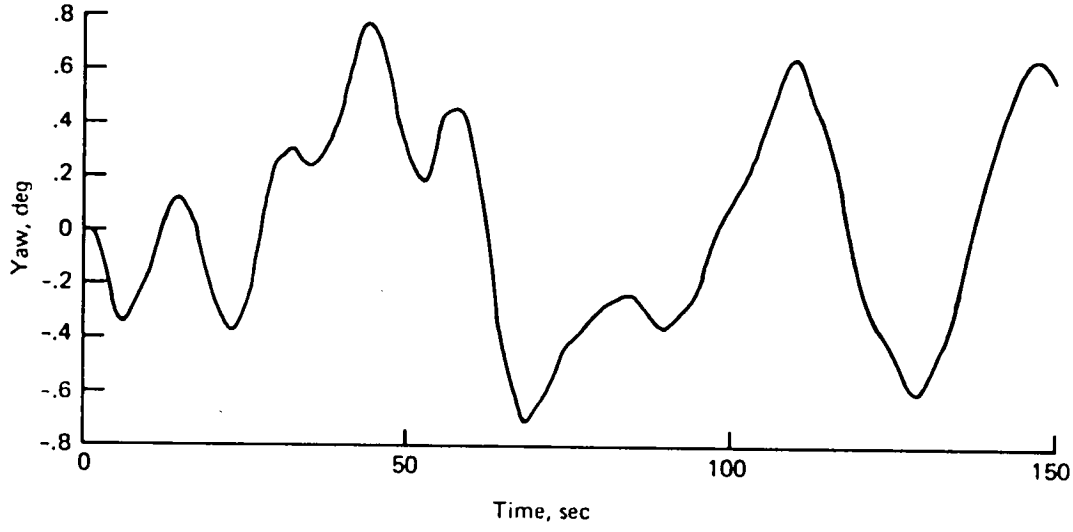

Figure 55. Yaw Angle

129044-61

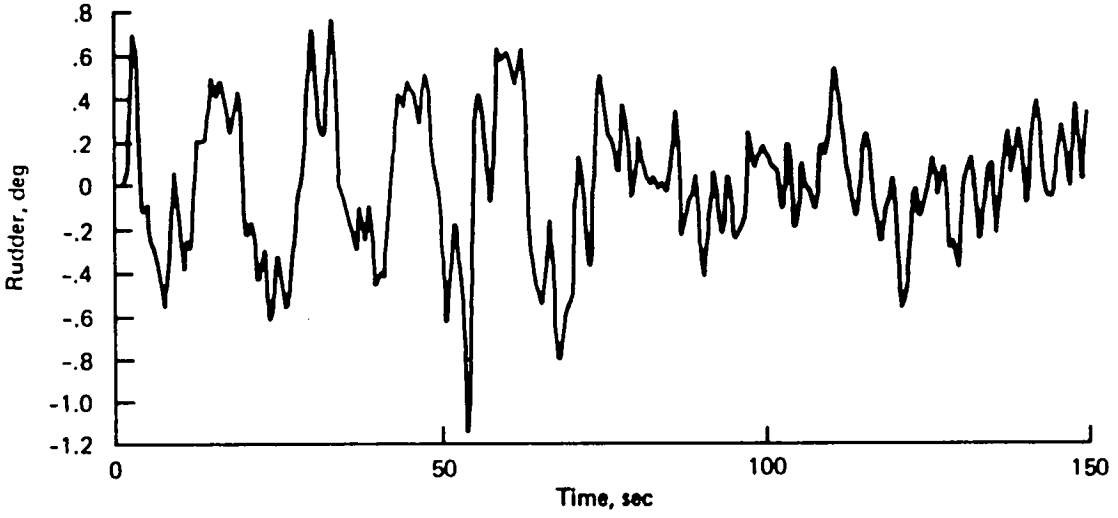

Figure 56. Rudder Angle

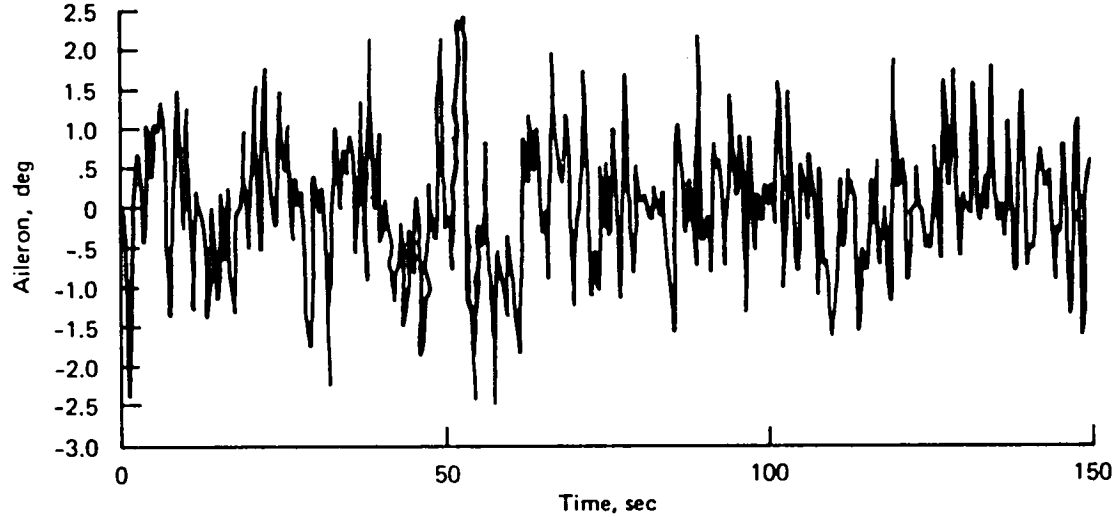

Figure 57. Aileron Angle

129044-62

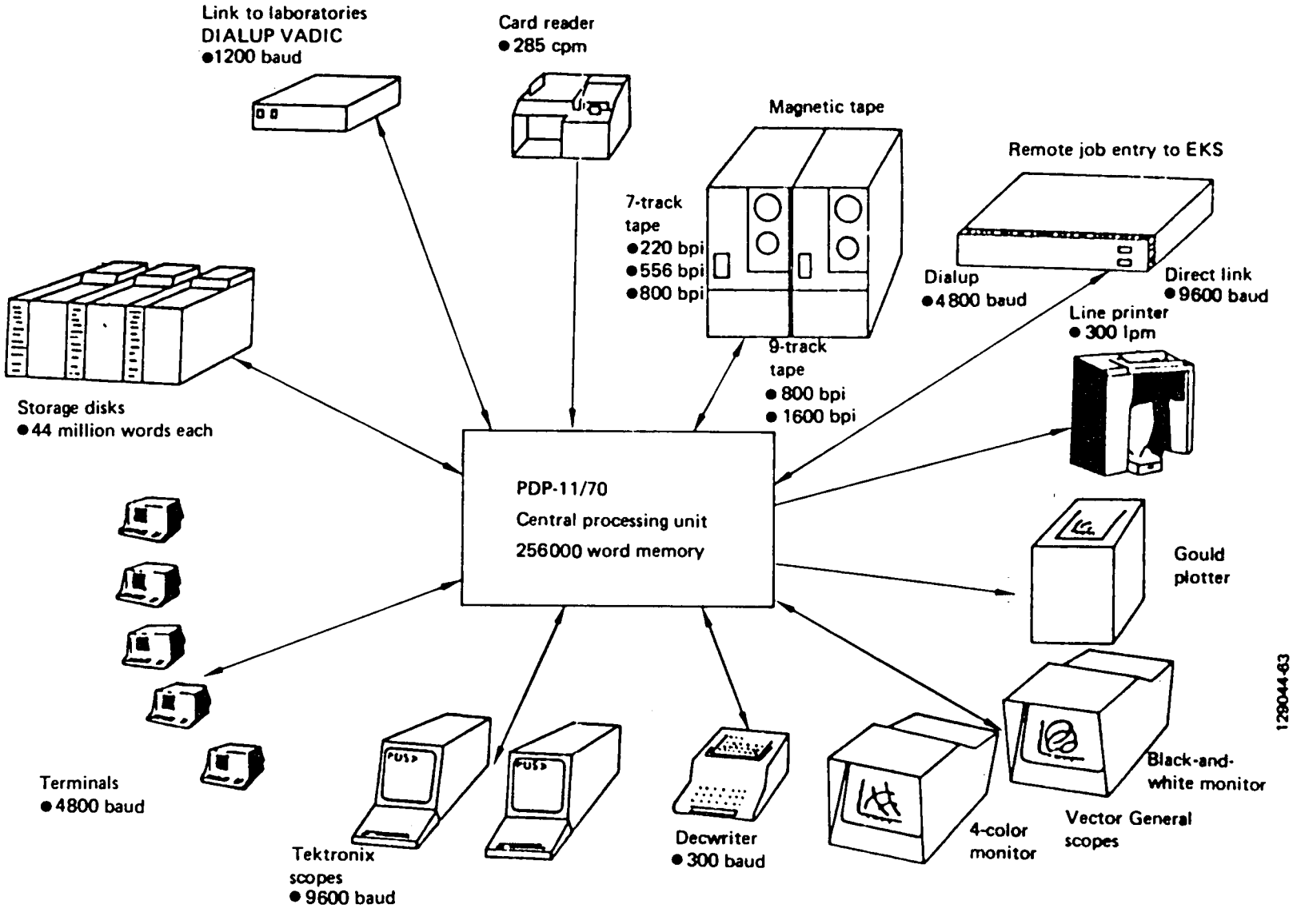

Figure A-1. Computer Facility

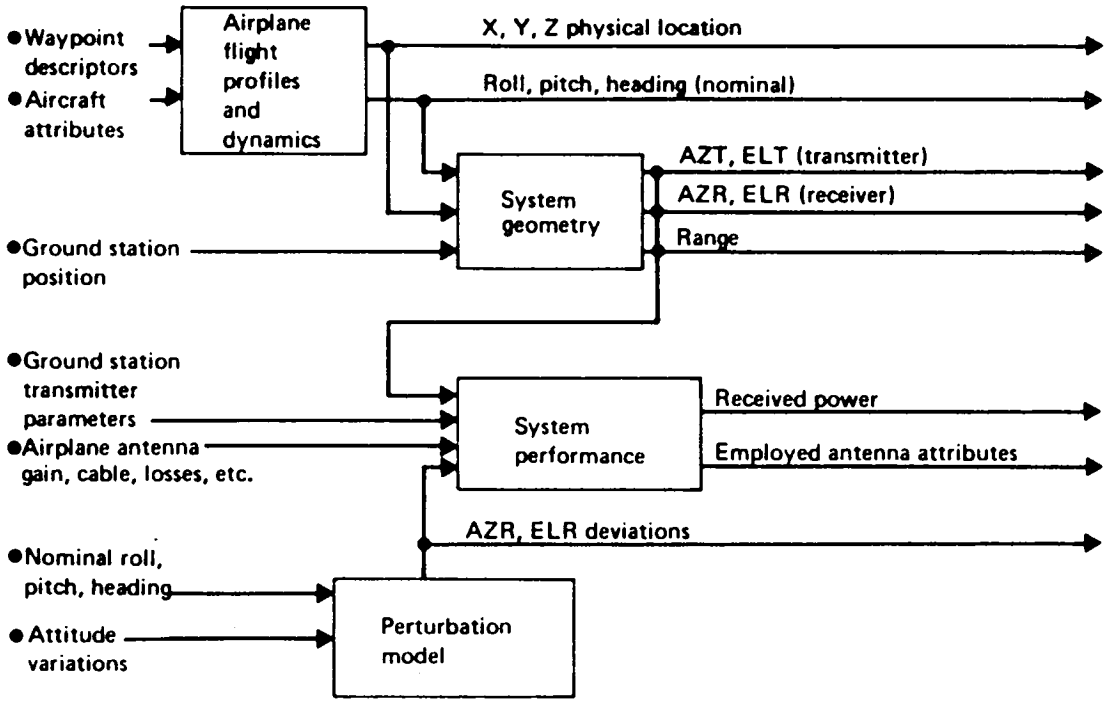

Figure A-2. Data Flow—Direct-Path Channel Characterization

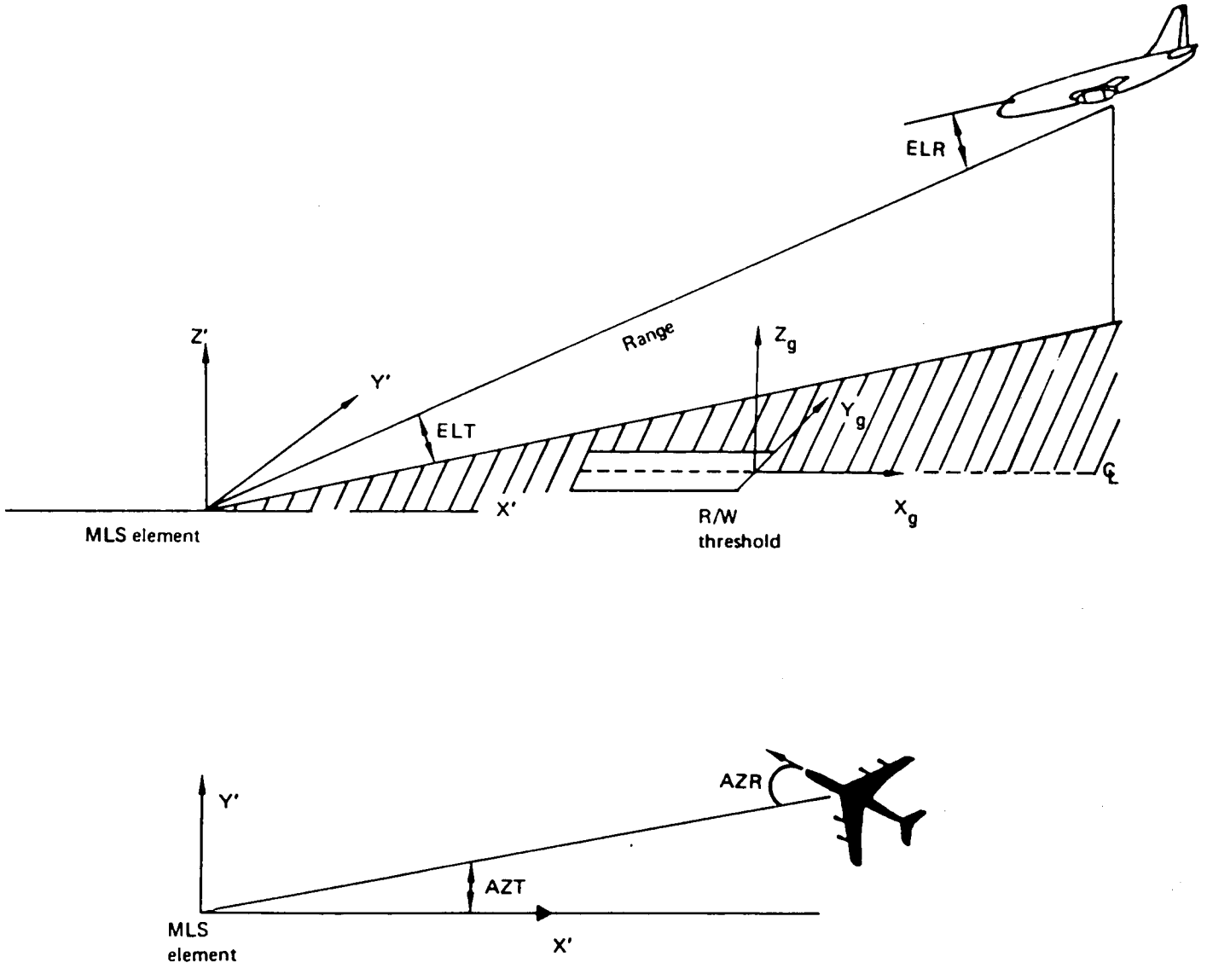

Figure A-3. System Geometry

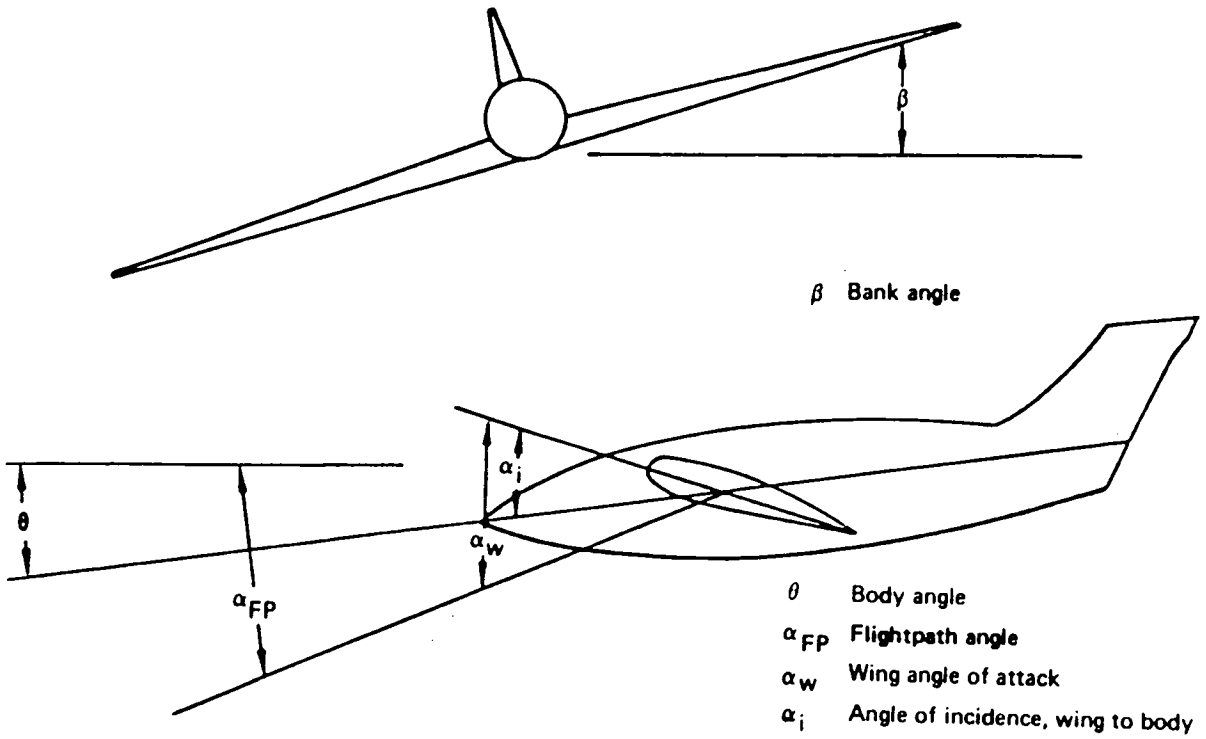

$$\theta = \alpha_{FP} + (\alpha_w - \alpha_i)$$

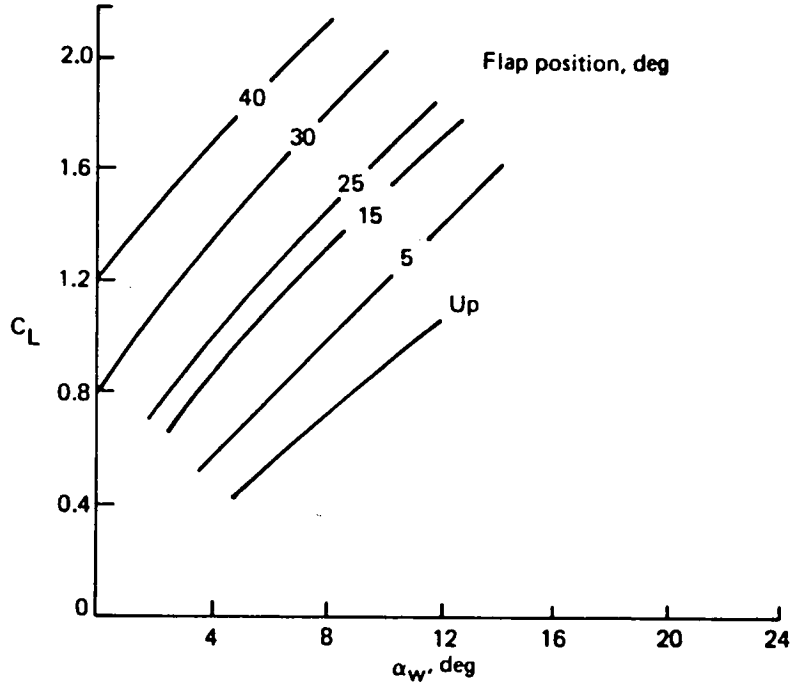

Figure A-4. Bank and Pitch-Angle Relationships

129044-66

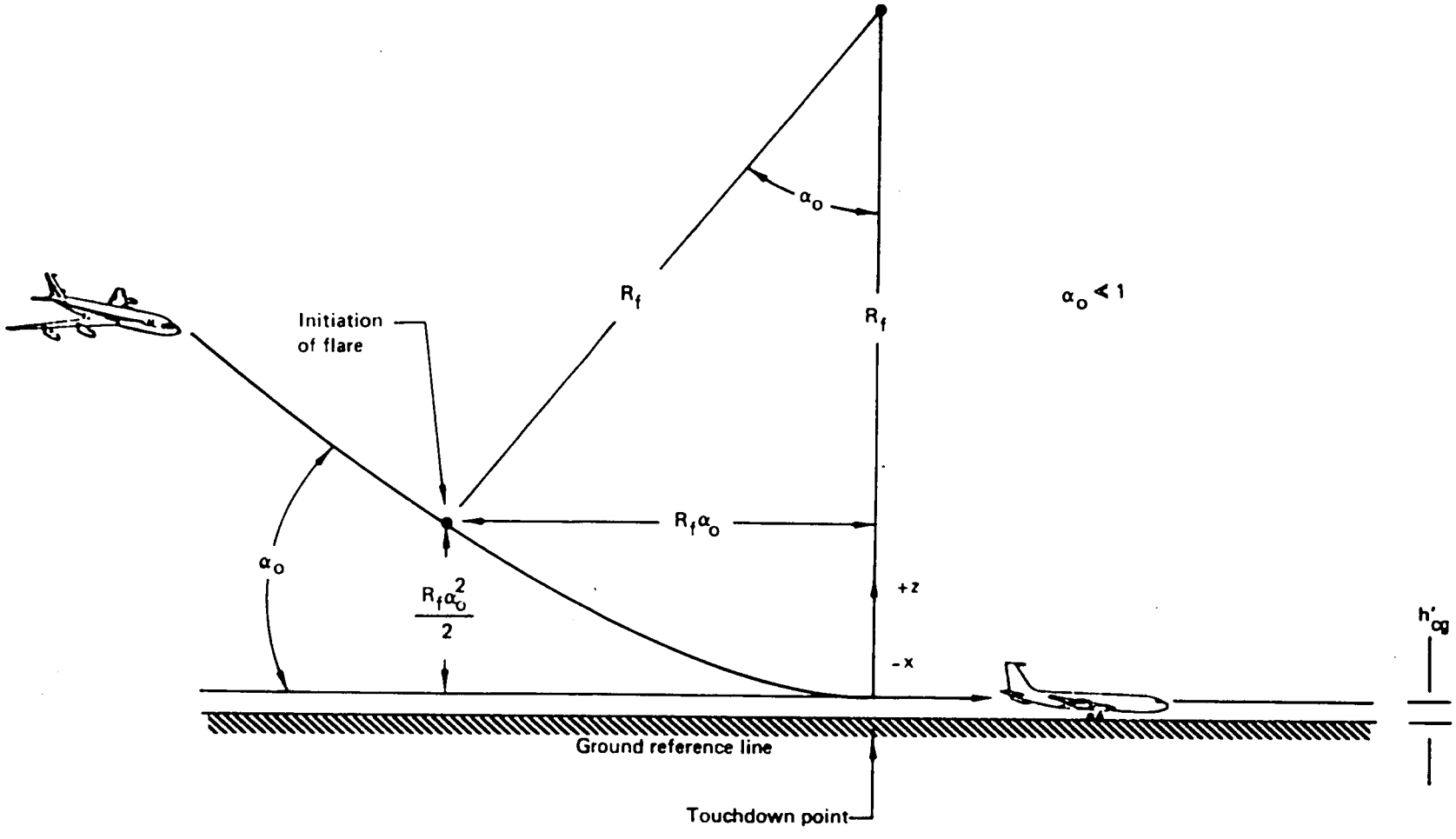

Figure A-5. Landing Flare Geometry

129044-67

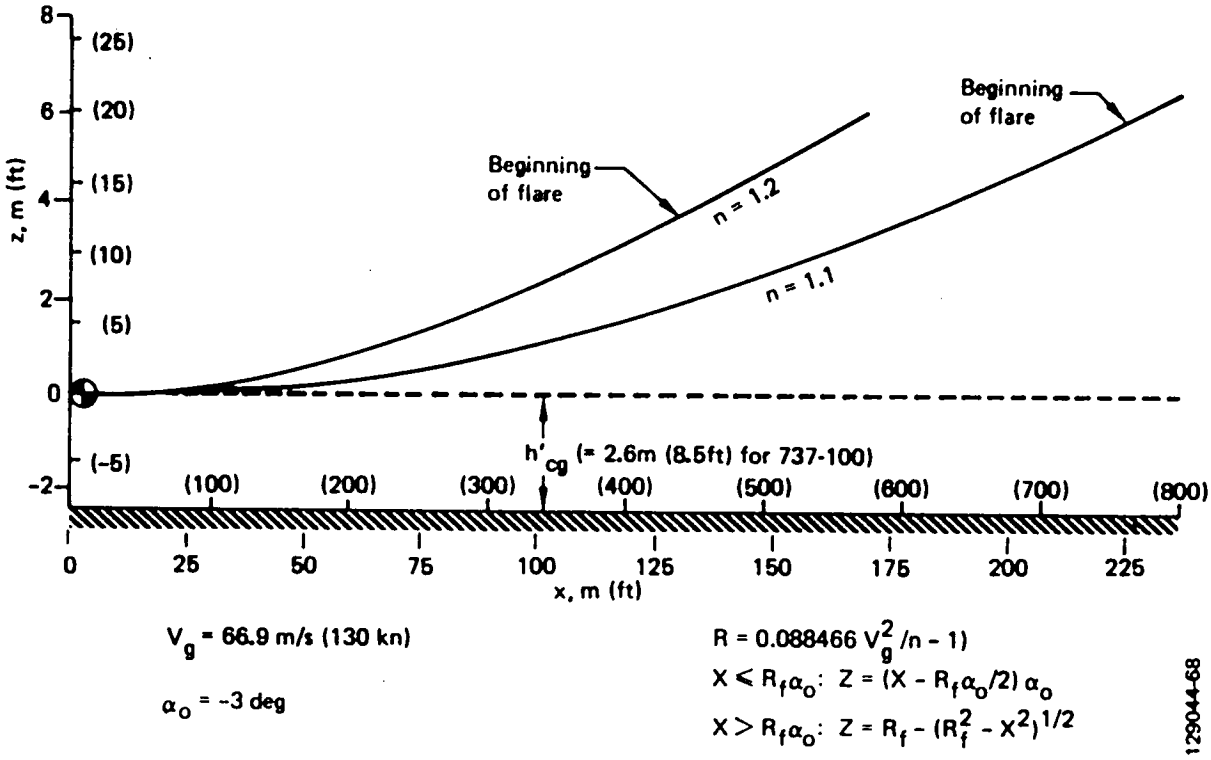

Figure A-6. Landing Flare Vertical Profile

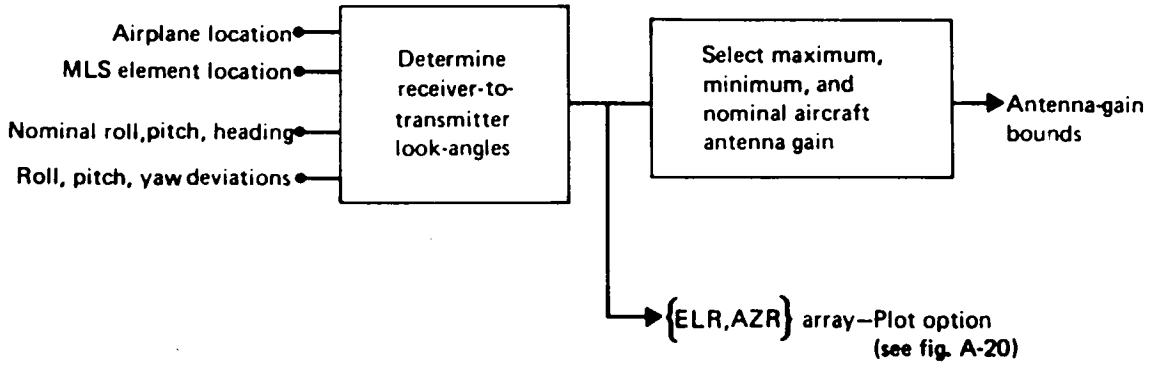

Figure A-7. Flight-Attitude and Antenna-Gain Bounds Procedure

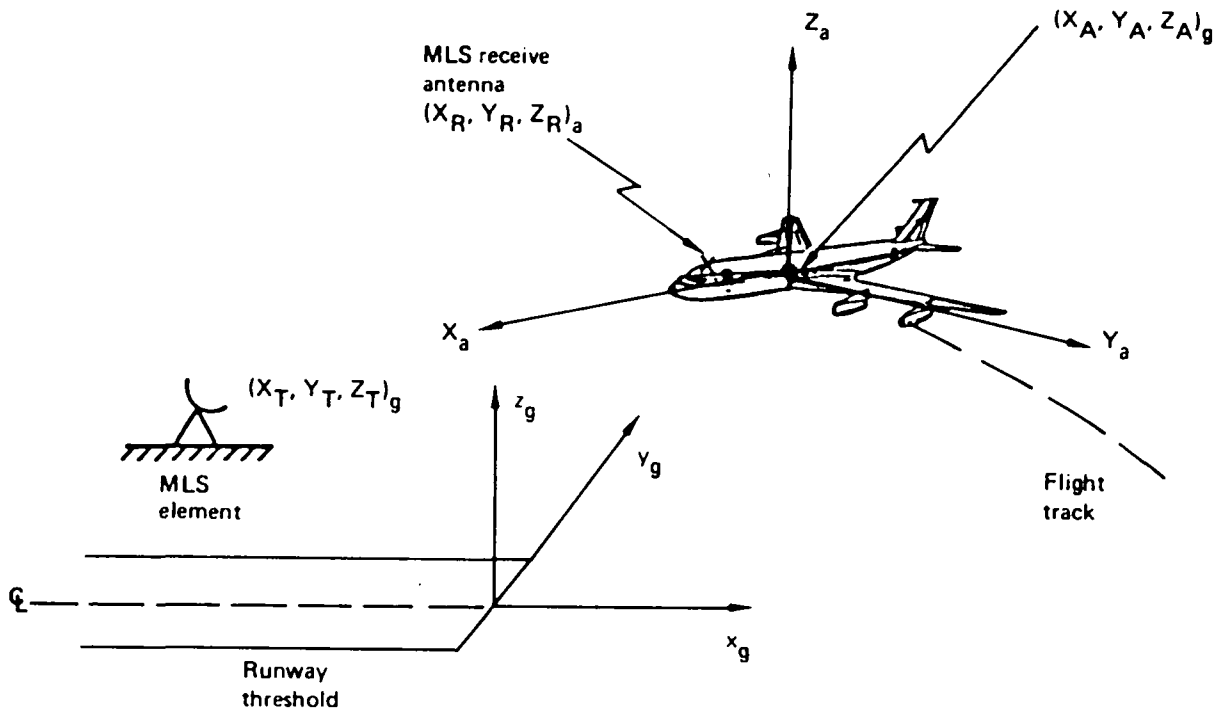

Figure A-8. Coordinate System Relationships

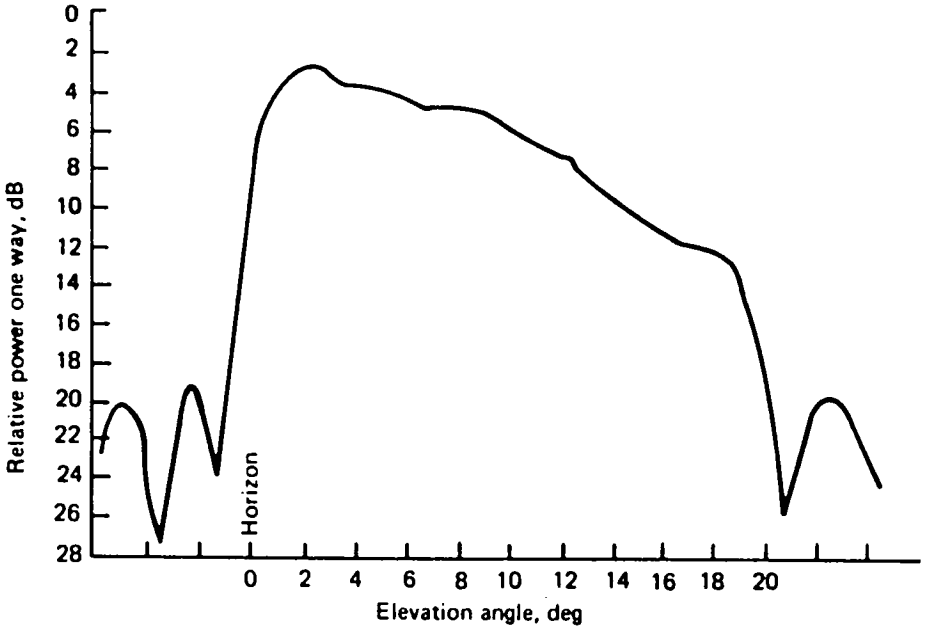

(a) Azimuth Angle and DPSK Antenna Vertical Pattern Control

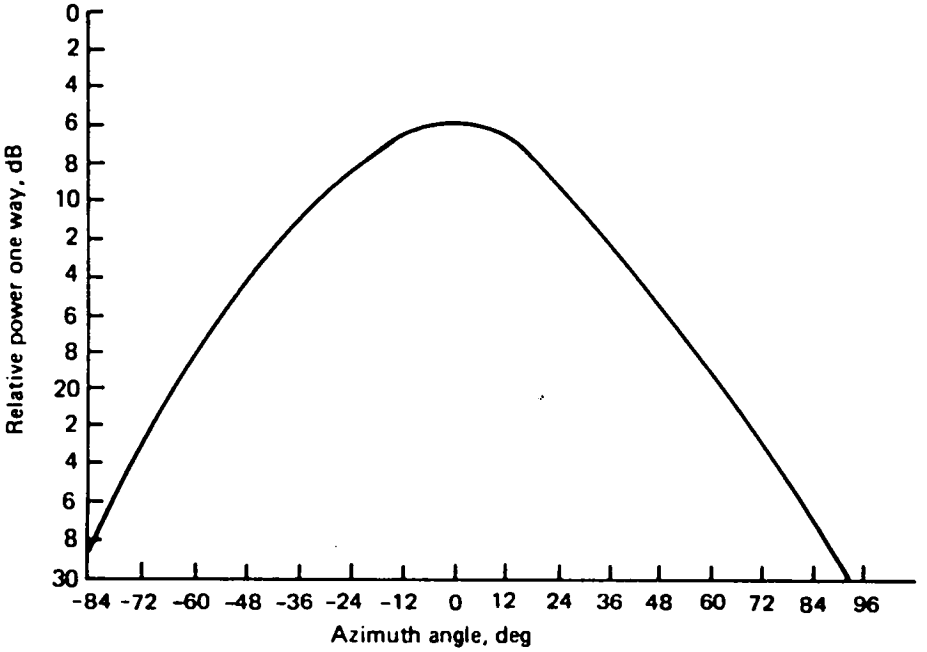

(b) Azimuth Pattern Control Elevation Antenna

Figure A-9. Pattern Control for Azimuth and Elevation Antennas

129044-71

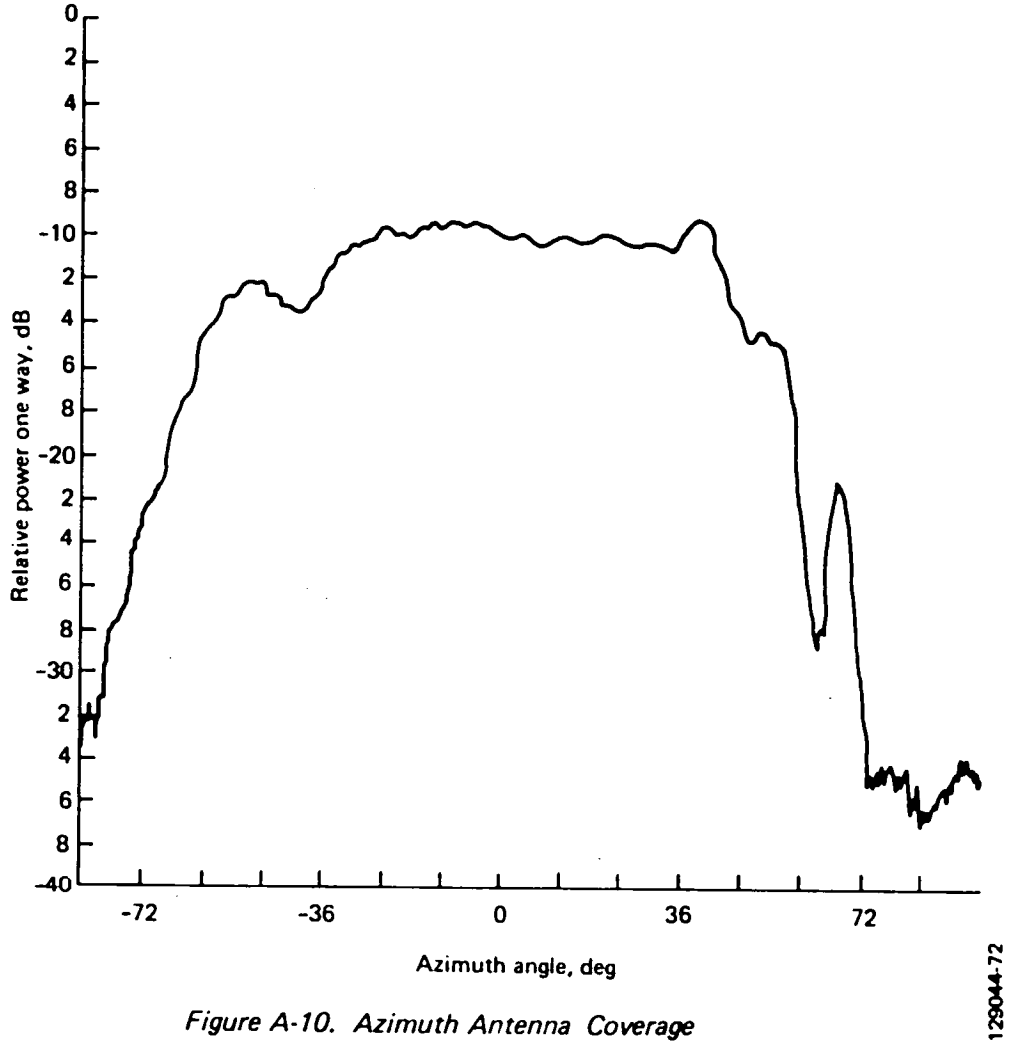

Figure A-10. Azimuth Antenna Coverage

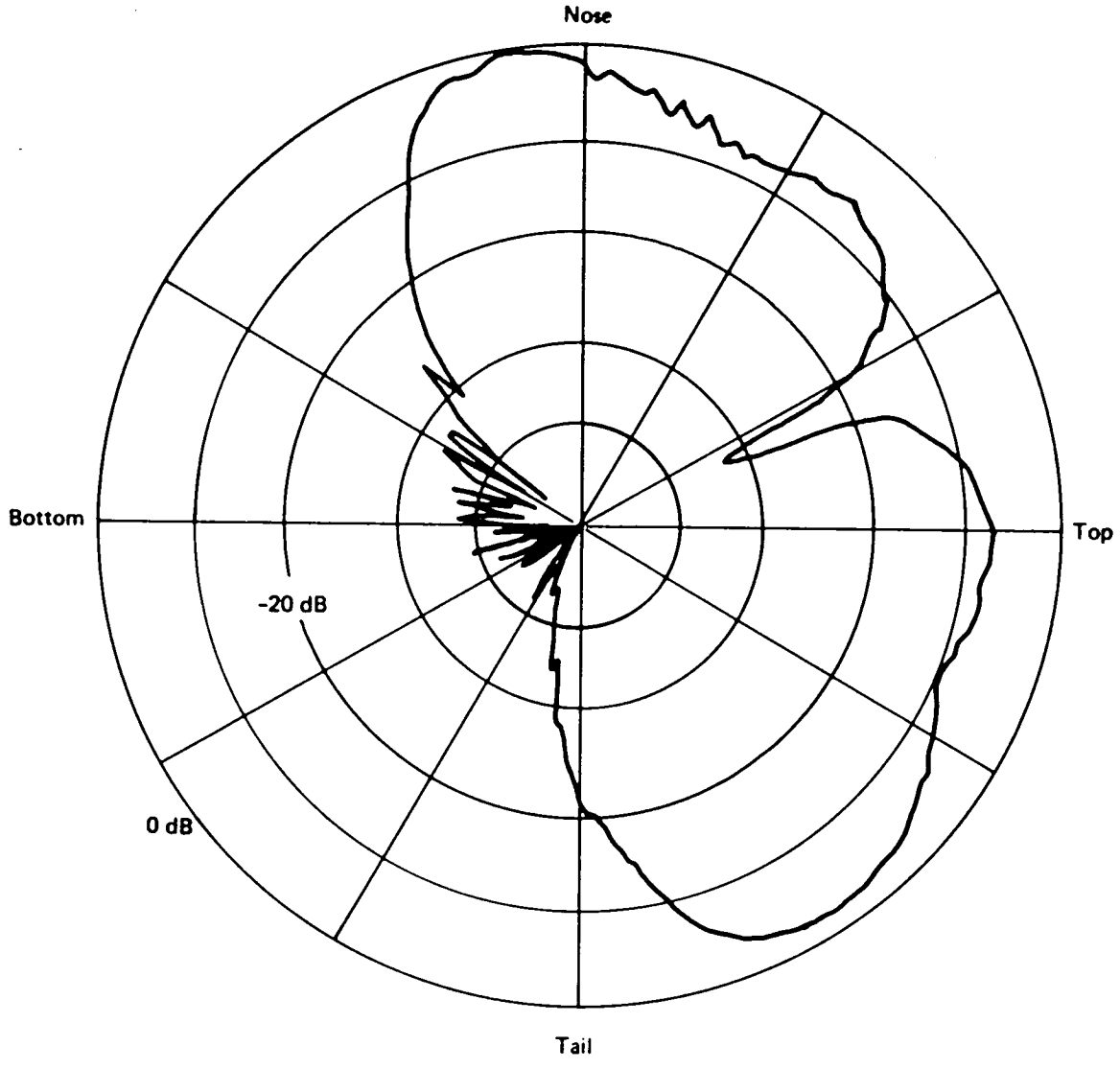

129044-73

Figure A-11. Top Antenna—Pitch-Plane Pattern

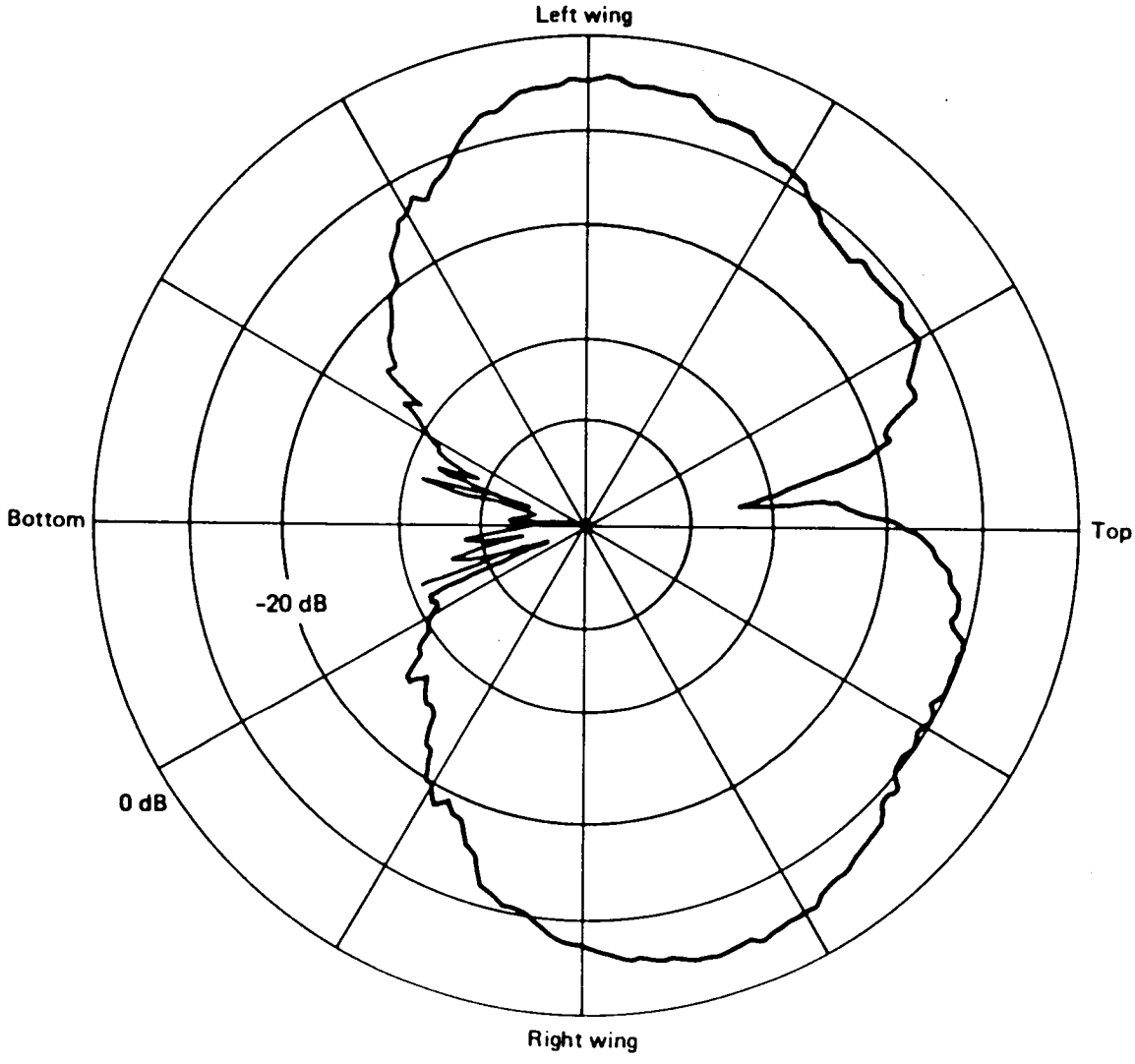

129044-74

Figure A-12. Top Antenna—Roll-Plane Pattern

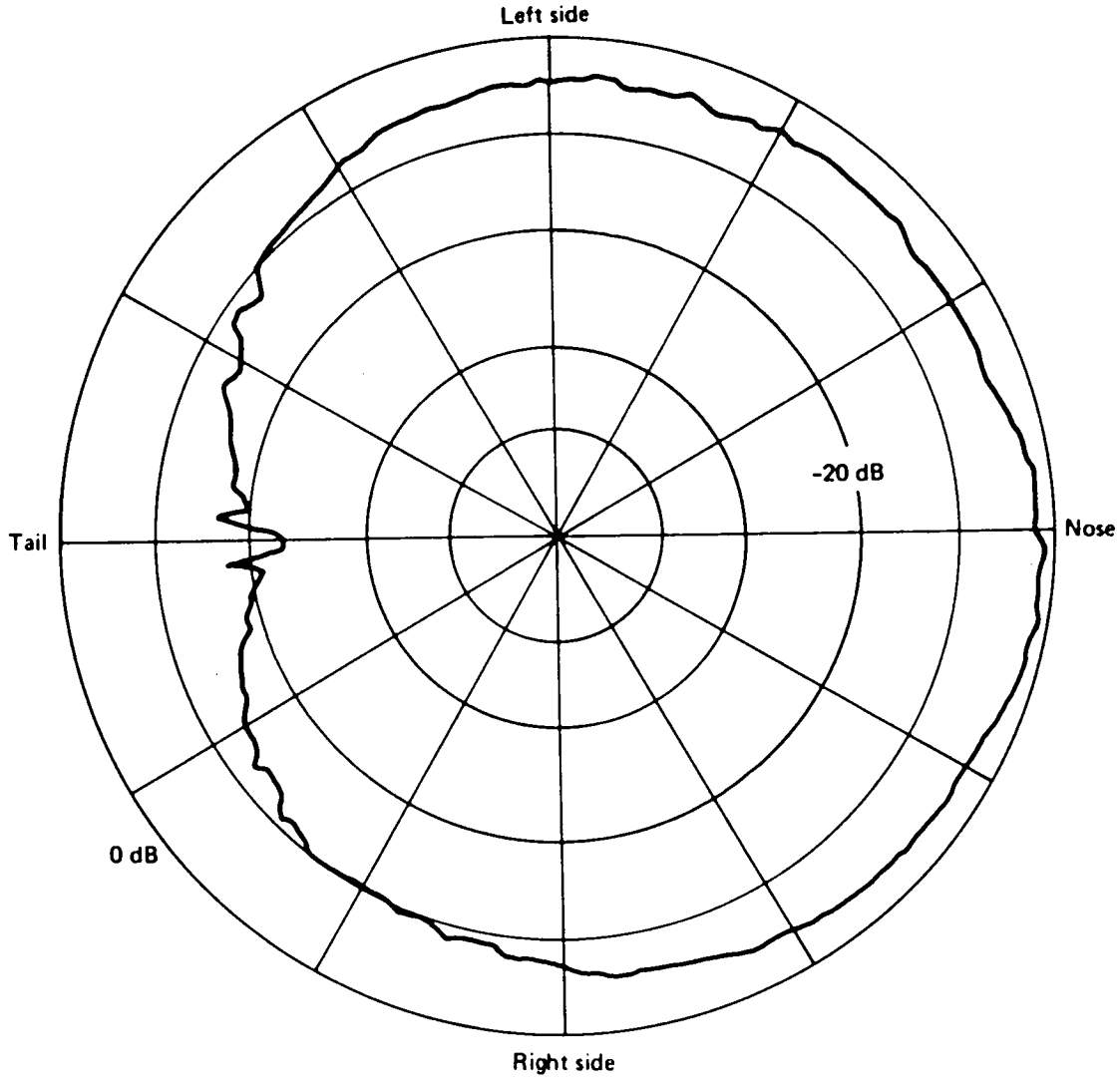

129044-75

Figure A-13. Top Antenna—Azimuth-Plane Pattern

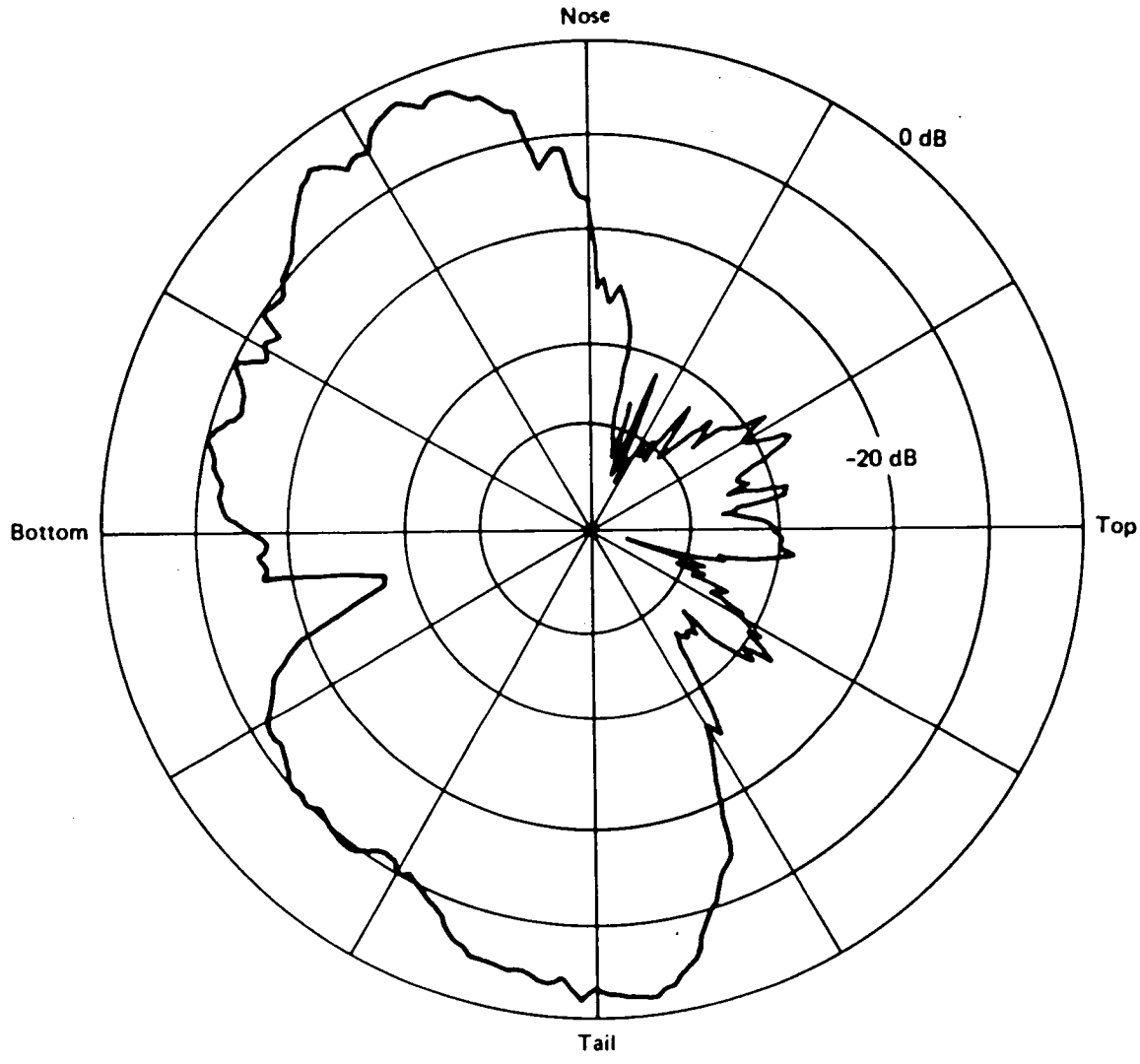

129044-76

Figure A-14. Bottom Antenna—Pitch-Plane Pattern

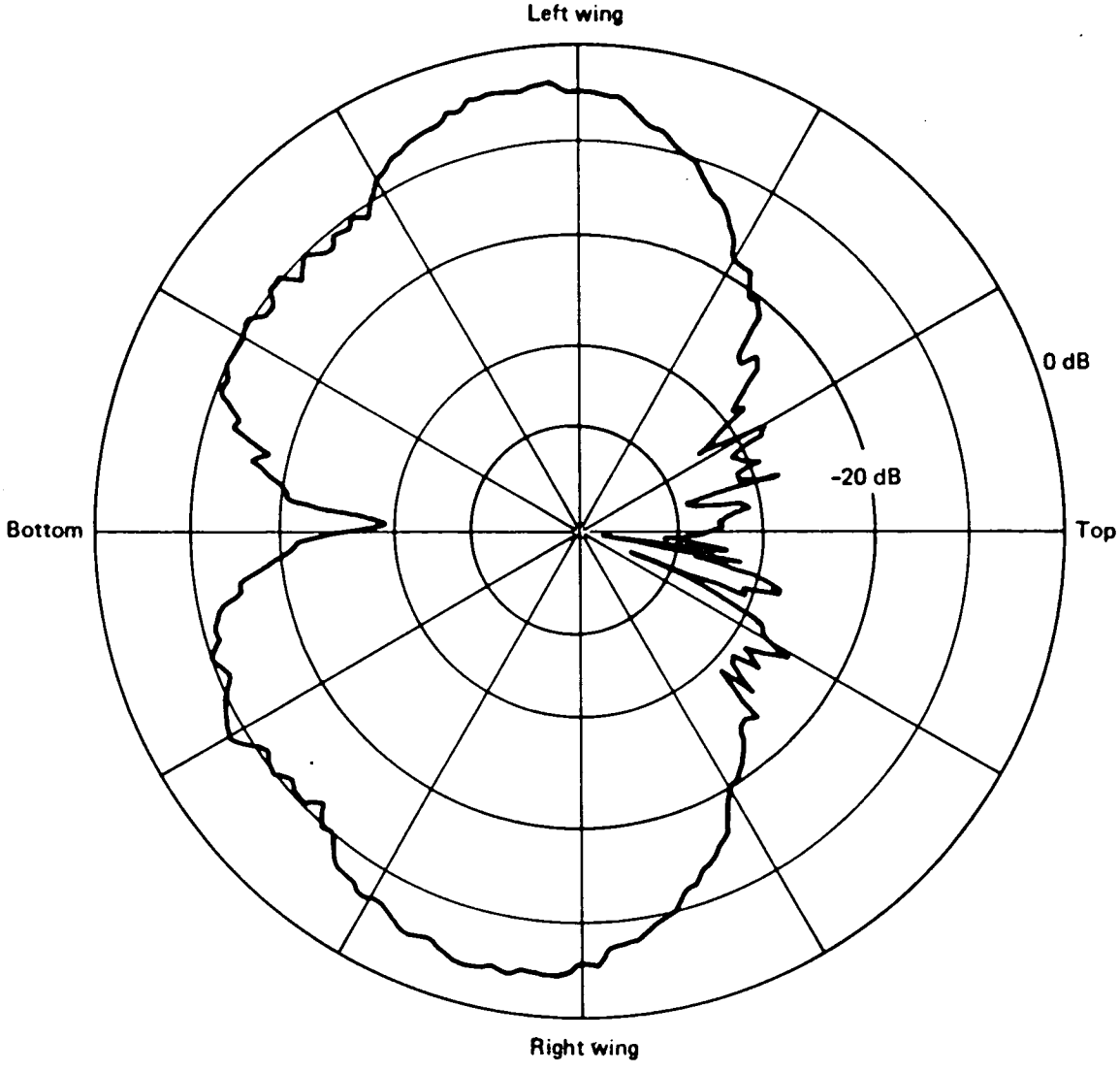

Figure A-15. Bottom Antenna—Roll-Plane Pattern

128044-77

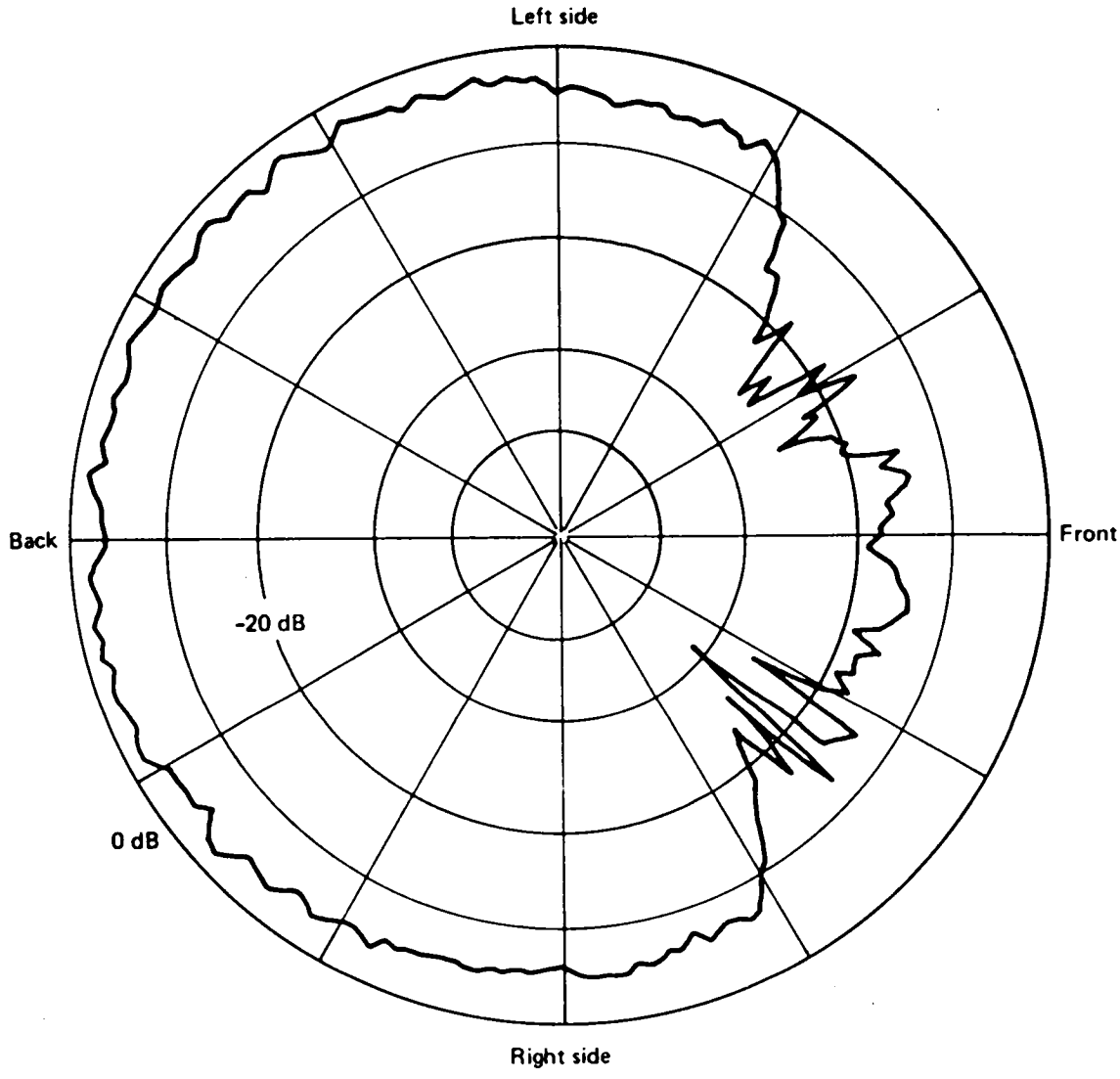

129044-78

Figure A-16. Bottom Antenna--Azimuth-Plane Pattern

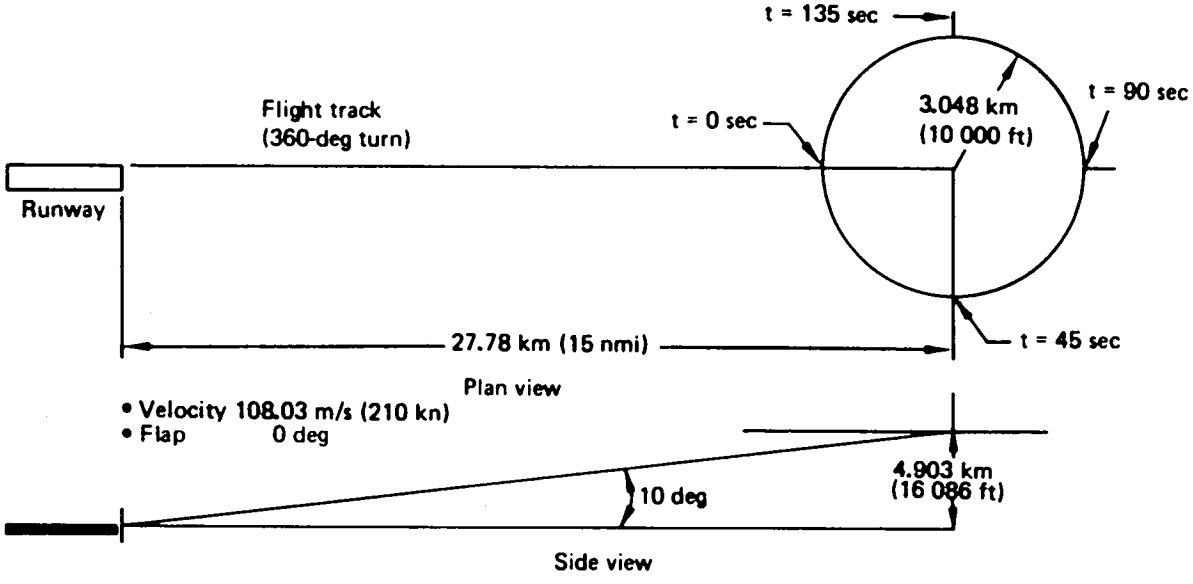

129044-79

Figure A-17. Sample Case 1—Flight Profile (V = 108.03 m/s (210 kn), Flap = 0 deg)

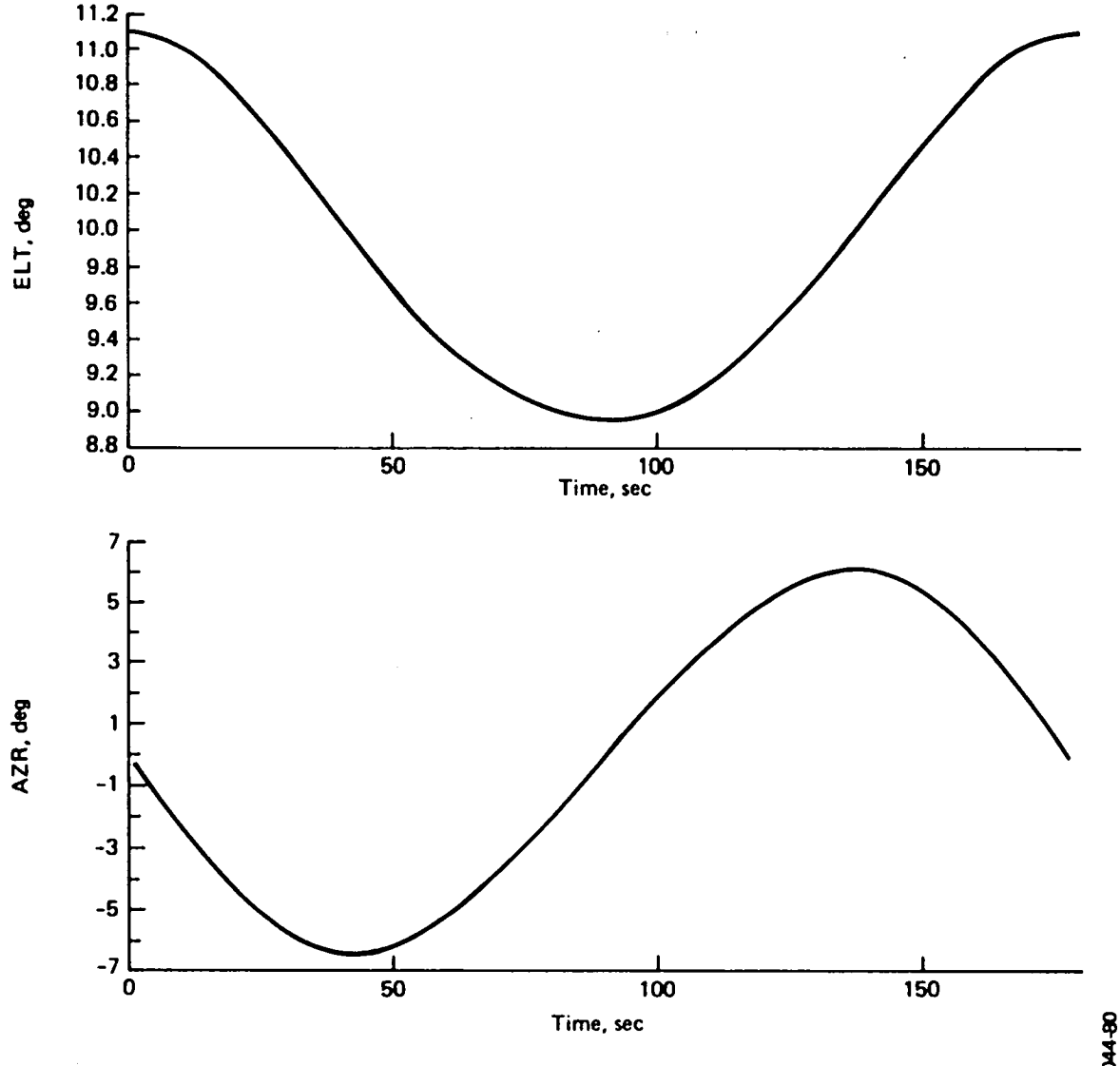

Figure A-18. Transmitter Look-Angle Time Histories

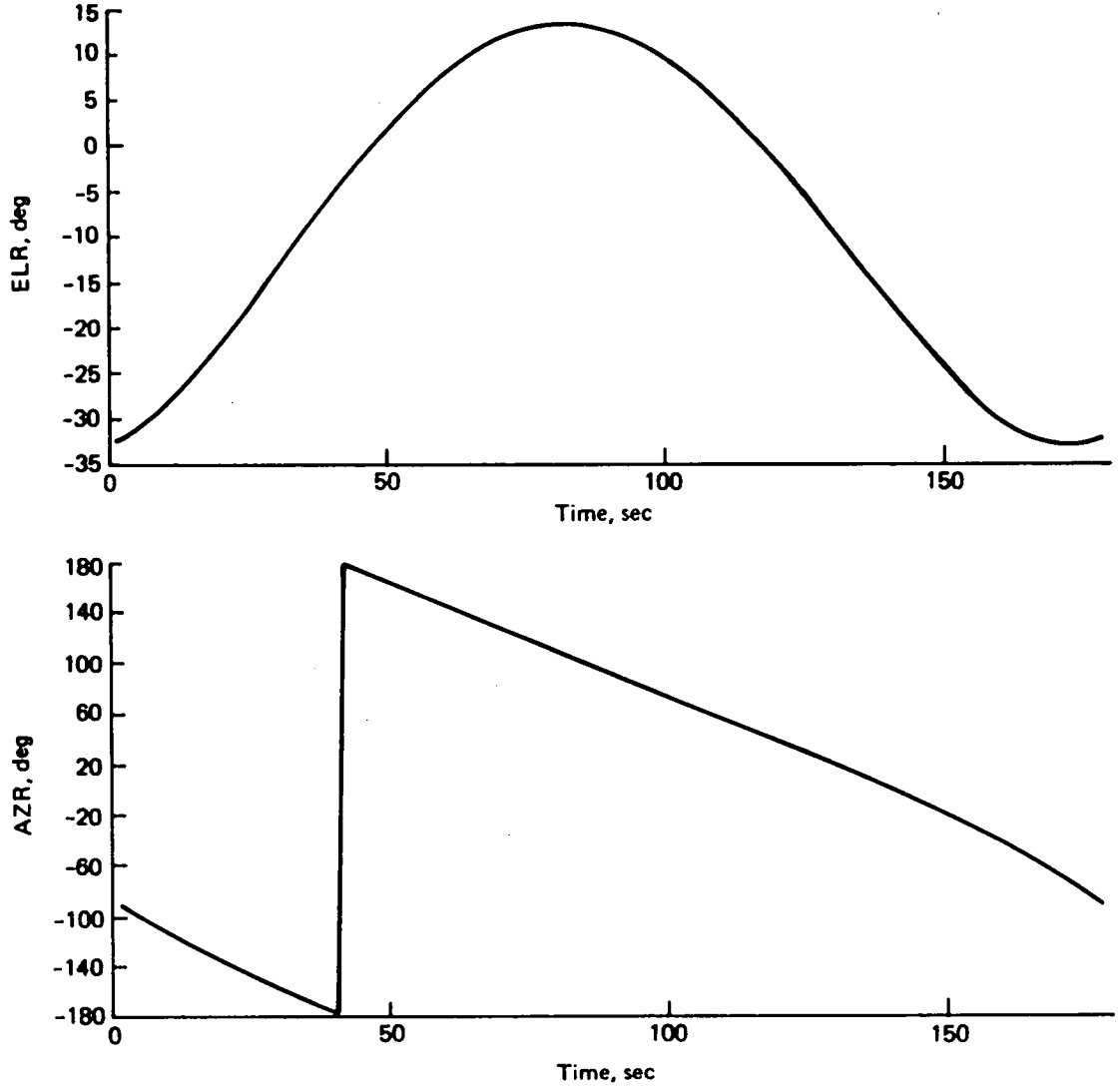

Figure A-19. Receiver Look-Angle Time Histories

129044-81

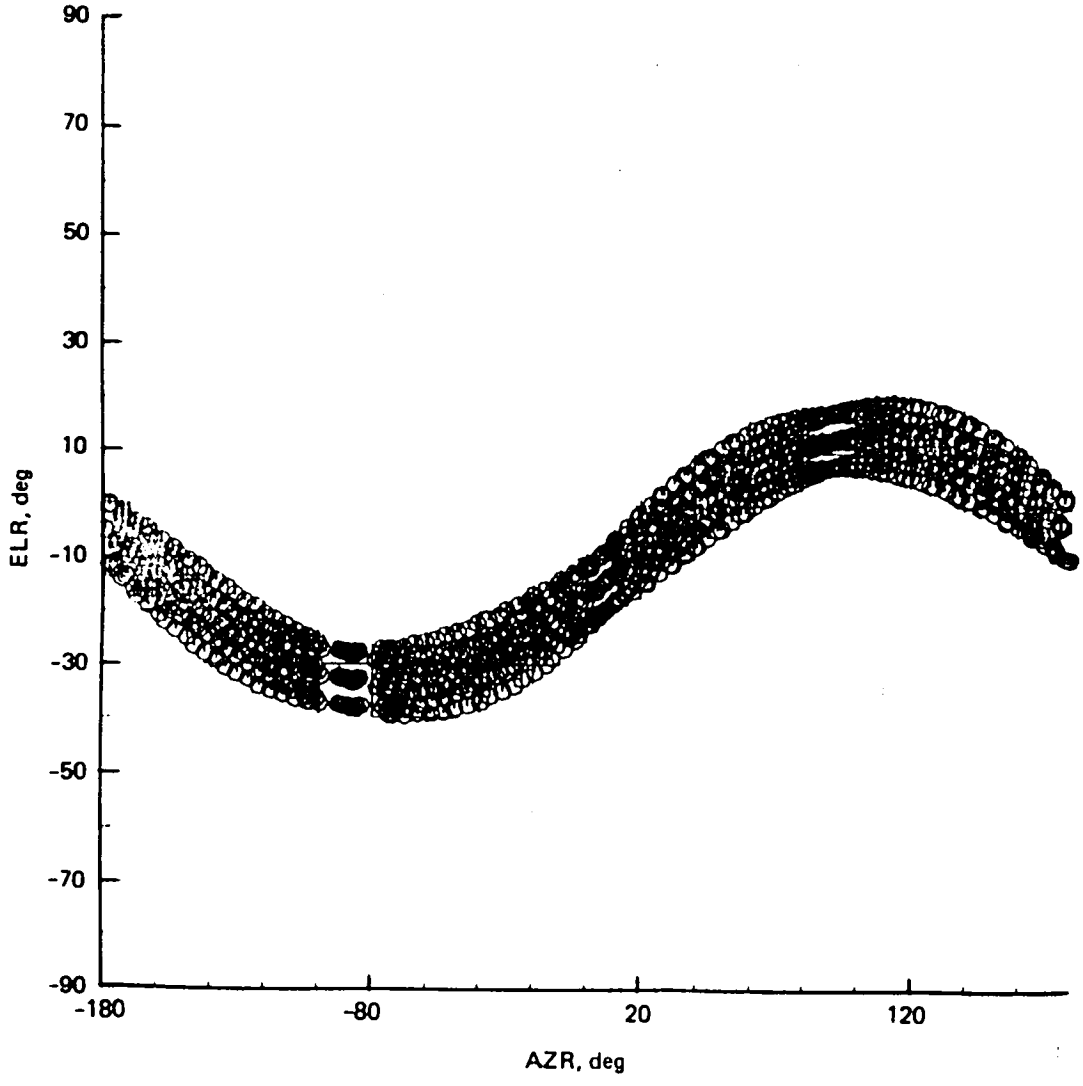

129044-82

Figure A-20. Receiver Look-Angle Mapping Results

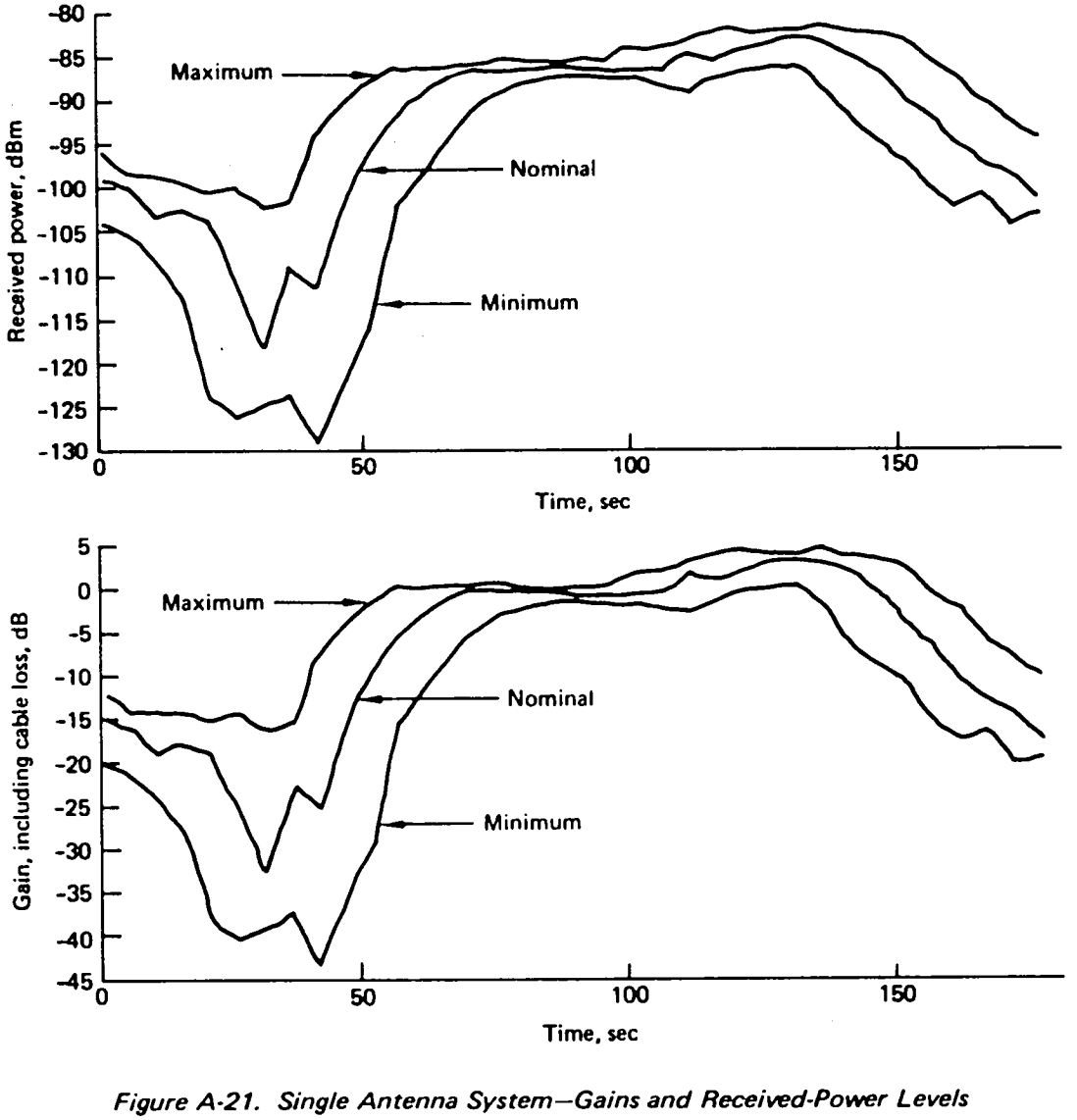

Figure A-21. Single Antenna System—Gains and Received-Power Levels

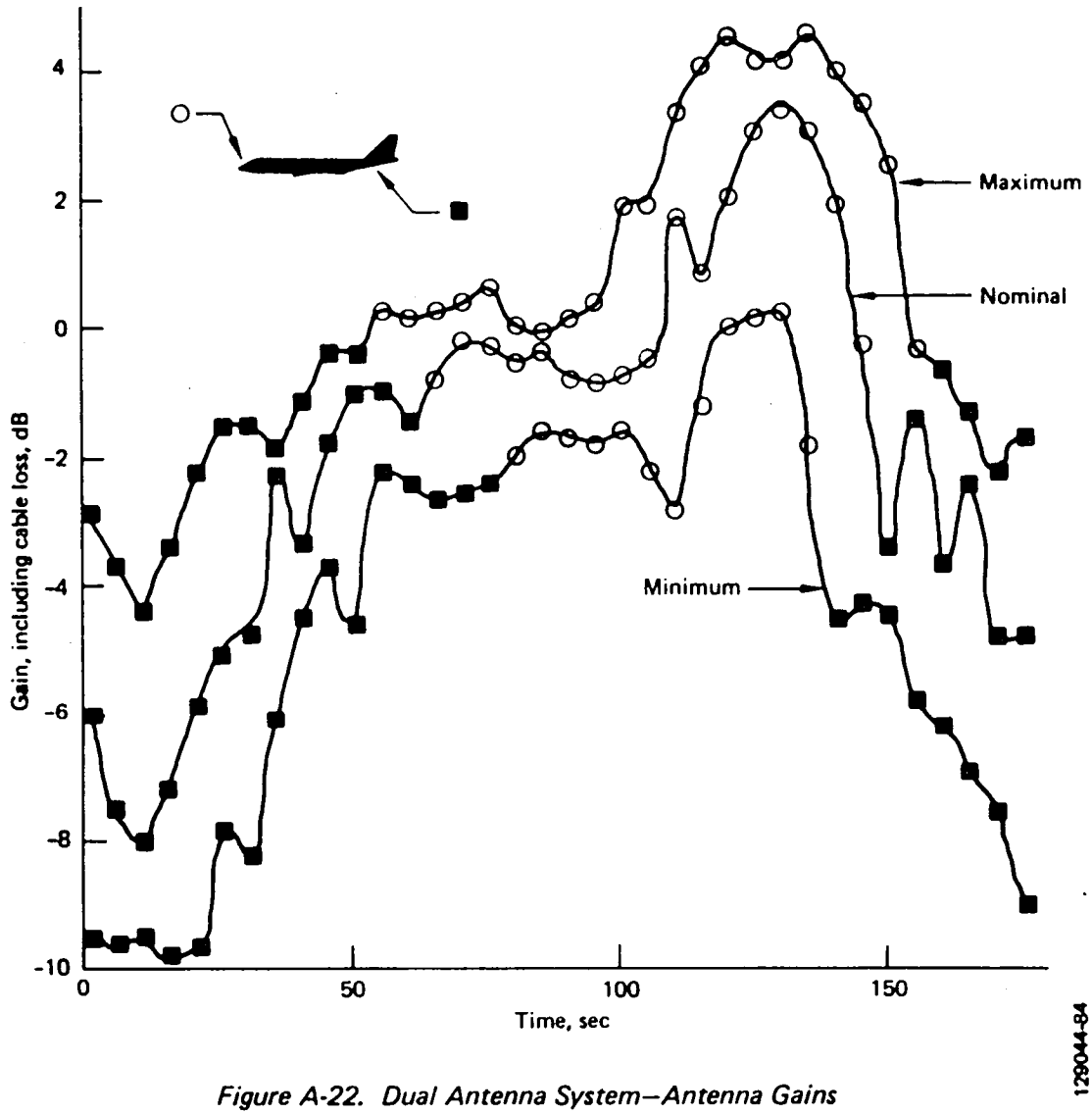

Figure A-22. Dual Antenna System—Antenna Gains

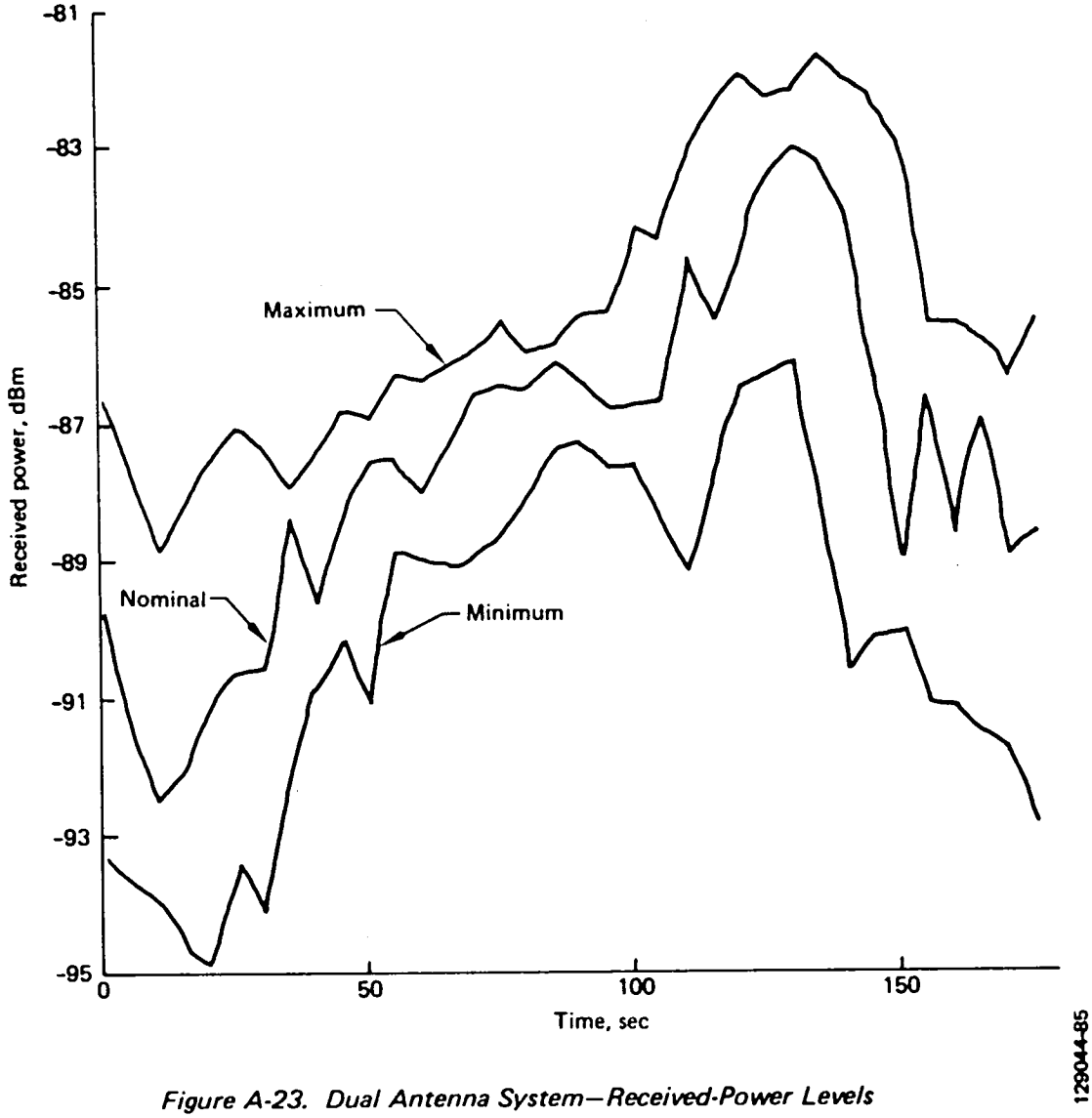

Figure A-23. Dual Antenna System—Received-Power Levels

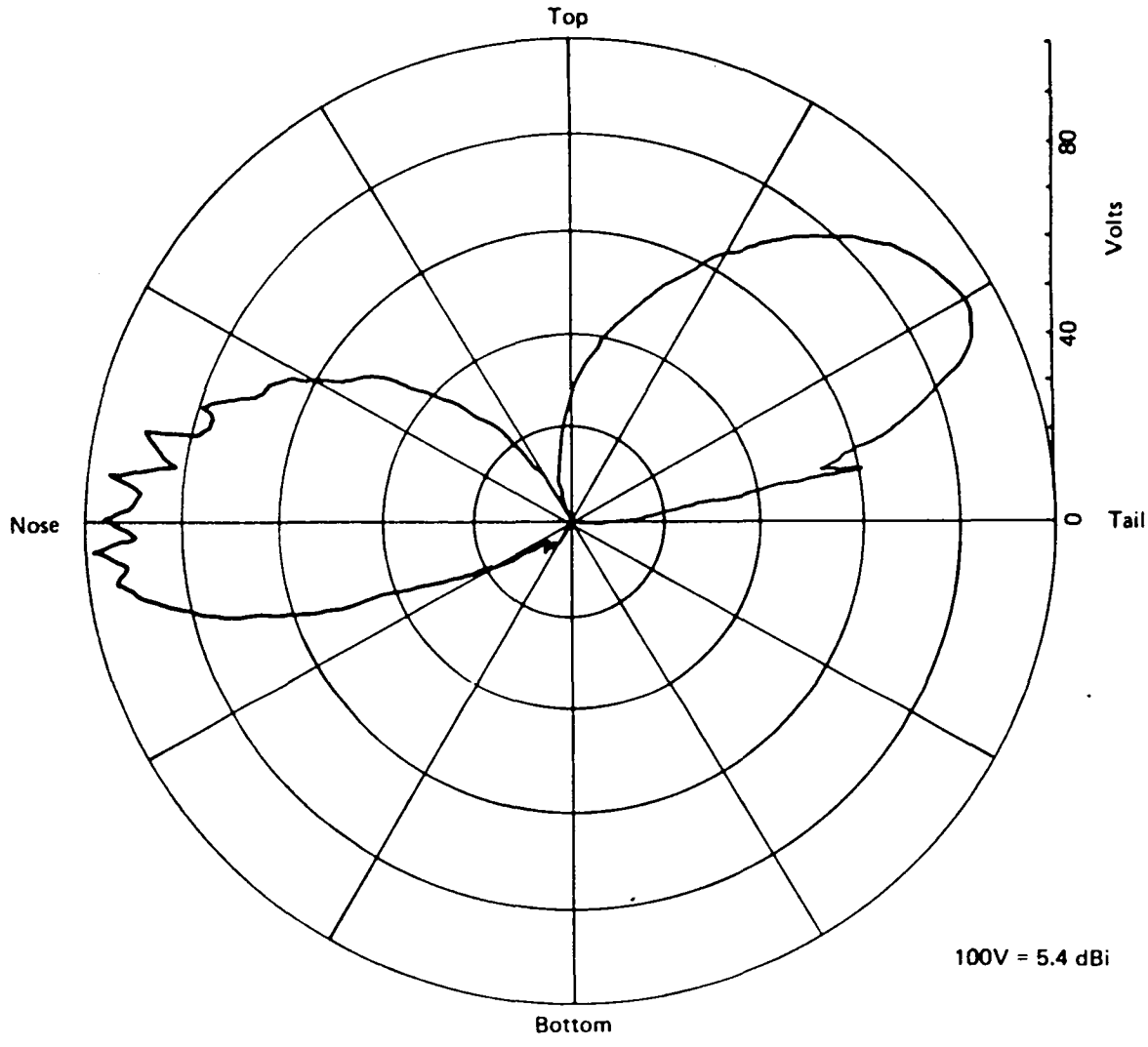

Figure B-1. 707 Top MLS Antenna—Pitch-Plane Pattern

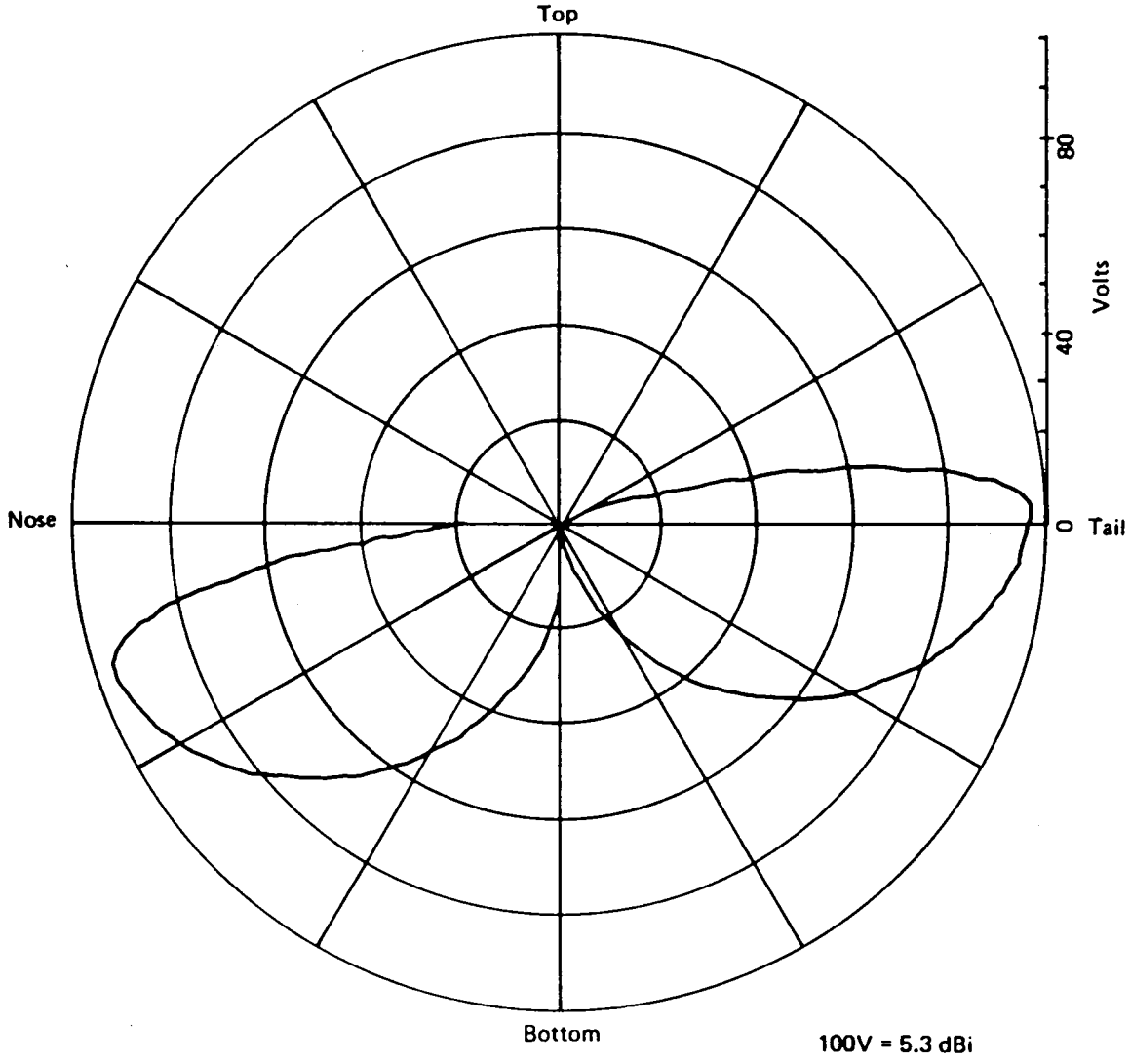

Figure B-2. 707 Bottom MLS Antenna—Pitch-Plane Pattern

129044-86

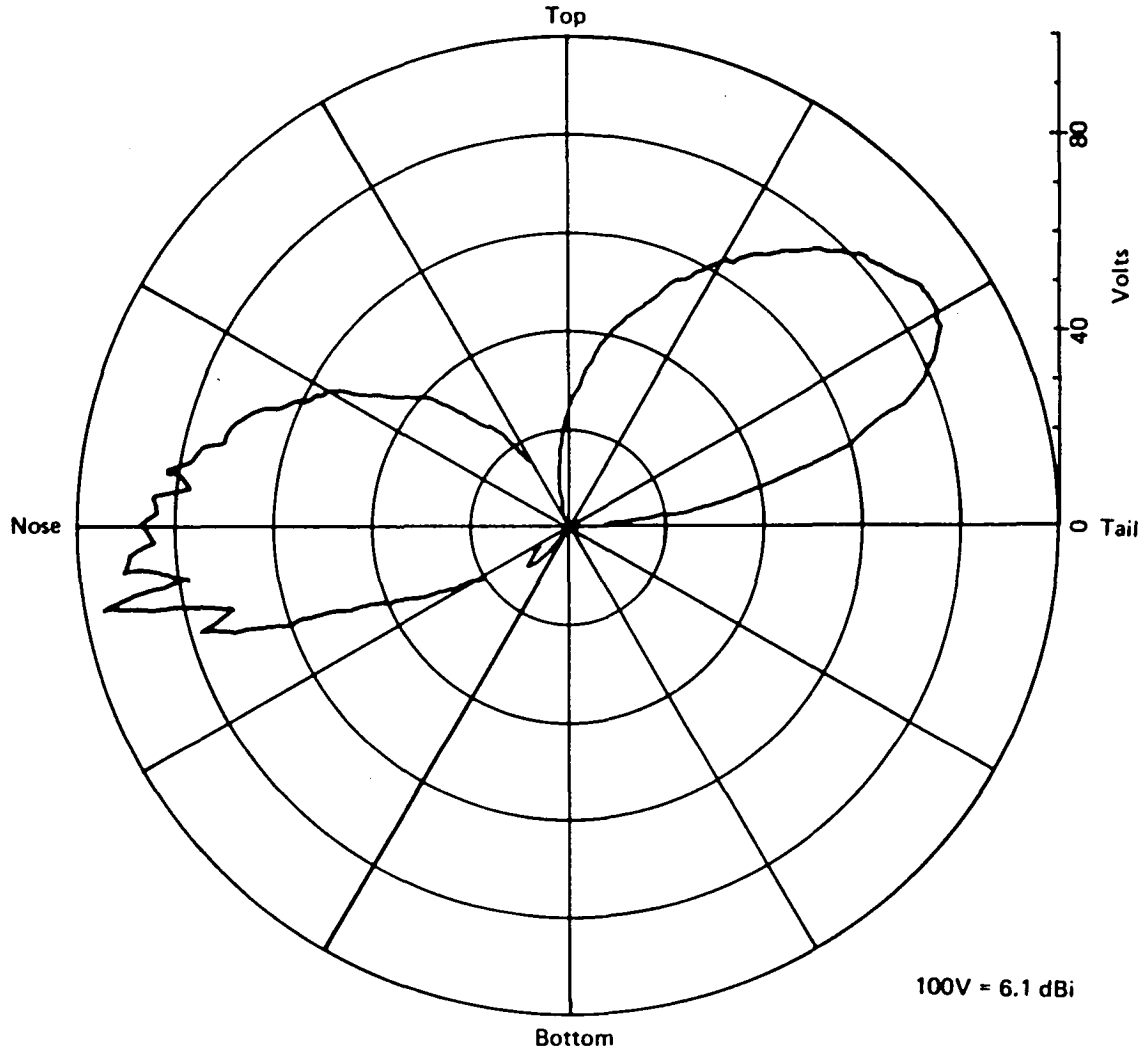

Figure B-3. 727 Top MLS Antenna—Pitch-Plane Pattern

129044-87

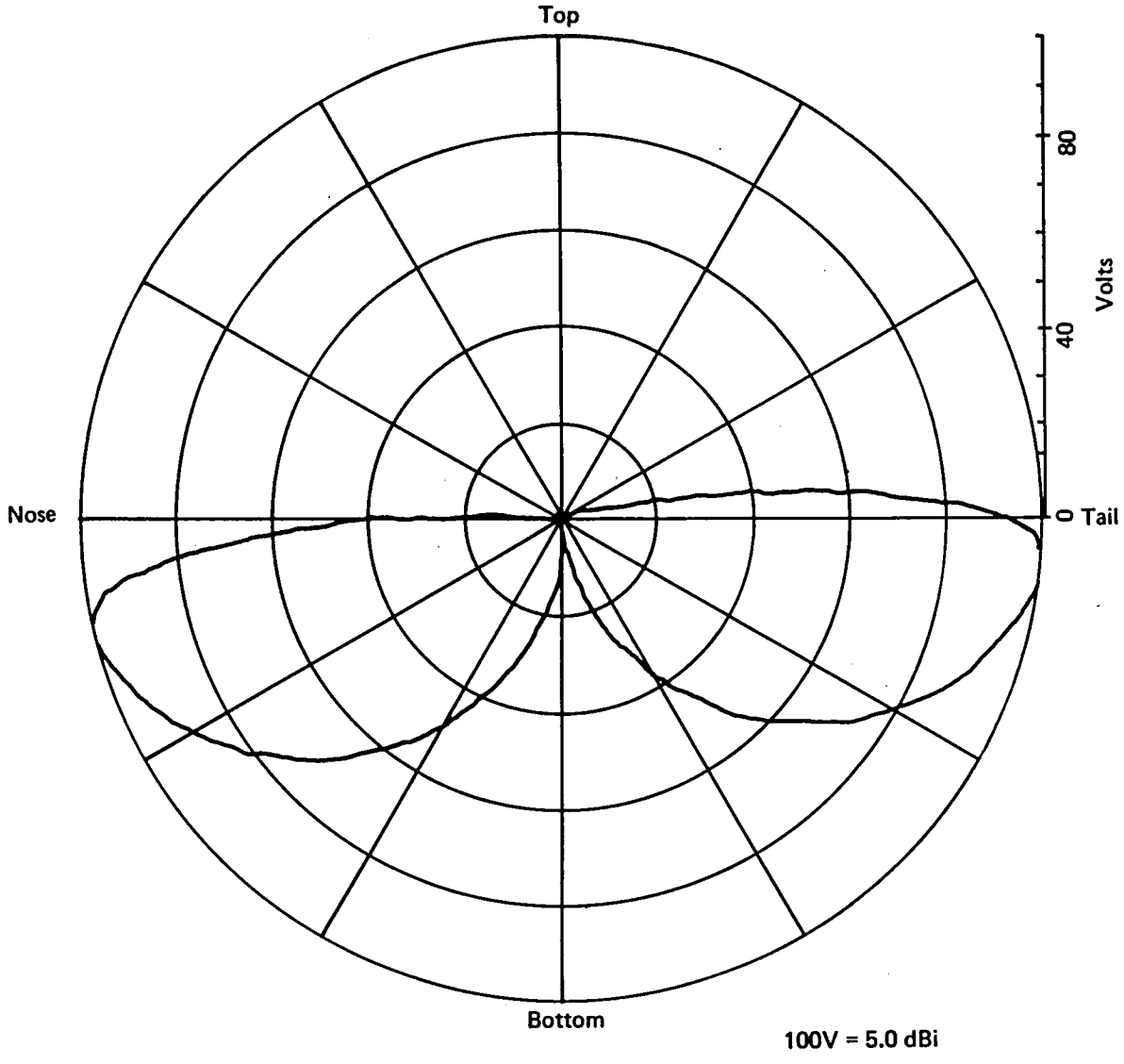

Figure B-4. 727 Bottom MLS Antenna—Pitch-Plane Pattern

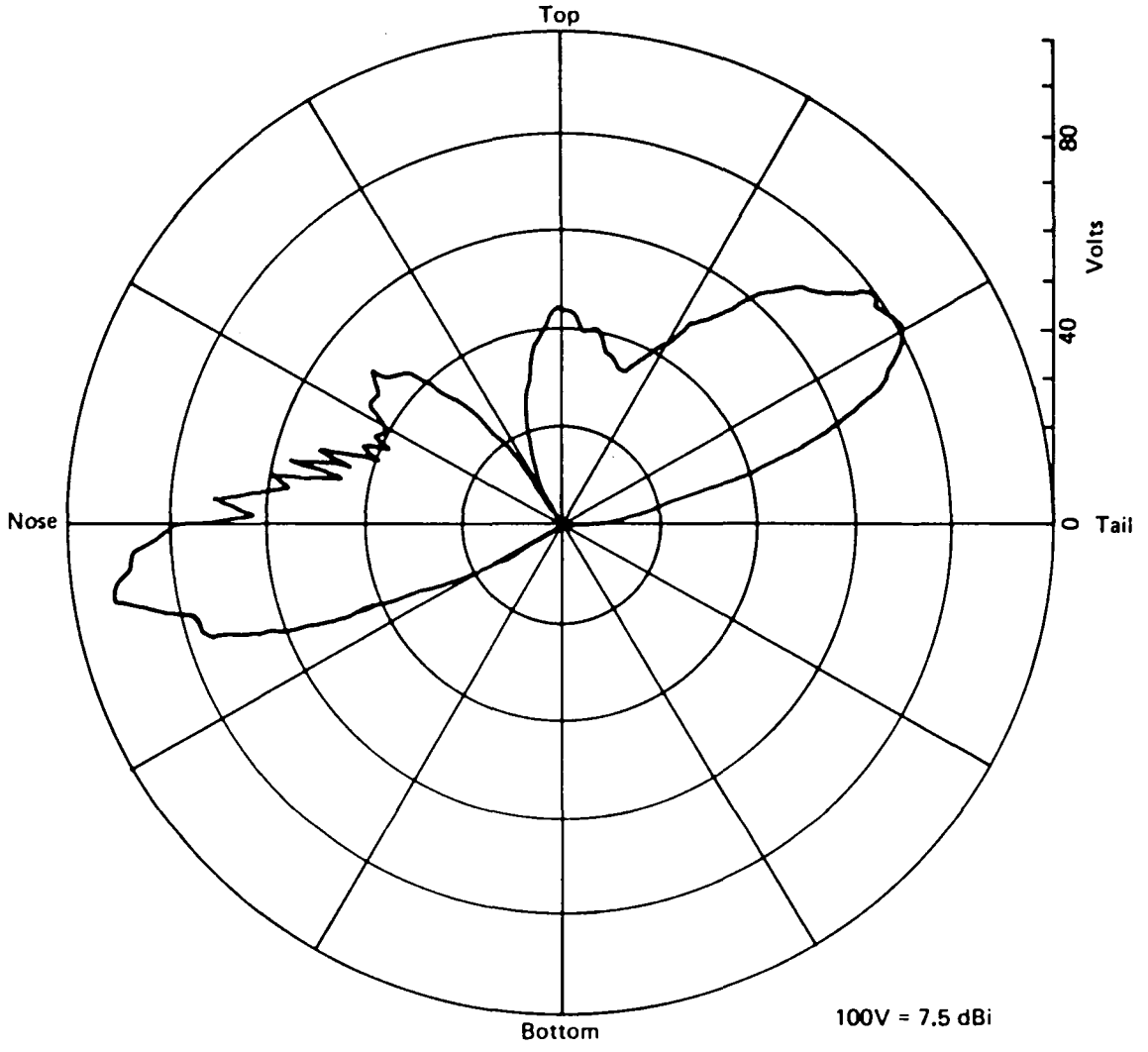

Figure B-5. 737 Top MLS Antenna–Pitch-Plane Pattern

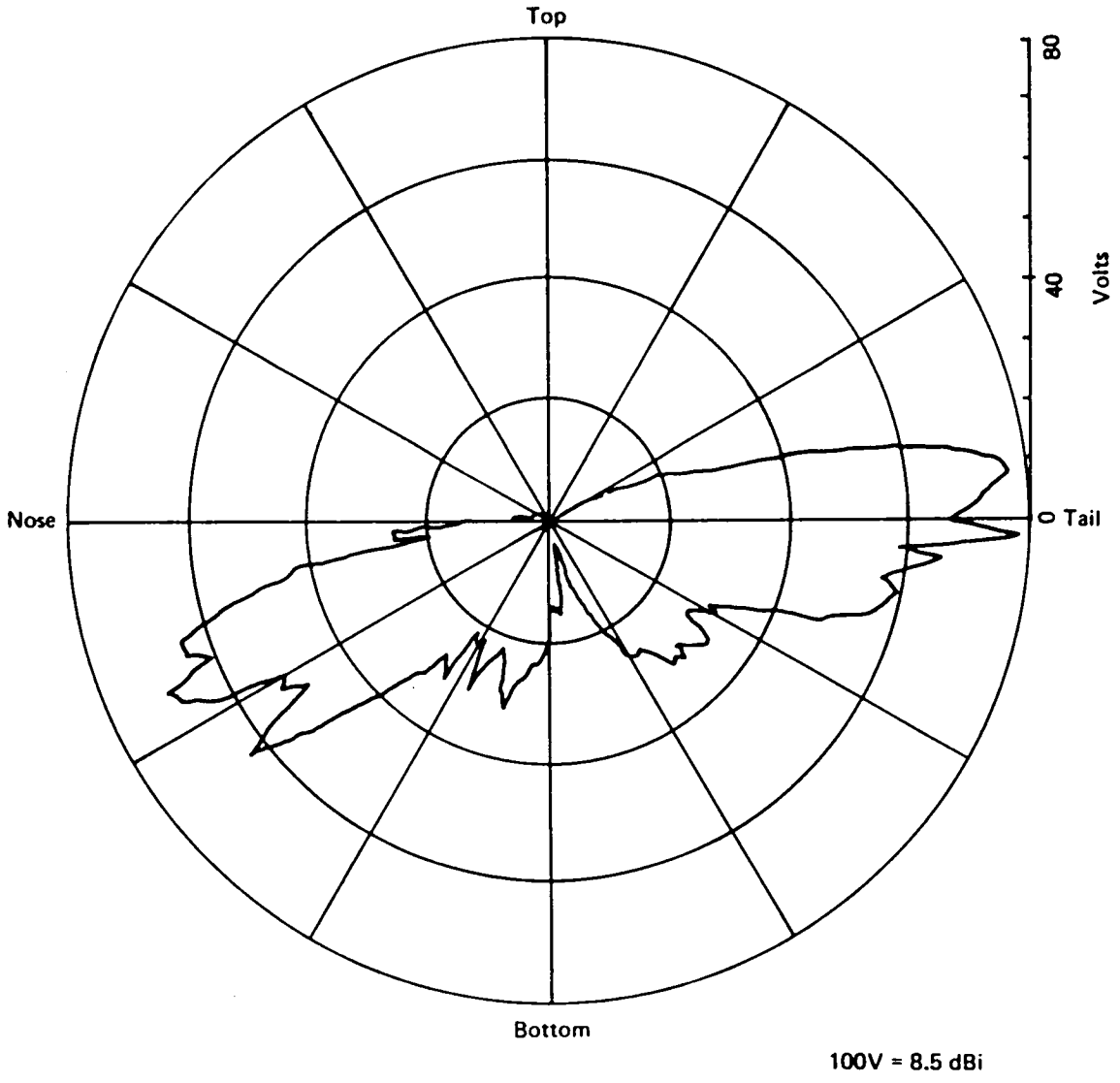

Figure B-6. 737 Bottom MLS Antenna—Pitch-Plane Pattern

129044-89

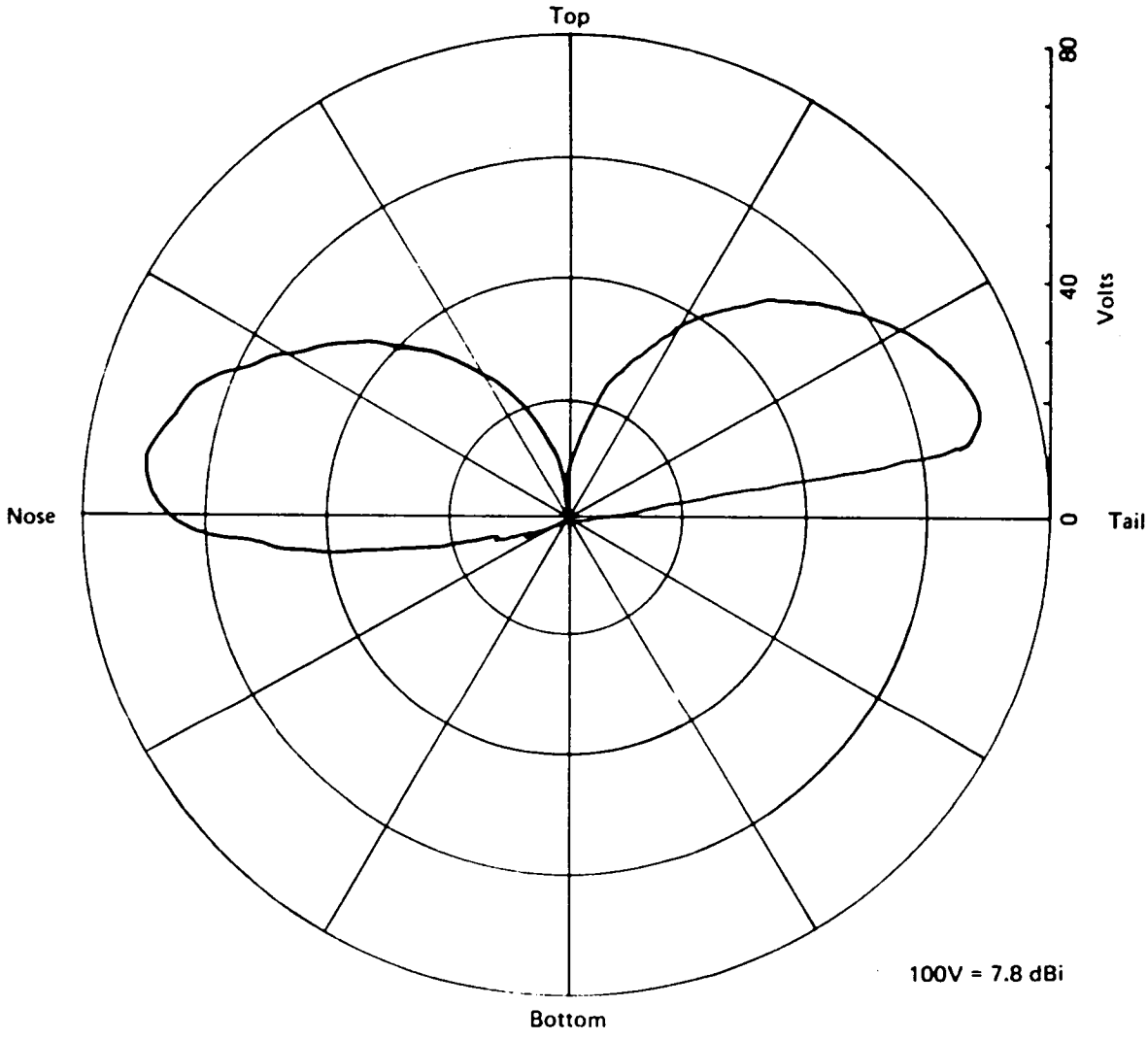

Figure B-7. 747 Top MLS Antenna—Pitch-Plane Pattern

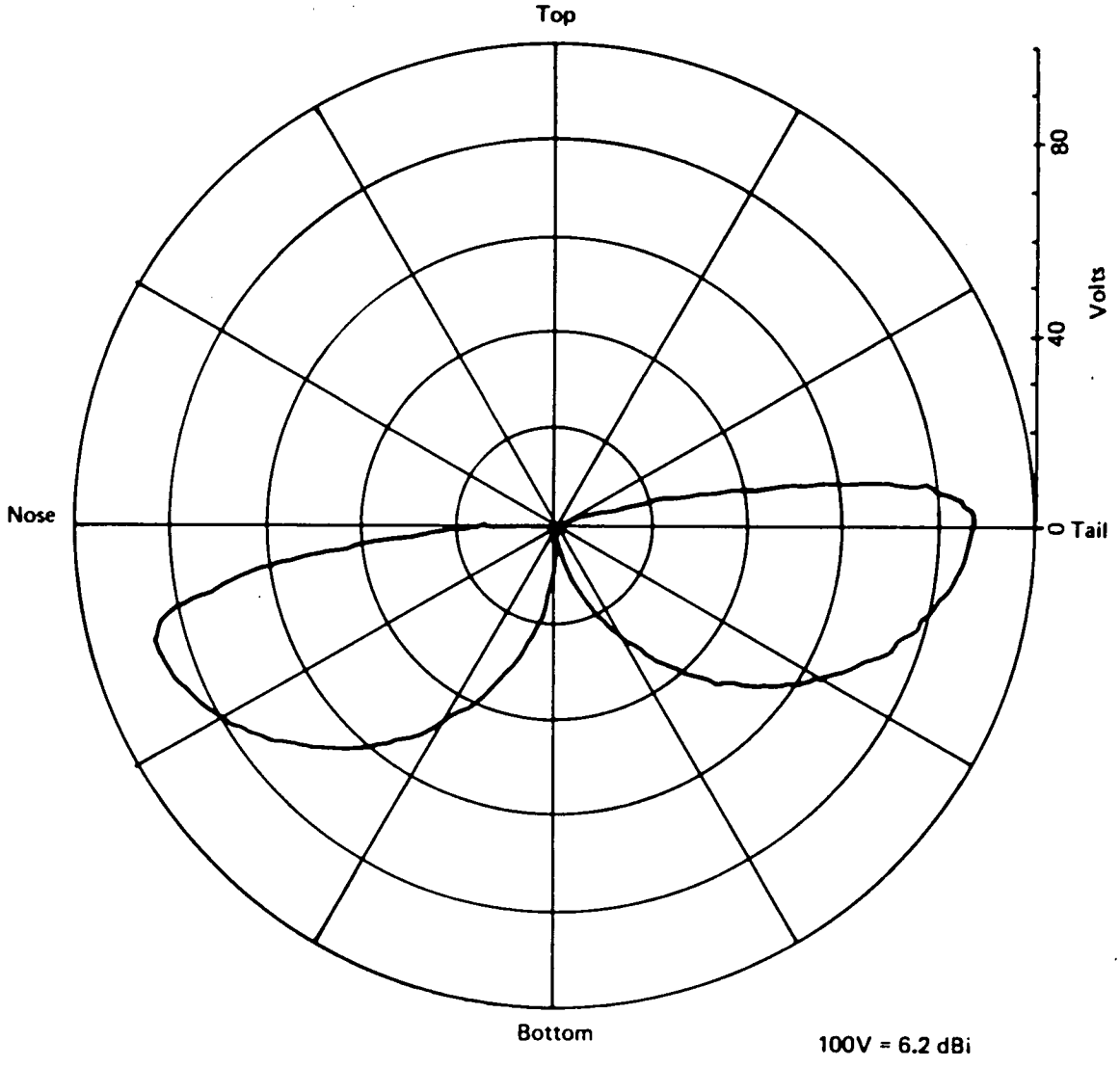

Figure B-8. 747 Bottom MLS Antenna—Pitch-Plane Pattern

129044-80

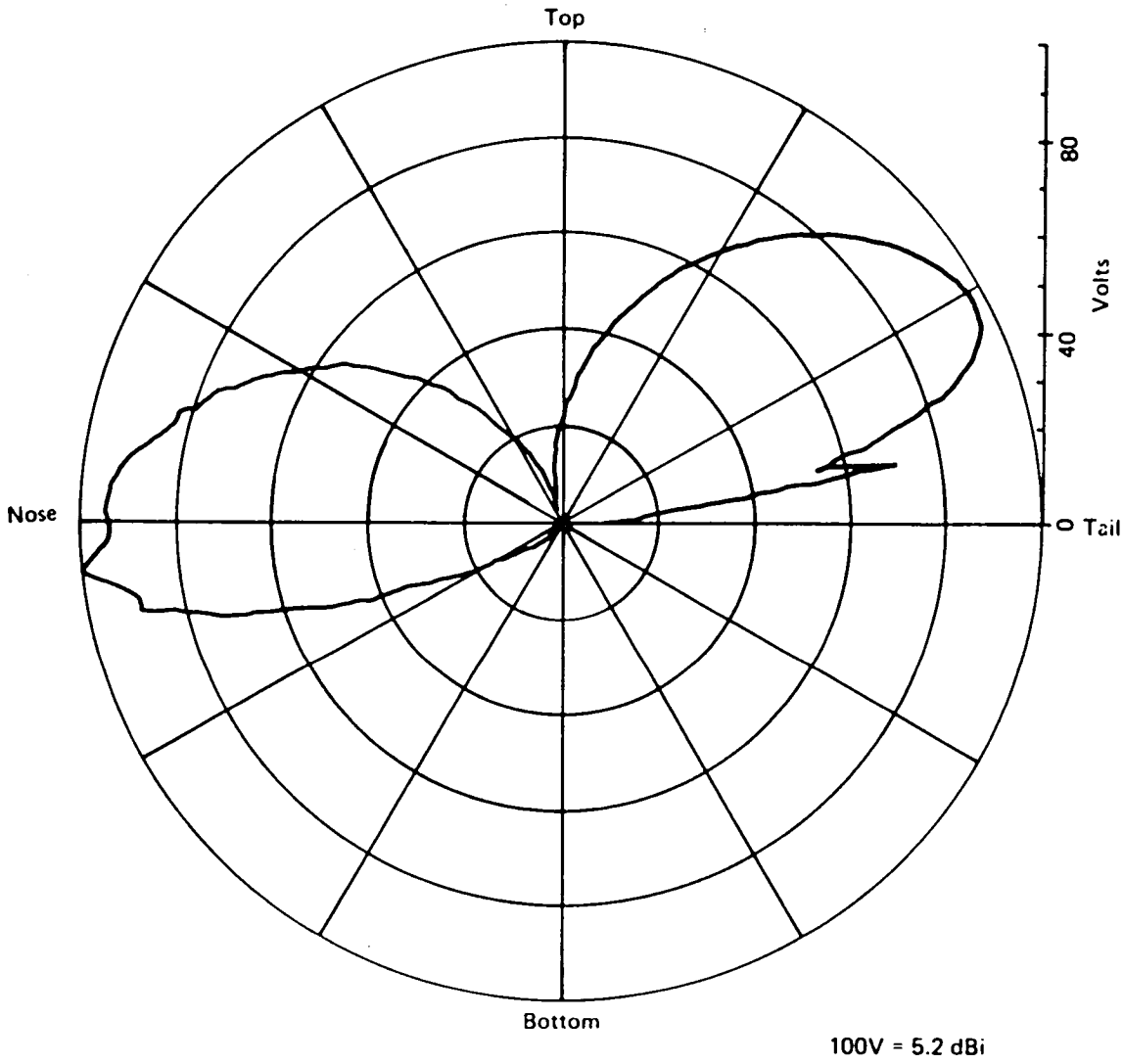

Figure B-9. 757 Top MLS Antenna—Pitch-Plane Pattern

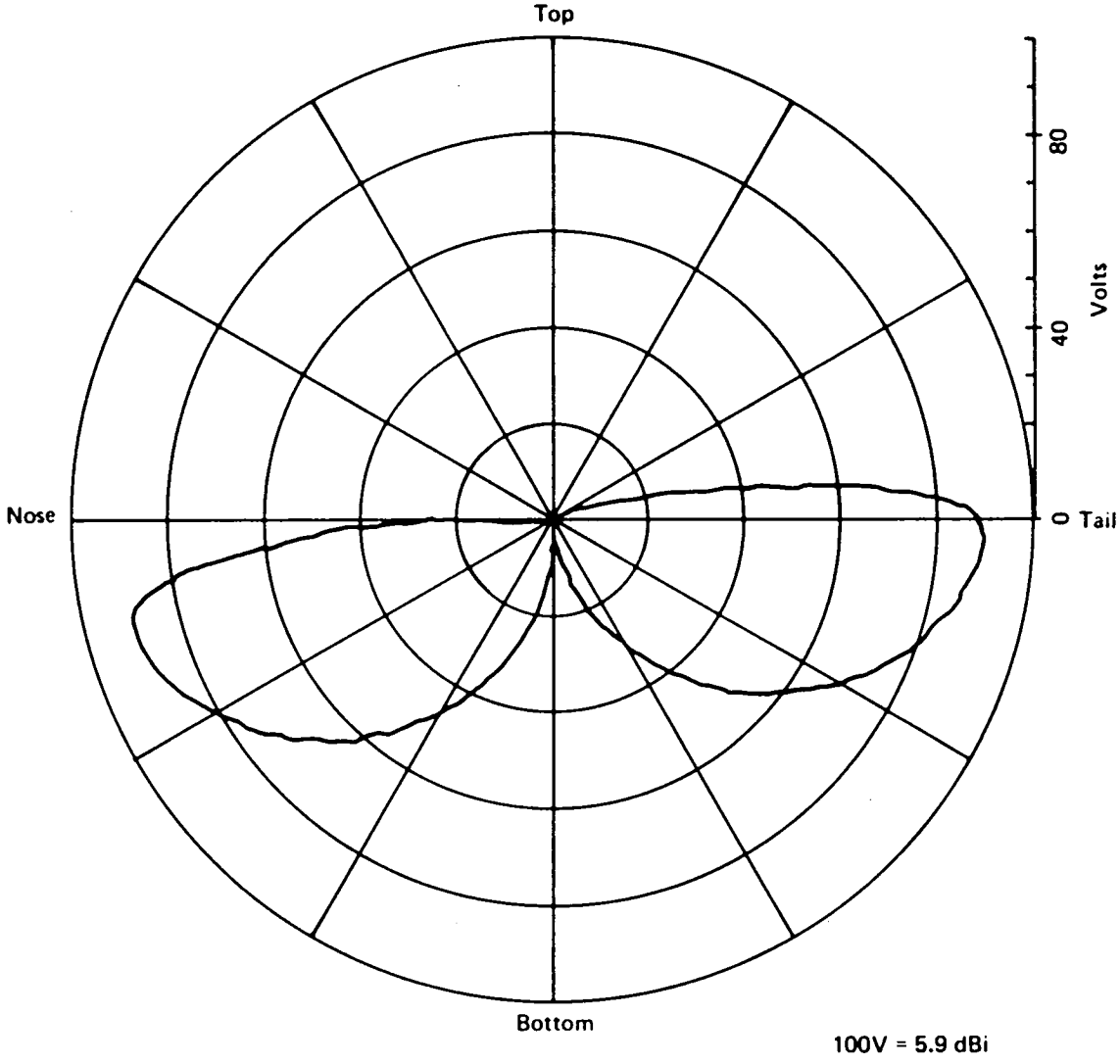

Figure B-10. 757 Bottom MLS Antenna—Pitch-Plane Pattern

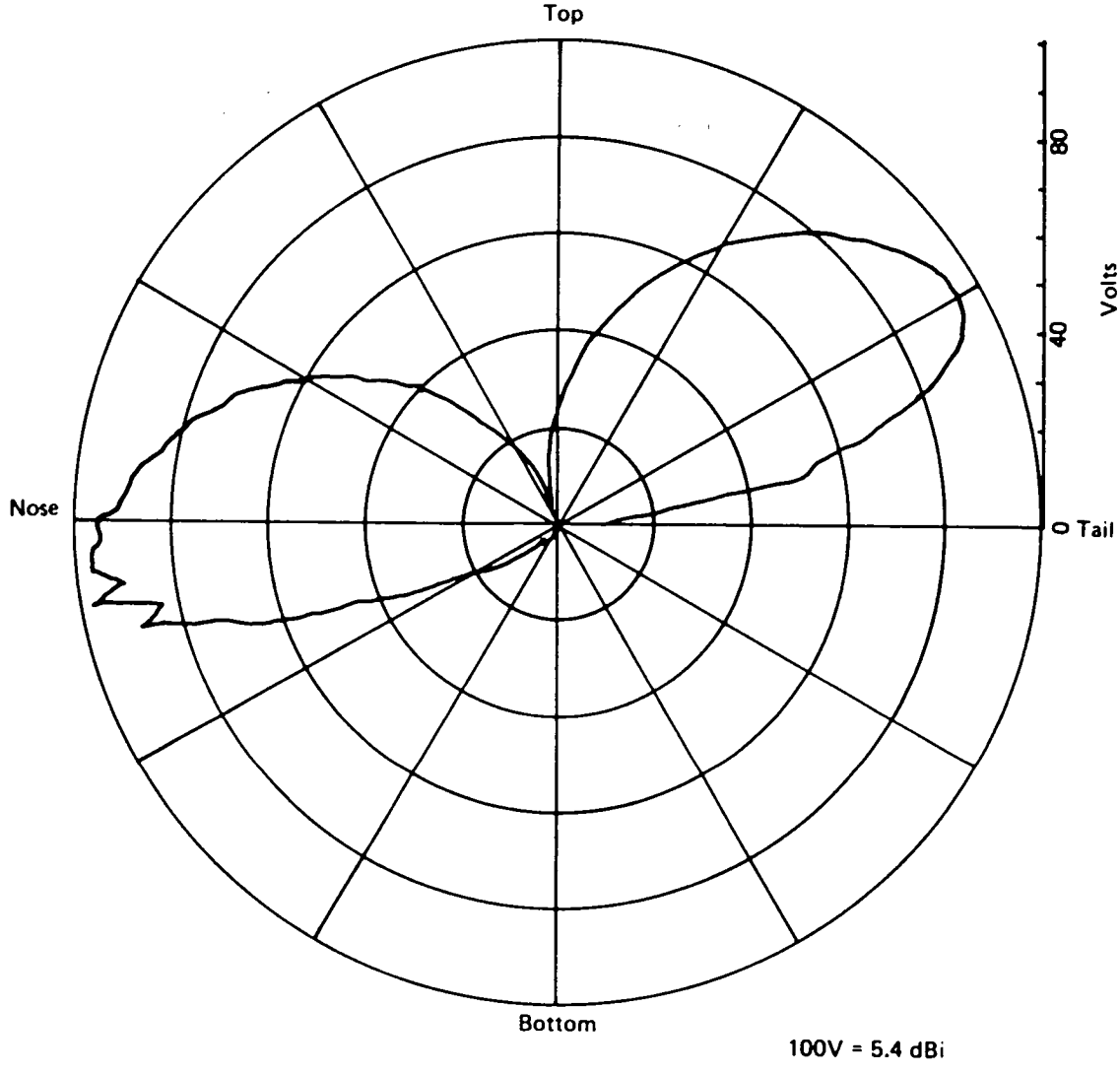

Figure B-11. 767 Top MLS Antenna—Pitch-Plane Pattern

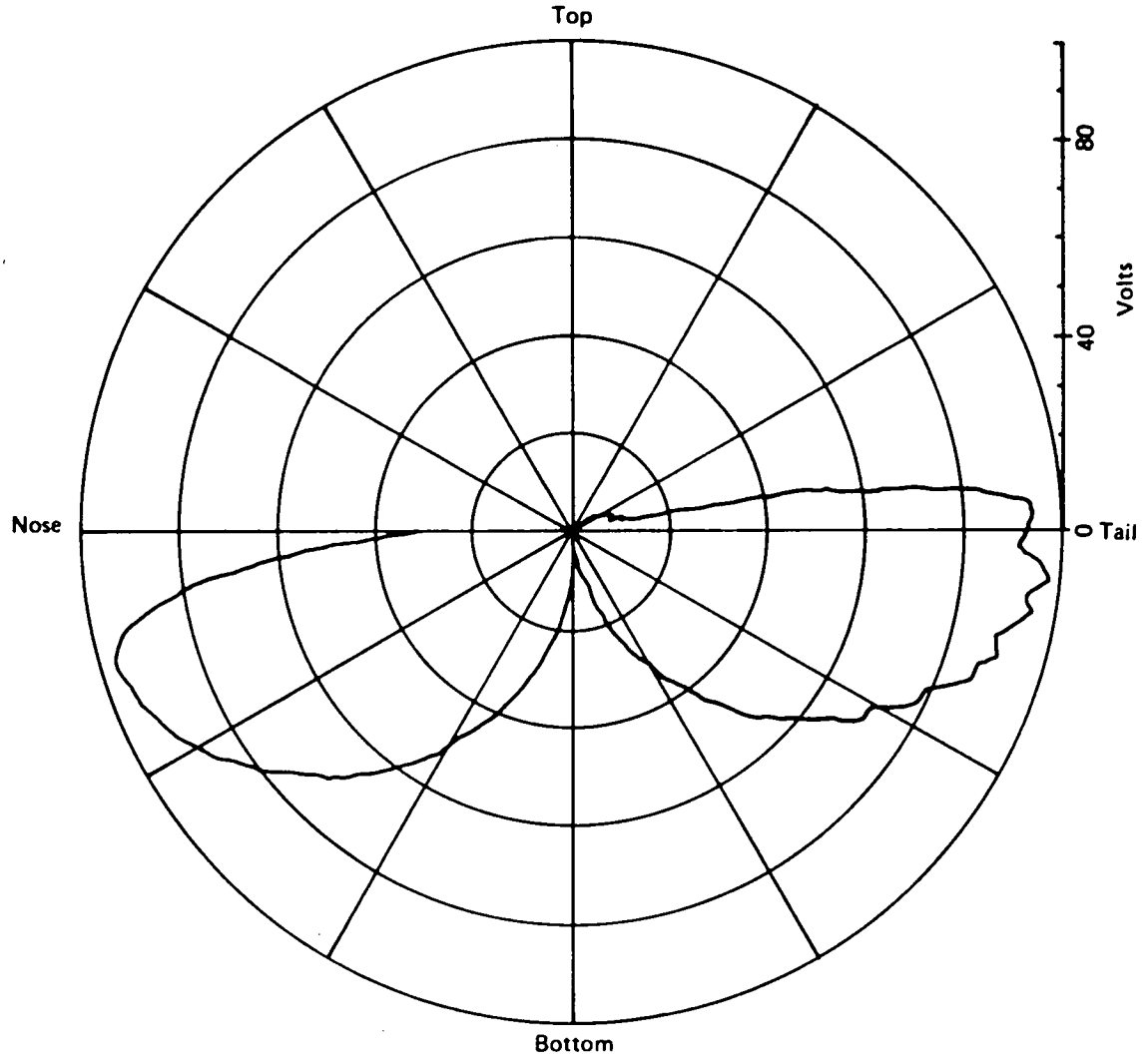

Fibure B-12. 767 Bottom MLS Antenna—Pitch-Plane Pattern

1. Report No.	2. Government Accession No.	3. Recipient's Catalog No.
NASA CR-165700		

4. Title and Subtitle	5. Report Date
MLS - Airplane System Modeling	April 1981
	6. Performing Organization Code

7. Author(s)	8. Performing Organization Report No
A. D. Thompson, B. P. Stapleton, D. B. Walen P. F. Rieder and D. G. Moss	D6-48724
	10. Work Unit No

9. Performing Organization Name and Address	11. Contract or Grant No
Boeing Commercial Airplane Company P.O. Box 3707 Seattle, Washington 98124	NAS1-14880
	13. Type of Report and Period Covered
12. Sponsoring Agency Name and Address	Contractor Report
National Aeronautics and Space Administration Washington, DC 20546	14. Sponsoring Agency Code

15. Supplementary Notes Technical monitor: William F. White
Mail Stop 265
NASA Langley Research Center
Hampton, VA 23665

16. Abstract

Analysis, modeling, and simulations have been conducted as part of a multiyear contract designed to address the more important airplane-system-related items of the microwave landing system (MLS). Particular emphasis was placed upon the airplane RF system, including the antenna radiation distribution, the cabling options from the antenna to the receiver, and the overall impact of the airborne system gains and losses upon the direct-path signal structure. In addition, effort was expended toward determining the impact of the MLS upon the airplane flight management system and developing the initial stages of a fast-time MLS automatic flight control system (AFCS) simulation model. Results of these studies are contained in this report.

17. Key Words (Suggested by Author(s))	18. Distribution Statement
Microwave landing system (MLS), Automatic flight control system (AFCS), Flight management system (FMS), Airplane, Antenna, Geometrical theory of diffraction (GTD)	Unclassified - Unlimited

19. Security Classif. (of this report)	20. Security Classif. (of this page)	21. No. of Pages	22. Price
Unclassified	Unclassified	127	

For sale by the National Technical Information Service, Springfield, Virginia 22161